DEVELOPMENT OF NONAQUEOUS ZINC-ION BATTERY BASED ON MANGANESE DIOXIDE CATHODE

Mr. Wathanyu Kao-ian

การพัฒนาแบตเตอรี่ไอออนสังกะสีซึ่งไม่ใช้น้ำฐานแคโทดแมงกานีสไดออกไซด์

นายวธัญญู เก้าเอี้ยน

จุฬาลงกรณ์มหาวิทยาลัย

CHULALONGKORN UNIVERSITY

วิทยานิพนธ์นี้เป็นส่วนหนึ่งของการศึกษาตามหลักสูตรปริญญาวิศวกรรมศาสตรดุษฎีบัณฑิต
สาขาวิชาวิศวกรรมเคมี ภาควิชาวิศวกรรมเคมี
คณะวิศวกรรมศาสตร์ จุฬาลงกรณ์มหาวิทยาลัย
ปีการศึกษา 2564
ลิขสิทธิ์ของจุฬาลงกรณ์มหาวิทยาลัย

Thesis Title	DEVELOPMENT OF NONAQUEOUS ZINC-ION BATTERY BASED ON MANGANESE DIOXIDE CATHODE
By	Mr. Wathanyu Kao-ian
Field of Study	Chemical Engineering
Thesis Advisor	Associate Professor SOORATHEP KHEAWHOM, Ph.D.

Accepted by the FACULTY OF ENGINEERING, Chulalongkorn University in Partial Fulfillment of the Requirement for the Doctor of Engineering

.... Dean of the FACULTY OF
ENGINEERING
(Professor SUPOT TEACHAVORASINSKUN, D.Eng.)

DISSERTATION COMMITTEE

.... Chairman
(Assistant Professor Pornchai Bumroongsri, D.Eng.)
.... Thesis Advisor
(Associate Professor SOORATHEP KHEAWHOM, Ph.D.)
.... Examiner
(Assistant Professor NATTAPORN TONANON, D.Eng.)
.... Examiner
(Associate Professor ROJANA PORNPRASERTSUK, Ph.D.)
.... Examiner
(Assistant Professor PIMPORN PONPESH, Ph.D.)

วธัญญ เก้าเอี้ยน : การพัฒนาแบตเตอรี่ไอออนสังกะสีซึ่งไม่ใช้น้ำฐานแคโทดแมงกานีสไดออกไซด์. (DEVELOPMENT OF NONAQUEOUS ZINC-ION BATTERY BASED ON MANGANESE DIOXIDE CATHODE) อ.ที่ปรึกษาหลัก : รศ. ดร.สุรเทพ เขียวหอม

แบตเตอรี่ไอออนสังกะสีนับว่าเป็นตัวเลือกหนึ่งที่มีแนวโน้มในการแทนที่แบตเตอรี่ไอออนลิเธียมเพื่อการประยุกต์ใช้ในระบบขนาดใหญ่ แม้ว่าแบตเตอรี่ไอออนสังกะสีที่ใช้อิเล็กโทรไลต์ฐานน้ำมีข้อดีหลายประการ เช่น มีต้นทุนต่ำ ปลอดภัย และเป็นมิตรกับสิ่งแวดล้อม แต่ข้อบกพร่องที่เกี่ยวข้องกับความเสถียร เช่น การกัดกร่อน การเกิดก๊าซไฮโดรเจน และการเกิดสังกะสีโครงสร้างกิ่ง ยังคงเป็นอุปสรรคต่อการประยุกต์ใช้งานจริง ดังนั้นอิเล็กโทรไลต์ที่ไม่ใช่น้ำ เช่น อิเล็กโทรไลต์อินทรีย์ และของเหลวไอออนิคที่อุณหภูมิห้อง ได้รับการพัฒนาเพื่อลดปัญหาเหล่านี้ อย่างไรก็ตาม ความเข้าใจเกี่ยวกับอิเล็กโทรไลต์ที่ไม่ใช่น้ำนั้นยังไม่ได้รับการอธิบายอย่างชัดเจน งานวิจัยนี้ระบุถึงความก้าวหน้าของอิเล็กโทรไลต์ที่ไม่ใช่น้ำ และพัฒนาระบบอิเล็กโทรไลต์ที่ไม่ใช่น้ำแบบใหม่สำหรับแบตเตอรี่ไอออนสังกะสีฐานแคโทดแมงกานีสไดออกไซด์ เพื่อจุดประสงค์นี้ เคมีของสังกะสี (กล่าวคือ การชุบ/การลอกออกของสังกะสี และการแทรกสอด/การแยกตัว) ในอิเล็กโทรไลต์ที่ไม่ใช่น้ำจะได้รับการพิจารณาและอธิบาย นอกจากนี้ยังมีการระบุช่องว่างของการวิจัยและพัฒนาในสาขาการวิจัยนี้ โดยสังเขป การทบทวนวรรณกรรมแสดงให้เห็นว่าอิเล็กโทรไลต์ที่ไม่ใช่น้ำสามารถระงับปัญหาดังกล่าวได้อย่างมีประสิทธิผล โดยยอมให้ใช้วัสดุเจ้าภาพที่มีศักย์ไฟฟ้าสูง และให้ปฏิกิริยาย้อนกลับของสังกะสีที่มีเสถียรภาพ (ประสิทธิภาพคูลอมบิก ~100%) นอกจากนี้ งานวิจัยนี้ยังสาธิตการใช้อิเล็กโทรไลต์สารละลายดีพยูเทคติก ได้แก่ โคลีนคลอไรด์-ยูเรีย และอิเล็กโทรไลต์อินทรีย์ ได้แก่ ไดเมทิลซัลฟอกไซด์ ในแบตเตอรี่ไอออนสังกะสีบนฐานแคโทดแมงกานีสออกไซด์ ผลการทดสอบแบตเตอรี่ชี้ให้เห็นว่าเซลล์แบตเตอรี่สังกะสี/แมงกานีสออกไซด์ที่ใช้โคลีนคลอไรด์-ยูเรีย แสดงความสามารถในการคายประจุสูงสุดที่ 170 mAh/g ที่ 50 mA/g และอัตราการเสื่อมของความจุ 0.7% ต่อรอบ ในทางตรงกันข้ามเซลล์แบตเตอรี่สังกะสี/แมงกานีสออกไซด์ที่ใช้ไดเมทิลซัลฟอกไซด์ สามารถถอัดคายประจุได้ถึง 1,000 รอบโดยให้ความสามารถในการคงความจุไว้ที่ 60% (0.047% ต่อรอบ) และความจุสูงสุด 159 mAh/g ที่ 50 mA/g นอกจากนี้ อิเล็กโทรไลต์ทั้งโคลีนคลอไรด์-ยูเรีย และไดเมทิลซัลฟอกไซด์ ยังแสดงให้เห็นสังกะสีที่ปราศจากเดนไดรต์และปราศจากการผลิตก๊าซไฮโดรเจน โดยรวมแล้ว ด้วยข้อดีในการปรับปรุงความเสถียรของแบตเตอรี่ อิเล็กโทรไลต์ที่ไม่ใช่น้ำที่นำเสนอมานั้น แสดงให้เห็นถึงสมบัติที่ดีสำหรับการใช้งานในแบตเตอรี่ไอออนสังกะสี และปูทางไปสู่การใช้งานจริงในอนาคต

สาขาวิชา	วิศวกรรมเคมี	ลายมือชื่อนิสิต	....
ปีการศึกษา	2564	ลายมือชื่อ อ.ที่ปรึกษาหลัก	....

5971474721 : MAJOR CHEMICAL ENGINEERING

KEYWOR
D:
Zinc-ion batteries; nonaqueous electrolytes; manganese dioxide cathode

Wathanyu Kao-ian : DEVELOPMENT OF NONAQUEOUS ZINC-ION BATTERY BASED ON MANGANESE DIOXIDE CATHODE. Advisor: Assoc. Prof. SOORATHEP KHEAWHOM, Ph.D.

Zinc-ion batteries (ZIBs) are considered promising candidates for large-scale applications replacing lithium-ion batteries (LIBs). ZIBs having aqueous electrolytes have many advantages being low-cost, safe, and eco-friendly. However, a number of shortcomings hinder their application e.g. self-corrosion, hydrogen evolution, and Zn dendrite-formation. To mitigate these issues, nonaqueous electrolytes i.e. organic-based and room temperature ionic liquid electrolytes have been proposed. Nevertheless, nonaqueous electrolytes are yet to be elucidated. Herein, this work identifies nonaqueous electrolytes' state of the art and develops a new nonaqueous electrolyte system for ZIBs based on a manganese dioxide (MnO_2) cathode. For this purpose, Zn chemistry in nonaqueous electrolytes is reviewed and described. In addition, gaps in this research area are highlighted. In brief, the review suggests that nonaqueous electrolytes can effectively suppress the above-mentioned issues allowing the use of high voltage host material and providing a reversible/stable Zn chemistry (~100% coulombic efficiency). Furthermore, this work demonstrates the use of deep eutectic electrolytes, namely chloride-urea (ChCl-urea) and organic electrolytes such as dimethyl sulfoxide (DMSO) in ZIBs based on MnO_2 cathode for the first time. Battery testing results indicate that Zn/MnO2 cell having ChCl-urea revealed the highest discharge capacity of 170 mAh/g at 50 mA/g and a capacity fading rate of 0.7 % per cycle. Moreover, Zn/MnO_2 and DMSO can cycle up to 1,000 cycles yielding capacity retention of 60 % (0.047 % per cycle) and the highest capacity of 159 mAh/g at 50 mA/g. In addition, both ChCl-urea and DMSO electrolytes are seen to be dendrite-free and gas-production-free. Overall, nonaqueous electrolytes as well as our proposed electrolytes indicate good promise for ZIBs and pave the way towards practical use in the future.

Field of Study:	Chemical Engineering	Student's Signature
		....
Academic Year:	2021	Advisor's Signature
		....

ACKNOWLEDGEMENTS

TABLE OF CONTENTS

จุฬาลงกรณ์มหาวิทยาลัย

CHULALONGKORN UNIVERSITY

List of Tables

List of Figures

CHAPTER 1
INTRODUCTION

1.1 Background

Environmental concerns regarding global warming and climate change have lead to the development of renewable energy technologies [1]. Several forms of renewable energy: solar energy, wind energy, and biomass have been used to produce electricity; unfortunately, such energy sources are intermittent and easily disrupted by the weather [2, 3]. To compensate for this behavior, electrical energy storage systems (ESS) have been employed to store the energy during the harvest periods and feed the grid during peak loads [3]. Rechargeable batteries, one of the ESSs, have been used extensively as an energy source for electrical devices since almost half a century ago [4]. Although many batteries i.e. Lithium-ion (LIBs), Nickel-Cadmium (Ni-Cds), and Lead-acid (LABs) have demonstrated their success at commercialization, their application on a large scale has been limited owing to their high cost, lack of safety and eco-unfriendliness [2] [5]. Thus, the trend today aims to develop a new battery system that meets the demand in terms of economic, environmental aspect, safety, and efficiency [6].

Due to its nontoxicity, inflammability, cheapness, and availability of raw material, zinc (Zn) is an attractive anode choice for rechargeable batteries: Zn, as an anode, possesses high specific and volumetric capacity (820 mAh/g and 5,845 mAh/cm^3, respectively), which benefits the compact design of the battery [2, 7, 8]. Several rechargeable battery systems based on Zn anode (rechargeable Zn battery, RZB) have been developed continuously and show great potential to replace traditional batteries in the future [9]. According to the literature, Zn-air batteries (ZABs) and Zn-ion batteries (ZIBs) are the most promising candidates among RZBs [10, 11].

ZABs and ZIBs operate under different pH levels: ZABs require a basic environment whereas ZIBs operate under a mild-acidic environment [12-14]. ZABs face several limitations regarding the reversibility of the Zn anode such as severe ZnO passivation upon discharging, high self-corrosion rate at rest state, and high fraction of hydrogen evolution (HER) during charging [14, 15]. Nevertheless, such issues are

found to be minimal in mild-acidic electrolytes. Thus, ZIBs, which operate under mild-acidic electrolytes, are found to be more stable [16]. During discharging, ZABs rely on oxygen reduction reaction (ORR) whilst during charging, ZABs rely on oxygen evolution reaction (OER): a three-phase reaction (solid-liquid-gas). In contrast, the process of charge storage of ZIBs occurs via a two-phase redox reaction (solid-liquid) [17, 18]. Further, it is noted that the design of ZABs face more challenging issues regarding mass transport than that of ZIBs [19].

Rechargeable Zn-ion intercalation-type batteries such as ZIBs having a Zn anode, MnO_2 cathode, and aqueous electrolyte ($ZnSO_4$ or $Zn(NO_3)_2$) was first proposed in 2011 [20]. As a result, ZIBs based on MnO_2 have received much attention among battery developers [16]. Several phases (α, β, γ, and δ) and nanostructures (nanowires, nanorods, nanoflowers etc.) of MnO_2 have been applied in ZIBs in order to increase their performance and cycling stability. Several workgroups succeeded in producing a thousand-cycle ZIB having a high specific capacity (>200 mAh/g of MnO_2), proving to be sufficient to produce a practical-scale battery [2, 14, 21]. In addition, the ZIB concept has been applied to other intercalation materials i.e. vanadium oxides, Prussian blue analogues as well as organic cathodes [2]. However, despite the reversible and energetic chemistry of aqueous ZIBs, their practical application is limited by H_2 production arising from self-corrosion and HER [1, 22]. It is significant that both Zn-hydrate passivation and dendrite-formation are found in aqueous ZIBs and have a role in degrading the performance and stability of ZIBs [1, 23].

To mitigate these issues, strategies such as the use of "water-in-salts" concept, the inhibitor addition, the artificial SEI, and the novel cathode design have been proposed [24-29]. Nevertheless, such problems cannot be entirely eliminated via the mentioned approaches: this is because the true cause of H_2 production is the existence of the proton (H^+) in the aqueous electrolyte, which consists of the proton-donor solvent (water) and Zn salt [30]. Thus, the best approach to eliminate the H_2 production issue is to use a non-proton donor electrolyte or a nonaqueous electrolyte [31]. Currently, there are mainly two groups of nonaqueous electrolytes found in the research on ZIBs: 1) organic solvent-based electrolytes and 2) room-temperature ionic liquid (RTIL)-based electrolytes [32].

Nonaqueous electrolytes provide not only a wider electrochemical stability window (2-3 V vs. Zn/Zn^{2+}) than that of aqueous electrolytes (< 2 V vs. Zn/Zn^{2+}), but also show a noncorrosive property onto the metallic Zn [1, 30, 33-35]. On average, RTIL-based electrolytes possess higher thermal stability than that of organic solvent-based electrolytes and aqueous electrolytes whereas organic solvent-based electrolytes provide more facile mass transport than that of RTIL-based electrolytes [32, 36]. Nonaqueous electrolytes exhibit great potential as an alternative electrolyte choice for ZIBs. Yet, due to limited information regarding cathode/electrolyte compatibility and lack of a basis for choosing the electrolyte components, nonaqueous electrolytes are, therefore, not widely applied in ZIBs [37]. Moreover, there are concerns regarding the performance of nonaqueous ZIBs (NZIBs) and the toxicity of nonaqueous electrolytes [1, 38]. To draw a clearer overall picture, research into NZIBs requires greater verification of their effectiveness and excellence.

Herein, this dissertation aims to determine the current state of NZIB research and to develop our own nonaqueous ZIB systems that feature high capacity, long-cycling life, and as such are eco-friendly and safe. The current state of NZIB research will be carried out by categorizing, reviewing, and benchmarking published articles regarding NZIBs. To develop new NZIB systems, MnO_2 was chosen to be the main cathode material. This is due to the availability, the nontoxicity, and the cheapness of MnO_2. Testing methods such as cyclic voltammetry (CV), electrochemical impedance spectroscopy (EIS), galvanostatic charge-discharge (GCD) cycling, X-ray diffraction (XRD), and scanning electron microscope (SEM) have been applied to investigate insight into the fabrication of this novel battery.

1.2 Objective

This research aims to determine the current state of NZIB research, to locate the limitation in NZIB research, and to develop a new NZIB prototype, which demonstrates high capacity, long-cycling life, is eco-friendly, and safe, based on MnO_2 cathode.

1.3 Scope of Research

1.3.1 Electrolytes for this study are in the range of nonaqueous electrolytes, including: 1) organic solvent-based electrolytes and 2) RTIL-based electrolytes.

1.3.2 The review part covers published articles regarding topics of Zn electrodeposition in nonaqueous media and topics of full cell NZIB proposition. All articles presented in this range are from early 2000 to the present 2021. Performance of both the Zn anode and intercalation cathode are highlighted.

1.3.3 In the new NZIB proposition sections, the main anode and cathode materials are discussed, as well as electrolytes that have been developed in the range of nonaqueous electrolytes.

1.3.4 The battery for electrochemical measurements is fabricated into CR2025 coin cell form. The Zn electrode is constructed via electrodeposition of Zn from an aqueous electrolyte. The δ-MnO_2 electrode is produced using simple doctor-blade ink coating methods.

1.4 Structure of the Dissertation

This dissertation comprises of five chapters, including Chapter 1 Introduction, Chapter 2 Literature Review, Chapter 3 Choline Chloride-Urea Electrolyte, Chapter 4 Dimethyl Sulfoxide Electrolyte, and Chapter 5 Conclusion and Suggestions.

Chapter 1: The Introduction describes the background and scope of the research, its objectives, related theories, and schedule plan. The necessary information regarding Zn based batteries and their development are further highlighted.

Chapter 2: The Literature Review provides general information and recent findings as regards nonaqueous electrolytes applied in rechargeable Zn battery research. The advantages and the limitation of nonaqueous electrolytes are outlined based on their performance. In addition, issues that need to be solved are introduced.

Chapter 3: Choline Chloride-Urea Electrolytes provides the data describing our first attempt on developing a Zn/MnO_2 battery system, which has been recently published: "Rechargeable Zinc-Ion Battery Based on Choline Chloride-Urea Deep

Eutectic Solvent". In this work, the choline-chloride/urea deep eutectic solvent enabled the smooth deposit of Zn. For the first time, the application of a Zn/MnO_2 battery is demonstrated. This chapter also reports on the experimental procedures, the evaluation results regarding the performance of both anode and cathode, as well as the limitation of this system.

To overcome the issues faced herein, a highly stable and safe aprotic solvent i.e. dimethyl sulfoxide was used as a solvent for the Zn/MnO_2 electrolyte. The result of this work has been published accordingly: "Highly stable rechargeable zinc-ion battery using dimethyl sulfoxide electrolyte" (see Chapter 4 for a full account). The results obtained and the testing conditions involved are provided in this chapter.

Chapter 5: Conclusion and Suggestions provides findings for both the review and further proposed works. In addition, possible enhancement approaches that can be used in future studies are also suggested.

1.5 Related Theories

1.5.1 Analytical techniques used in ZIB research

1.5.1.1 Galvanostatic charge-discharge (GCD)

The standard method used to evaluate the performance of a battery is to repeat the constant current charging and discharging, called GCD [39]. To conduct the GCD test, it requires a battery tester, which is equipment that can control the charge-discharge current of the battery. The capacity or the amount of charge transferred upon charging/discharging of the battery can be counted via an integral equation, as shown:

$$Capacity = \left(\int_{t_0}^{t_f} I dt \right) \tag{1.1}$$

where, I, t, t_0, t_f is current value, time, starting time and ending time, respectively. In addition, by including a voltage (V) into account, the charging/discharging energy can also be calculated using the GCD result via the equation as follows:

$$Energy = \left(\int_{t_0}^{t_f} IV dt \right) \tag{1.2}$$

Another important parameter in the battery test that can be obtained via GCD is the coulombic efficiency. Coulombic efficiency describes how much discharging capacity the battery can deliver with respect to the charging capacity:

$$Coulombic\ Efficiency = \frac{Discharging\ Capacity}{Charging\ Capacity} x 100\% \tag{1.3}$$

1.5.1.2 Cyclic voltammetry (CV)

The common technique for investigating the characteristic of the redox reaction is CV [39]. Via this method, the potential of a working electrode is ramped linearly starting from an initial point moving to the vertex point, then, turning back to the final point. The output from this action gives the rate of the redox reaction in current form, as shown in Fig. 1.1.

The influential parameters in this characterization include the potential range and scan rate (potential ramp rate). According to Fig. 1.1 b , E_{pa}, E_{pc}, I_{pa} and I_{pc} show their anodic peak potential, cathodic peak potential, anodic current and cathodic current, respectively. The inclined straight line represents the background current, which is the effect of capacitance.
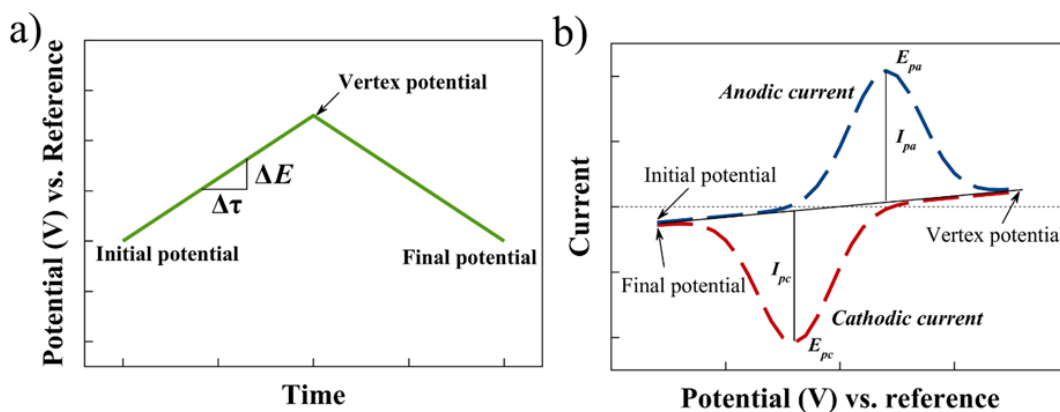
Figure 1.1 Schema of a) the input potential profile and b) the typical cyclic voltammogram of the reversible reaction

1.5.1.3 Electrochemical impedance spectroscopy (EIS)

EIS [40] is a technique used to analyze an electrochemical cell by applying both a frequency-varying sinusoidal potential (2-10 mV) and a static potential to the cell. The result of the output is the impedance spectra, which is comprised of the size of the impedance as well as the phase lag between input and output signal, at each frequency.

In battery applications, this technique is a powerful tool for interpreting the change in charge transfer characteristic upon the cycling. Impedance spectra can be fitted with some proposed model to retrieve parameters such as internal resistance, double-layer capacitance, charge transfer resistance and other associate parameters involved in the charge transport of the battery. The models used in impedance analysis are always constructed based on basic electrical components such as resistor, capacitor, and inductor, as seen in table 1.1
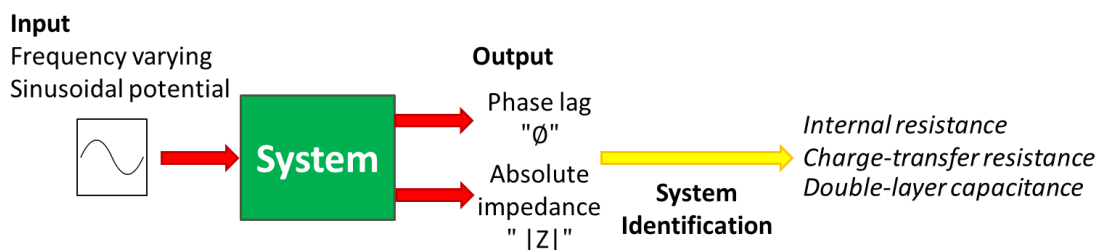
Figure 1.2 Schematic illustration of the electrochemical system analysis via EIS technique

Table 1.1 Basic equivalent circuit components for interpretation of impedance spectra

Description	Symbol	Relation
Resistance	R	$Z_R = R$
Capacitance	C	$Z_c = 1/j\omega C$
Constant-Phase Element	Q	$Z_Q = 1/[Y_0(j\omega)^n]$
Warburg	W	$Z_W = 1/[Y_0\sqrt{j\omega}]$

1.5.1.4 X-ray diffraction (XRD)

X-ray diffractometry [41] is a characterization technique used in analyzing the crystalline structure of materials. XRD works based on applying an X-ray beam to the sample at various angles; thus, the scattering reflected beam will be detected. The output is the relation between the intensity of the reflected beam and the angle. Such a result can be used to identify the allocation of the lattice structure, and the distance between inter-atoms.

1.5.1.5 Scanning electron microscope (SEM)

SEM [41] is a traditional characterization technique used to observe the morphology of materials. In battery application, SEM is used to investigate the morphology of synthesized material, the fabricated electrode, the cycled electrode etc.

1.5.2 Performance indicators in ZIB research

1.5.2.1 Anode [7, 26]

Cycling stability- is evaluated via time spent upon GCD cycling (h) whereby a Zn symmetrical cell can perform before failure.

Plating/stripping overpotential- is evaluated via measured voltage when the GCD cycling is performed on Zn symmetrical cell.

Plating/stripping coulombic efficiency **(%)** - is calculated via the capacity of Zn that the current collector/Zn cell can deliver divided by the capacity used to plate the Zn and multiplied by 100.

Morphology of plated Zn- is observed graphically i.e. whether there is dendrite formation or not.

1.5.2.2 Cathode or full cell [42, 43]

Discharge capacity- is evaluated, depending on the capacity that the full cell can deliver upon discharging.

Specific discharge capacity- is calculated via the discharge capacity divided by mass loading of the cathode material.

Coulombic efficiency- is calculated via the discharge capacity that the full cell can deliver divided by the capacity used to charge the cell and multiplied by 100.

Specific energy- is calculated via the discharge energy divided by mass loading of the cathode material.

Cyclability- is evaluated via how much capacity the battery can maintain after multiple times of repeated charging-discharging.

Rate capability- is evaluated via how much capacity the battery can maintain when the current is increased.

1.5.3 Criterion used for considering the electrolyte system

1.5.3.1 Ionic conductivity

Ionic conductivity [39] is a parameter that describes the motion of ions. The higher the ionic conductivity means that more charge can be transferred through the media. Thus, all battery systems prefer the electrolyte with high ionic conductivity.

1.5.3.2 Ion transference number

Ion transference number is a parameter that describes the movement of each single ion in comparison with bulk ion movement in the electrolyte [39]. Low transference number of the main charge-transfer species can lead to inferior performance of the battery [44]. For instance, the ZIB system prefers an electrolyte that provides a high Zn^{2+} transfer number.

1.5.3.3 Electrochemical stability window (ESW)

The electrochemical stability window [44] of an electrolyte is the potential range where the electrolyte is neither oxidized nor reduced. The stability window should cover the range of operation for both anode and cathode.

1.5.3.4 Thermal stability

During operation of a battery, generation of heat is unavoidable [45]. Heat is generated due to the current flowing through the battery, which has internal resistance. Such heat can result in the degradation or evaporation of the electrolyte [44]. Thus, the electrolyte having high thermal stability is preferable.

1.5.4 Desolvation penalty

The factor that can influence the performance of a battery is known as a desolvation penalty. Basically, desolvation penalty refers to energy loss due to the desolvation process, which can occur before plating of Zn^{2+} at the anode upon charging and before intercalation of Zn^{2+} during discharging. It is noted that such a loss strongly relates to the divalent nature of Zn^{2+} and the effect of nonaqueous media [1]. Kundu et al. [46] proved that there is a significant difference in terms of performance between a ZIB based on a vanadium oxide cathode having an aqueous electrolyte or a nonaqueous electrolyte; such a difference arises from the effect of the desolvation penalty.

1.5.5 Commercialization target in terms of performance
1.5.5.1 Target for anode

Ma et al. [7] demonstrated that the commercial target of a Zn anode is as follows: 1) plating/stripping coulombic efficiency of 100 % 2) capacity of 5 mAh/cm^2 with depth of discharge of 80 % 3) cycling stability of 2,000 cycles or cumulative plated capacity of 10 Ah/cm^2, and 4) fast rate availability at 2C or 10 mA/cm^2.

1.5.5.2 Target for full cell

ZIBs have been developed with the intent to replace LIBs. Although ZIBs cannot provide higher voltage than LIBs, at least, their energy density must be in the same range as LIBs, which provide 200 to 300 Wh/kg [47].

1.6 Schedule Plan

Table 1.2 Schedule plan for the research project.

List/Years	2019				2020				2021			
	Jan.-Mar.	Apr.-Jun.	Jul.-Sep.	Oct.-Dec.	Jan.-Mar.	Apr.-Jun.	Jul.-Sep.	Oct.-Dec.	Jan.-Mar.	Apr.-Jun.	Jul.-Sep.	Oct.-Dec.
Review of the literature	■	■	■	■	■	■	■	■	■	■	■	
Learning the battery fundamentals												
Electrochemical characterization section and Battery testing section	■	■	■	■	■	■	■	■				
Discussion of obtained data	■	■	■	■				■	■	■	■	
Repeat of experiment				■	■	■	■	■	■			
Conclusion of research project and preparation of complete dissertation									■	■	■	

CHAPTER 2

LITERATURE REVIEW

Review article: Stability enhancement of zinc-ion batteries using nonaqueous electrolytes

Author Names: Wathanyu Kao-ian[1], Ahmad Azmin Mohamad[2], Wei-Ren Liu[3], Rojana Pornprasertsuk[4,5,6,7], Siwaruk Siwamogsatham[8] and Soorathep Kheawhom[1,6,9,*]

Affiliation(s):
[1] Department of chemical engineering, Faculty of engineering, Chulalongkorn University, Bangkok 10330, Thailand
[2] School of Materials and Mineral Resources Engineering, Universiti Sains Malaysia, Nibong Tebal 14300, Malaysia
[3] Department of Chemical Engineering, R&D Center for Membrane Technology, Research Center for Circular Economy, Chung Yuan Christian University, Chung Li, Taiwan (R.O.C.)
[4] Department of Materials Science, Faculty of Science, Chulalongkorn University, Bangkok 10330, Thailand
[5] Center of Excellence in Petrochemical and Materials Technology, Chulalongkorn University, Bangkok 10330, Thailand
[6] Research Unit of Advanced Materials for Energy Storage, Chulalongkorn University, Bangkok 10330, Thailand
[7] Department of Materials Science and Technology, Nagaoka University of Technology, Niigata, 940-2188, Japan
[8] National Science and Technology Development Agency, Pathumthani 12120, Thailand
[9] Bio-Circular-Green-economy Technology & Engineering Center (BCGeTEC) Faculty of Engineering, Chulalongkorn University, Bangkok 10330, Thailand
* Corresponding authors: soorathep.k@chula.ac.th

(Manuscript)

Abstract

Owing to their high energy density and low cost, zinc-ion batteries (ZIBs) are gaining much in popularity. However, in practice, issues with hydrogen evolution, zinc dendrite development, corrosion, and passivation persist. Such drawbacks prove difficult to eradicate completely. To address these difficulties, many techniques have been proposed including inhibitor addition, artificial SEI, and Zn electrode modification. As a result, some researchers believe that using non-proton donor electrolytes or nonaqueous electrolytes can fundamentally solve these problems. Herein, the efforts to apply nonaqueous electrolytes such as organic electrolytes, room-temperature ionic liquids, and deep-eutectic solvents to ZIBs are described. An understanding of the mechanics of nonaqueous ZIBs (NZIBs) regarding zinc plating/stripping and intercalation/deintercalation are also highlighted. Importantly, research gaps are identified in order to pave the way for future study. In addition, an attempt is made to offer a viewpoint on critical topics as well as a benchmarking and enhancement of NZIB technologies.

Keywords: non-proton donor electrolyte; deep eutectic solvent; organic; ionic liquid; costs; zinc.

2.1 Introduction

At present, due to the enormous demand for efficient energy storage systems (ESSs), battery systems have become one of the hottest topics of research. Even though various systems using Li-ion batteries (LIBs), Ni-MH batteries, and Pb-acid batteries dominate the ESS market, research into alternative battery systems having additional critical attributes such as safety, sustainability, and eco-friendliness is still ongoing [37]. Multivalent metals i.e. zinc (Zn), calcium (Ca), and aluminum (Al), have received much attention for use as battery electrodes owing to their large volumetric capacity (Zn, Mg, Ca and Al: 5851, 3833, 2073, and 8046 mAh/cm^3, respectively) as well as their safety, resource availability and nontoxicity [1]. Nonetheless, most of them suffer from poor electrochemical reversibility caused by the passive layer formation at solid-liquid interfaces upon dissolution. This shortcoming limits their application in rechargeable

batteries. However, through the use of mild-acid electrolytes based on water, reversibility of metallic Zn electrodes can be achieved [2]. This type of electrolyte has been applied to intercalation type batteries based on Zn i.e. Zn-ion batteries (ZIBs). As proposed by Xu et al. (2011)[20], ZIBs utilizing manganese dioxide (MnO_2) and aqueous electrolytes have captured much attention worldwide.

The charge-storage mechanism of ZIBs rely on two processes: namely, the intercalation/deintercalation of Zn^{2+} at cathode i.e. $xZn^{2+}+2xe^-+\mathbf{H} \leftrightarrow Zn_x\mathbf{H}$**,** where $\mathbf{H}$ is host material, or also called intercalation material and the dissolution/deposition of Zn at anode e.g. $Zn \leftrightarrow Zn^{2+}+2e^-$, as illustrated in Fig. 2.1. Theoretically, Zn, as an electron source, can deliver a large capacity of 820 mAh/g via dissolution reaction. In most cases, the capacity of ZIBs have been limited by the lower capacity of host material [2, 44]. To date, several kinds of host material i.e. transition metal (Mn, V, Mo, Co and Ni) oxides, transition-metal sulfides, transition-metal phosphates and Prussian blue analogues have been undertaken in the study of ZIBs.
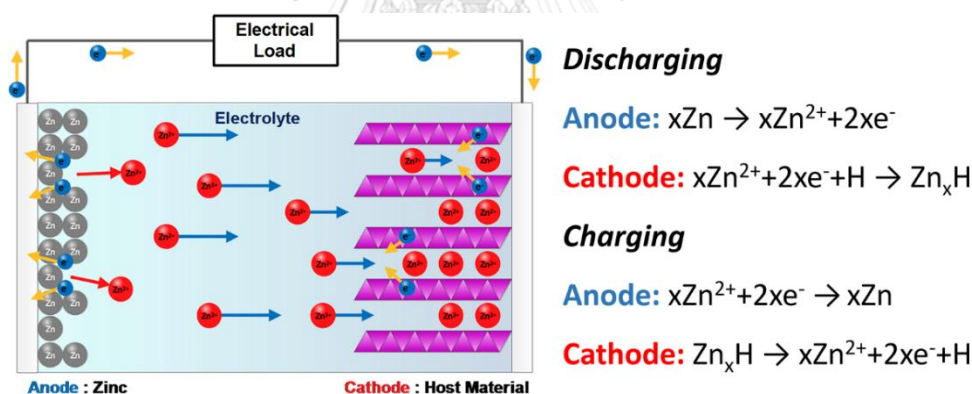
Figure 2.1 Schema of the charge-storage mechanisms of ZIBs

Water-based or aqueous electrolytes, because of their simplicity, non-toxicity and cheapness, are the most widely applied electrolytes in the study of ZIBs [48]. A variety of Zn salts viz. $ZnSO_4$, $ZnCl_2$, $Zn(ClO_4)_2$, $Zn(NO_3)_2$, $Zn(OTf)_2$, and $Zn(TFSI)_2$ have been used as a Zn^{2+} source[2]. Generally, electrolytes based on these mentioned salts are neutral or mild-acid, and result in a better surface quality of electrodeposited Zn at the anode and lower self-corrosion than that of alkaline electrolytes [49]. Aqueous ZIBs (AZIBs) show great potential as a battery system for the next generation. Several AZIBs recently proposed are seen to be very promising both in terms of performance

and cyclability viz. those having a specific capacity of more than 200 mAh/g (weight of host material) and achieving thousands of cycles of repeated charging/discharging [50-52]. However, up to now, no ZIBs have been recommended for the commercialized battery market [1]. This outcome points to the fact that there are a number of barriers, which limit their application in practice. According to the literature, the issues within the AZIBs system are as follows:

(I)   **Hydrogen evolution reaction (HER):** since water is a protic solvent, which can dissociate and provide proton (H^+), the contribution of H^+ upon charging is unavoidable. Thus, the H^+ reduction reaction ($2H^+(aq) + 2e^- \rightarrow H_2(g)$; $E^0 = 0.00$ V), also called HER, which generates H_2 gas, is considered to be a competitive reaction resulting in lower charging efficiency and excessive pressure within the battery package[31]. In practice, the high concentration of Zn salts, as well as the addition of some inhibitor can suppress HER[53].

(II) **Dendrite formation:** dendrite formation is not such a new issue in battery researches, especially in the system where metallic anodes are used. In AZIBs, Zn dendrites can be formed due to the uneven Zn-ion flux and electric field above the Zn anode, and can lead ZIBs to failure because of short-circuit[54, 55]Moreover, the operating conditions i.e. current density and areal capacity involves the evolution of Zn morphology and can further lead to the formation of dendritic structure in long-term cycling.

(III) **Corrosion of Zn:** self-corrosion of Zn is a different scenario from HER[53]. Due to the fact that aqueous mild-acid electrolytes always contain protons (H^+), and the H^+ ($2H^+(aq) + 2e^- \rightarrow H_2(g)$; $E^0 = 0.00$ V) has a higher standard potential than Zn^{2+} ($Zn^{2+}(aq) + 2e^- \rightarrow Zn(s)$; $E^0 = -0.76$ V), these H^+ can withdraw the electron from the metallic Zn. Accordingly, Zn is corroded and changed into Zn^{2+}, and pressure is built-up within the cell due to the H_2 produced. Such an outcome can occur at the rest (inactive) state of the battery.

(IV) **Passivation:** one of the issues concerned in AZIB development is the formation of a passive layer, which can reduce the performance of AZIBs in long-term cycling [44, 55]. In the most widely used electrolytes such as

aqueous $ZnSO_4$ electrolytes, zinc hydroxysulfate ($Zn_4(OH)_6SO_4 \cdot nH_2O$, ZHS) is found to be the main passivation species. ZHS can form well at the local position where H^+ is consumed due to the redox reaction i.e. HER and H^+ intercalation. At such a position, accumulation of hydroxide ion (OH^-) occurs, which can aggregate with Zn^{2+}, and SO_4^{2-} to form ZHS. Due to the reduction in the amount of active Zn^{2+} and SO_4^{2-} and the passivation effect of the formed layer, performance and charging efficiency of ZIBs are reduced tremendously.

Many approaches have been proposed to solve these issues e.g. the inhibitor addition, the artificial SEI, the modification of Zn electrode etc[14, 56]. However, some researchers believe that these approaches are only passive strategies; such problems cannot be entirely eliminated[30]. Three out of four issues mentioned in AZIB studies involve the existence of H^+. Accordingly, some researchers believe that these issues can be avoided fundamentally by employing non-proton donor electrolytes or nonaqueous electrolytes. Due to their wide-stability window, nonaqueous electrolytes such as organic electrolytes have been extensively used in LIBs for more than a decade [57, 58]. In recent years, several efforts have been initiated to apply nonaqueous electrolytes i.e. organic electrolytes, room-temperature ionic liquids (RTILs) and deep-eutectic solvents (DESs) to ZIBs. Most nonaqueous ZIB (NZIB) studies guarantee that the HER and Zn corrosion can be effectively inhibited [30, 31, 59, 60]. Besides, nonaqueous electrolytes are stable enough to be used with high voltage host materials i.e. Prussian blue analogue, cobalt oxide, polyanion-type phosphates and graphite, which are unstable in aqueous electrolytes [61-66]. However, NZIB technologies still lack categorization: a review, an overall picture, a benchmarking and finally, a target. In addition, it is immensely important to clarify what is missing in the researches in order to pave the way towards further development and to produce a clear understanding as regards the mechanisms of NZIB reactions. In this review, an attempt is made to provide a perspective with respect to the important issues and a benchmarking of NZIB technologies in order to make possible the enhancement of NZIBs.

2.2 Nonaqueous Electrolytes, Their Stability and Their Transport Properties

2.2.1 Organic electrolytes

The development of nonaqueous electrolytes for ZIBs originated from basic requirements viz. a wide operation window, noncorrosive and high ionic conductivity. Han et al. (2016) [35] first introduced the polar-aprotic solvents i.e. acetonitrile (AN), diglyme (G2), propylene carbonate (PC) and N,N-dimethylformamide (DMF), having Zn salts (i.e. $Zn(TFSI)_2$, $Zn(OTf)_2$, $Zn(PF_6)_2$ and $Zn(BF_4)_2$), as an electrolyte for Zn electrodeposition. AN-$Zn(TFSI)_2$ shows very impressive anodic stability (up to ~3.8 V vs Zn/Zn^{2+}), high ionic conductivity (28 mS/cm, 0.5 M), exhibiting ≥99% coulombic efficiency upon the deposition/dissolution of Zn. The superior ionic conductivity of AN-$Zn(TFSI)_2$, which is nearly on a par with mild-acid aqueous electrolyte, is due to the weaker coordination between AN and Zn^{2+} than in other solvents, and the highly dissociated anion such as $TFSI^-$. It is also suggested that the key to attain high electrochemical stability for organic electrolytes comprises 1) the choice of solvent and 2) the choice of anion species i.e. $TFSI^-$, OTf^- or others. Such findings have inspired other research groups to explore the new organic electrolyte systems that meet their requirements, such as triethyl phosphate (TEP), trimethyl phosphate (TMP), tetraethylene glycol dimethyl ether and dimethyl sulfoxide (DMSO), as shown in Table 2.1. A wider stability window means that higher voltage host material can be applied. Thus, organic electrolytes receive much attention among high voltage host materials e.g. Prussian blue analogue, graphite (anion intercalation) and the cobalt oxide developers.

Table 2.1 Organic electrolytes in ZIB application

Name	Applicable Zn salts	Compatible host materials	Anodic stability (V vs. Zn/Zn^{2+})	Conductivity range (S/cm)	Ref.
Acetonitrile (AN)	$Zn(TFSI)_2$ $Zn(OTf)_2$ $Zn(ClO_4)_2$ $Zn(PF_6)_2$ $Zn(BF_4)_2$	V_2O_5 $V_3O_7 \cdot H_2O$ $VOPO_4 \cdot 2H_2O$ PPy-$VOPO_4$ δ-MnO_2 $K_xNi[Fe(CN)_6]_{1-y}(H_2O)_z$ $ZnAl_xCo_{2-x}O_4$ $ZnNi_xMn_xCo_{2-2x}O_4$ Graphite*	2.2-3.8	~10^{-2}	[35, 46, 62, 63, 66-71]

Diglyme (G2)	$Zn(TFSI)_2$ $Zn(OTf)_2$ $Zn(PF_6)_2$	N/A	2.3-2.6	$\sim 10^{-3}$	[35]
Propylene carbonate (PC)	$Zn(TFSI)_2$ $Zn(OTf)_2$ $Zn(PF_6)_2$ $Zn(BF_4)_2$	Polyaniline (PANi)*	3.3-3.4	$\sim 10^{-3}$	[35, 72]
N,N-dimethylformamide (DMF)	$Zn(TFSI)_2$ $Zn(OTf)_2$ $Zn(PF_6)_2$ $Zn(BF_4)_2$	Phenanthrenequinone macrocyclic trimer (PQ-MCT)	2.5-2.9	$\sim 10^{-2}$	[35, 59]
Triethyl Phosphate (TEP)	$Zn(OTf)_2$	Copper hexacyanoferrate (KCuHCf)	2.25	$\sim 10^{-3}$	[61]
Trimethyl phosphate (TMP)	$Zn(OTf)_2$	$Na_3V_2(PO_4)_2O_2F$ (NVPOF) VS_2	2.8	$\sim 10^{-3}$	[64, 73]
Tetraethylene glycol dimethyl ether (TEGDME)	$(Zn(ClO_4)_2)$	$K_{1.6}Mn_{1.2}Fe(CN)_6$ (MnHCf)	N/A	N/A	[60]
Dimethyl Sulfoxide (DMSO)	$Zn(OTf)_2$	δ-MnO_2 α-MnO_2	2.0	$\sim 10^{-2}$	[31, 74]
Cosolvent propylene carbonate (PC)/ Triethyl Phosphate (TEP)	$Zn(OTf)_2$	Polytriphenylamine composite (PTPAn)	2.8	$\sim 10^{-3}$	[75]
Cosolvent dimethylamine (DMA)/ Tetrahydrofuran (THF)	$Zn(TFSI)_2$	N/A	N/A	$\sim 10^{-3}$	[76]

*Anion intercalation

2.2.2 Room-temperature ionic liquid (RTIL) and deep-eutectic solvent (DES) based electrolytes

RTIL is one class of a room-temperature molten salt, which is formed from a bulky organic cation i.e. imidazolium ion, pyridinium ion, ammonium ion and phosphonium ion and an organic or inorganic anion[77]. Such groups possess several beneficial basic features such as intrinsic ion conductivity, negligible volatility, high chemical/thermal stability and a wide electrochemical stability window. According to the literature, there are mainly two groups of conventional RTILs being studied in Zn electrodeposition and in Zn battery researches, classified by their cation species e.g. alkyl imidazolium and alkyl pyrrolidinium[78]. Simons et al. (2014)[79] indicated the possibility of using RTILs in Zn battery applications. 1-ethyl-3-methylimidazolium dicyanamide ([C2mim]dca) and 1-butyl-1-methylpyrrolidinium dicyanamide ([C4mpyrr]dca), containing 3 wt.% water and 9 mol% Zn dicyanamide (Zn(dca)2), have been examined

as an electrolyte for a Zn symmetrical (Zn/Zn) cell. Although, such work did not demonstrate very good reversibility of Zn at cycling, it proved that the deposition/dissolution of Zn from/into RTIL can exist. Lately, [C$_2$mim] based RTILs, having different anion species i.e. OTf$^-$, BF$_4$, OAc$^-$, have been found in several studies [30, 65, 80, 81]. RTILs have still not received much attention in Zn battery studies; yet they cannot be overlooked.

Another type of RTIL: namely, a deep eutectic solvent (DES), has been formed from a mixture of hydrogen bond donor (HBD) and hydrogen bond acceptor (HBA) i.e. quaternary ammonium salt, leading to a complex formation, and further resulting in the depression of the freezing point[32, 82]. Abbott et al. (2003)[83] first introduced DES. Due to the fact that DESs can contain a huge amount of multivalent cations and provide comparable properties as in traditional RTILs, DESs have become one of the interesting solvent choices for ZIBs[34, 84]. In addition, DESs have proved that they are more environmentally friendly than traditional RTILs. RTIL and DES electrolytes previously studied in Zn batteries are shown in Table 2.2.

Table 2.2 RTIL and DES electrolytes in ZIB application

Name	Applicable Zn salts	Compatible host materials	Anodic stability (V vs. Zn/Zn^{2+})	Conductivity (S/cm)	Ref.
[C$_2$mim]OTf	Zn(OTf)$_2$	Graphite	2.8	~10^{-3}	[65]
[C$_2$mim]BF$_4$	Zn(BF$_4$)$_2$	CoHCf	2.3-2.8	~10^{-2}	[30, 80]
[C$_2$mim]dca	Zn(dca)$_2$	N/A	1.95**	~10^{-2**}	[79, 85, 86]
[C$_4$mpyrr]TFSI	Zn(TFSI)$_2$	Expanded graphite (EG)	2.6-2.7	~10^{-3}	[77, 87-90]
[C$_4$mpyrr]dca	Zn(dca)$_2$	N/A	2.0*	~10^{-2**}	[79, 91]
ChCl/ Urea	ZnCl$_2$	δ-MnO$_2$	1.4 (vs. metallic Ag in ChCl/ Urea)	~10^{-3}	[8, 92]
Ace/Zn(TFSI)$_2$	Zn(TFSI)$_2$	V$_2$O$_5$	2.4	~10^{-4}	[34]
Ace/Zn(ClO$_4$)$_2$	Zn(ClO$_4$)$_2$	γ-MnO$_2$	N/A	~10^{-3}	[93]

Urea/LiTFSI/Zn(TFSI)$_2$	Zn(TFSI)$_2$	LiMn$_2$O$_4$	2.5*	~10^{-5} (neat)	[33]
				~10^{-3}*	

Measured from the solution containing water

2.3 Zn Anode Performance within Nonaqueous Electrolytes

2.3.1 Organic electrolytes

2.3.1.1 Cyanomethane-based electrolytes

The N-donor cyanomethane solvent such as AN has proven to be one of the most promising choices for NZIBs. Han et al. (2016)[35] highlighted the effect of solvent choice and the effect of Zn salt choice on the plating/stripping performance of Zn. Thus, it was found that the weak coordination of Zn^{2+} with AN and the low viscosity proved to be the origin of the high mobility of both cations and anions in AN, especially when combined with Zn(TFSI)$_2$. The electrodeposition of Zn on a platinum electrode using Zn(TFSI)$_2$-AN and Zn(OTf)$_2$-AN electrolyte provided significantly higher current density, better %CE (>99% upon -1.0 V to upper anodic limit point) and wider anodic limit (>3.5 V, Fig. 2.2a) than the use of other organic electrolytes i.e. G2, PC and DMF based on Zn(TFSI)$_2$ and Zn(OTf)$_2$ salts. Furthermore, the additional redox reaction trend was clearly observed when Zn(TFSI)$_2$-G2, Zn(TFSI)$_2$-PC, Zn(TFSI)$_2$-DMF, Zn(OTf)$_2$-G2, Zn(OTf)$_2$-PC, and Zn(OTf)$_2$-PC were used as electrolytes, whereas in the Zn(TFSI)$_2$-AN and Zn(OTf)$_2$-AN samples, there were no such reactions. Such outcomes were also found in the case of Zn(BF$_4$)$_2$-AN and Zn(PF$_6$)-AN. However, details in depth regarding these additional redox reactions, as well as the relationship between electrolyte properties and electrodeposition of Zn, are not given in this work. Chae et al. (2017)[70] claimed that 99.9% CE was achieved over the 20th cycle of CV test for the 0.5 M Zn(ClO$_4$)$_2$-AN electrolyte , whereas it was lower than 80% for the aqueous electrolyte (0.5 M Zn(ClO$_4$)$_2$, 0.1 M ZnSO$_4$ and 0.1 M ZnSO$_4$-water) at the same cycle number; however, Zn-dendrite was found to be unavoidable.

As regards practical performance, galvanostatic charge-discharge (GCD) cycling results are presented. Zhang et al. (2019)[66] stated that 99.5% CE upon GCD test (Ti/Zn cell) was achieved via 1 M Zn(TFSI)$_2$-AN electrolyte (Fig. 2.2b). In addition, Zn/Zn cell having this electrolyte displayed a very stable operation upon 1000

cycles of GCD cycling (0.5 h charge/0.5 h discharge, 0.5 mA/cm^2) 1C; the cycled electrode was found to be dendrite-free and ZnO passivation-free (Fig. 2.2c and d). Likewise, Etman et al. (2020)[67] noted that AN having 0.5 M of Zn(TFSI)$_2$ and Zn(OTf)$_2$ provided reversible Zn plating/stripping for over 500 cycles achieving 99.8% CE (current density: 1.25 to 10 mA/cm^2); additionally, the AN-Zn(OTf)$_2$ demonstrated better cyclability and slightly lower plating–stripping voltage (Fig. 2.2e). Based on both CV and GCD results, the reversible chemistry of Zn in the AN electrolyte is thus substantiated.
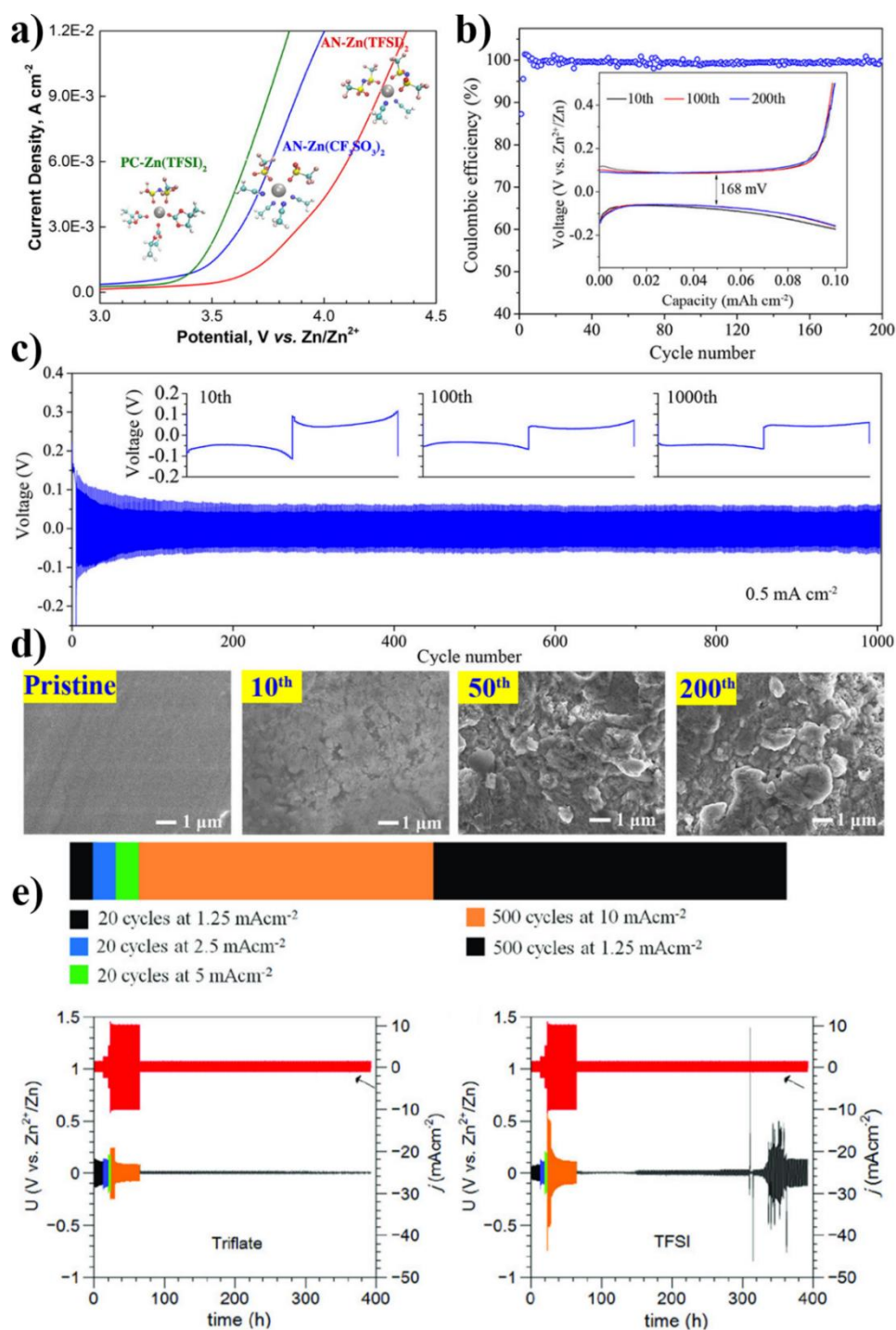
Figure 2.2 Electrochemical testing results using AN electrolyte: a) Anodic stability of AN and PC electrolytes. Reproduced with permission [35]. Copyright, 2016 American Chemical Society. b) Zn plating/stripping testing results using Zn/Ti cell at 0.2 mA/cm² (1 M Zn(TFSI)2-AN) c) GCD cycling results using Zn/Zn cell at 0.5 mA/cm2 (1 M Zn(TFSI)2-AN) d) SEM images of pristine Zn anode and Z anode after 10, 50, 200 cycles). Reproduced with permission [66]. Copyright, 2019 American

Chemical Society. e) GCD cycling results using Zn/Zn cell at 1.25, 2.5, 5, 10 mA/cm^2 of current density (0.5 M Zn(OTf)$_2$ vs. 0.5 M Zn(TFSI)$_2$ in AN). Reproduced from Reference [67] (CC BY 4.0).

2.3.1.2 Carbonate-based electrolytes

Over the past decade, due to their low-cost, high electrochemical stability and high Li salts solubility, organic carbonate solvents e.g. ethylene carbonate (EC), dimethyl carbonate (DMC), dimethyl carbonate (DEC), ethyl methyl carbonate (EMC) and propylene carbonate (PC) have been extensively used in LIBs [57, 94]. Guerfi et al. (2014) [72] revealed the feasibility of using PC as an electrolyte for Zn batteries. However, despite the fact that the Zn/PANi (polyaniline) cell having PC electrolyte (0.3 M Zn(TFSI)$_2$) possessed high cycling stability, high reversibility of the Zn in PC is observed. Han et al. (2016) [35] reported the use of PC electrolytes containing Zn(TFSI)$_2$, Zn(OTf)$_2$, and Zn(PF$_6$)$_2$ achieving ~100% of CE and higher than 3.3 V vs. Zn/Zn^{2+} of anodic limit (Fig. 2.3a). Furthermore, by applying the novel technique called "Zn CE protocols", as proposed by Ma et al. (2020) [95], the CE value was evaluated more precisely (Fig. 2.3b and c). It was found that the PC electrolyte (0.5 M Zn(TFSI)$_2$) possessed high CE values (99.1, 99.0, 98.8 and 98.0% at current densities of 0.25, 0.5, 1.0, 2.5 mA/cm^2, respectively) upon GCD Zn deposition/dissolution whereas the water-based electrolyte (1 m ZnSO$_4$ and 2 m Zn(OTf)$_2$) could not even pass the test and did not yield any result. In spite of its high CE, the PC electrolyte was not dendrite-free. Furthermore, according to Chen's work[96], the PC having Zn(ClO$_4$)$_2$ can be used in a Zn/V$_2$O$_5$ battery. The battery for the GCD test in this research was set up using a coin cell configuration having a Zn foil anode. It is seen that the full cell passed 5000 cycles of GCD test at high current (10 A/g of V$_2$O$_5$), indicating the high cyclability of the Zn anode within this electrolyte system.
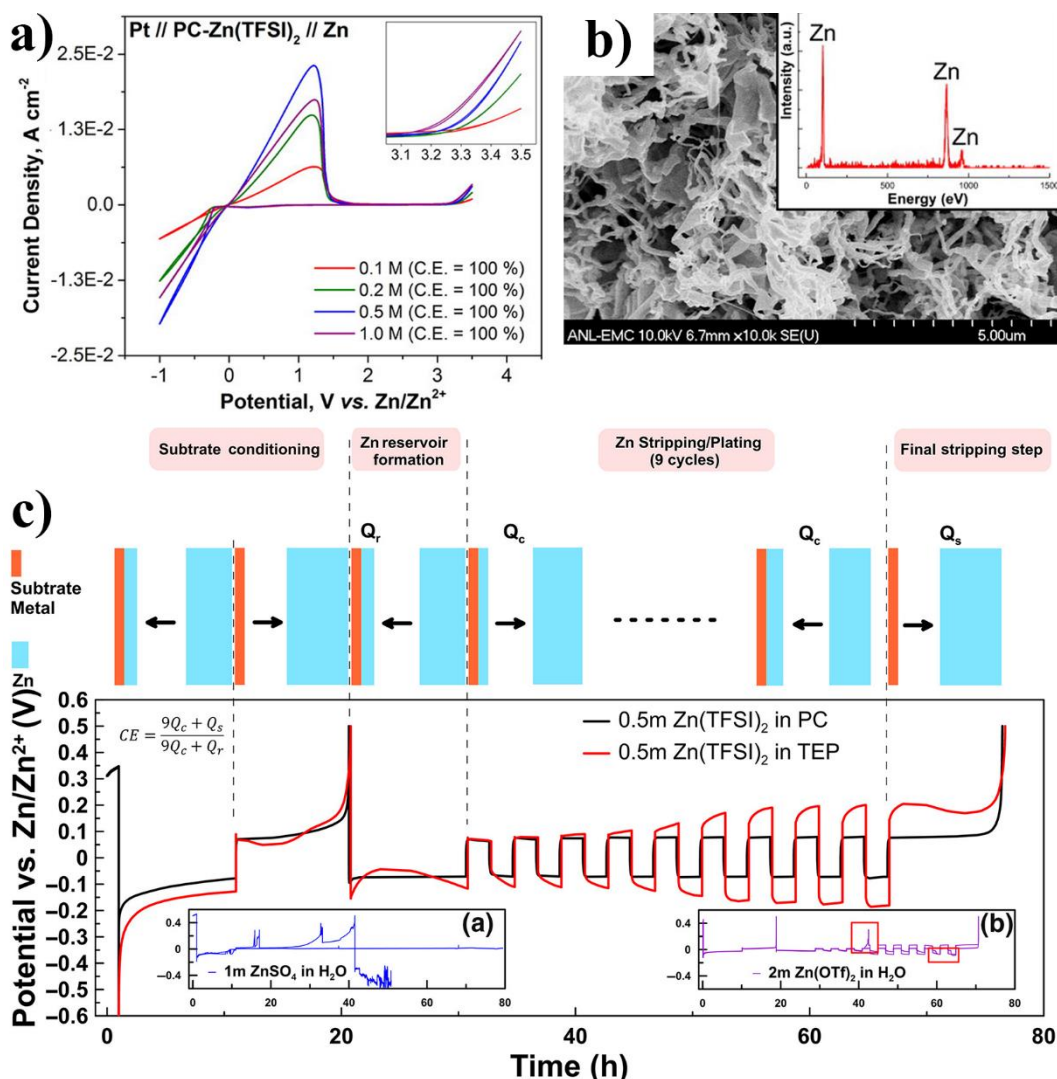
Figure 2.3 Electrochemical testing results using PC electrolyte: a) CV curves of Pt/Zn(TFSI)$_2$-PC/Zn cell with various concentration of Zn(TFSI)$_2$ (0.1-1.0 M). b) Deposited Zn on Pt electrode after deposition overnight (Zn(TFSI)$_2$-PC) Reproduced with permission [35]. Copyright, 2016 American Chemical Society. c) Implementation of Zn CE protocol to the 0.5 m Zn(TFSI)$_2$-PC, 0.5 m Zn(TFSI)$_2$-TEP, 1.0 m ZnSO$_4$-water and 2.0 m Zn(OTf)$_2$-water. Reproduced with permission [95].

2.3.1.3 Amide-based electrolytes

Several Zn salts i.e. Zn(TFSI)$_2$, Zn(OTf)$_2$, Zn(PF$_6$)$_2$ and Zn(BF$_4$)$_2$ can dissolve in DMF and provide Zn electrodeposition. Han et al. (2016) [35] reported that only 50.8% of CE was achieved via CV (-1.0 V to upper anodic limit point of ~2.8 V) test for the Zn(TFSI)$_2$-DMF electrolyte. The maximum concentration of Zn(OTf)$_2$ in DMF was found to be above 1.0 M. The 0.5 M electrolyte yielded the highest ionic conductivity

of 18.9 mS/cm and the widest anodic limit of 2.5 V vs Zn/Zn^{2+}. Wang et al. (2020) [59] found that Zn/Zn cell having 0.5 M Zn(OTf)$_2$-DMF can pass at least 2800 h of GCD test without failure (1.0 mA/cm^2 having a discharge/charge time of 1.0 h) (Fig. 2.4a). The high CE (>99.8%) was achieved via SS (stainless-steel)/Zn cell, thus implying the high reversibility chemistry of Zn within the Zn(OTf)$_2$-DMF electrolyte. Furthermore, via SEM, it was noted that no dendrite formation upon cycling occurred (Fig. 2.4b).
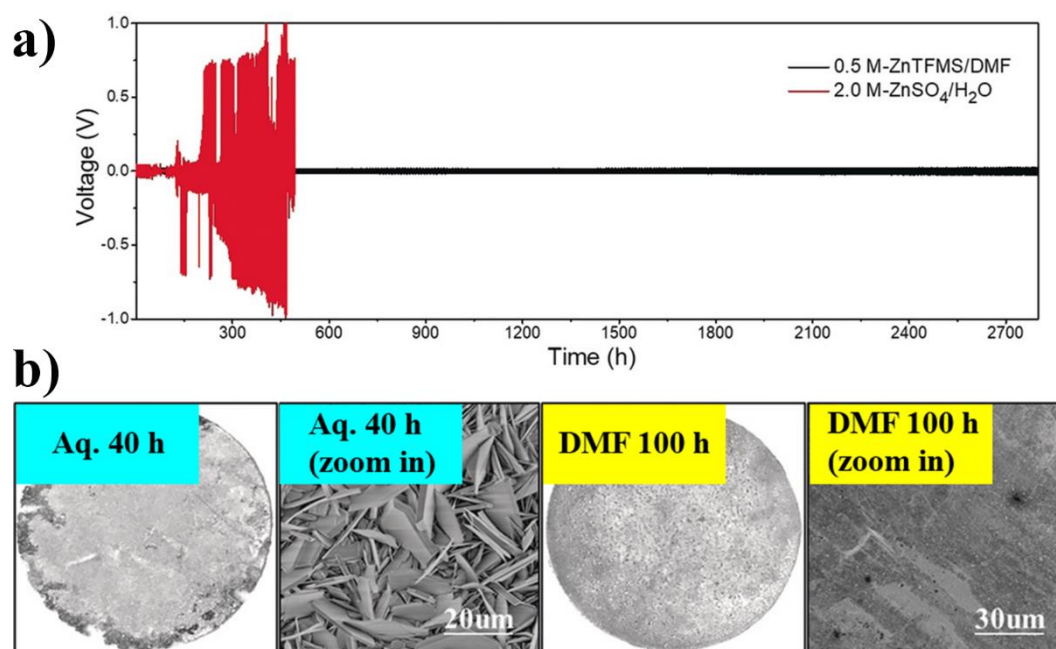
Figure 2.4 a) GCD cycling results of Zn/Zn cell having 0.5 M Zn(OTf)$_2$ (TFMS)-DMF and 2.0 M ZnSO$_4$-water electrolytes at 1.0 mA/cm^2 b) SEM images of cycled electrodes at 1.0 mA/cm^2 (light blue: 2.0 M ZnSO$_4$, 40 h cycling time) (yellow: 0.5 M Zn(OTf)$_2$-DMF, 100 h cycling time). Reproduced with permission [59].

2.3.1.4 Phosphate-based electrolytes

Two organic phosphate solvents being used in NZIBs include triethyl phosphate (TEP) and trimethyl phosphate (TMP) [61, 64]. Notably, the dry Zn(OTf)$_2$-TEP solution (0.5 M), as an electrolyte, is seen to provide stable cycling of 3000 h via Zn/Zn cell-GCD test at 0.1-0.5 mA/cm^2 of current density; the high CE (99.86% at 0.5 mA/cm^2) attained 1000 cycles via SS/Zn cell-GCD test, and wide anodic limit (2.25 V vs. Zn/Zn^{2+}) [61] (Fig. 2.5a and b). Besides, the Zn/Zn cell having this electrolyte can pass a long-period of cycling (10 h Charge/10 h Discharge, 0.5 mA/cm^2) and can last for 2000 h of total

time. The main morphology of Zn after cycling was found to be a cage-like porous network (Fig. 2.5c); this kind of Zn morphology came about by following an in-situ-formed molecular template, which was initiated by the $Zn_3(PO_4)_2$ layer between the Zn-electrolyte interface. However, the full cell, having dry TEP electrolyte and Prussian blue cathode, was not successful at cycling; there was an electrolyte modification by adding water into the electrolyte. It is noted that adding water into the solvent formed the 7:3-TEP:water by volume such that it enhanced the full cell cyclability tremendously. However, it also reduced the CE of Zn anode and the anodic limit of the electrolyte.

According to Naveed et al. (2019)[73], Zn can also be deposited through the TMP electrolyte that contained $Zn(OTf)_2$. The TMP electrolyte (0.5 M $Zn(OTf)_2$-TMP) provided not only a high CE value (99.57% via SS/Zn cell-GCD test), but also exhibited very stable plating/stripping via Zn/Zn cell-GCD test (>2,000 h at 0.1, 0.25, 0.5 and 1.0 mA/cm^2). In addition, 1000 h of rigorous GCD tests, having 10 h of charge/discharge time and 0.5-1 mA/cm^2 of current density, were achieved using this electrolyte. The main Zn morphology developed upon cycling was found to be a graphene-like porous structure, which allows for the high rate of Zn plating/stripping and the facile Zn^{2+} transport. This kind of Zn structure was formed by a mechanism similar to that of the TEP electrolyte.

However, Dong et al. (2020)[64] noted that $Zn(OTf)_2$-TMP electrolyte is unstable when operated at a high voltage. To overcome such an issue, a CV test was performed using a higher upper potential limit (-0.6 to 1.25 V vs. Zn/Zn^{2+}) than what it was in Naveed's research (-0.5 to 3.0 V vs. Zn/Zn^{2+}). As a result, deterioration of the current was observed in the 0.5 M $Zn(OTf)_2$-TMP sample after only a few cycles of the CV test (Fig. 2.5d). Dong et al. also indicated that this issue can be effectively suppressed using $NaClO_4$ as an electrolyte additive. Furthermore, at 0.5 M/1.0 M of $Zn(OTf)_2$/$NaClO_4$ concentration in TMP, both electrochemical stability and thermal stability can be tremendously enhanced (anodic limit: from 2.0 V to 2.8 V). The characterization e.g. FTIR and Raman results showed that the $NaClO_4$ addition resulted in reducing free solvents and free anions, thus leading the electrolyte to be more stable (Fig. 2.5e). In addition, the Zn/Zn cell passed 5000 h of total time via the GCD test at

0.5 mA/cm^2 of current density, and an average 99.8% CE was achieved over 1000 cycles (0.2 mA/cm^2, 1 h of deposition time) of Ti/Zn cell-GCD test (Fig. 2.5f). After cycling, no Zn dendrite was observed.
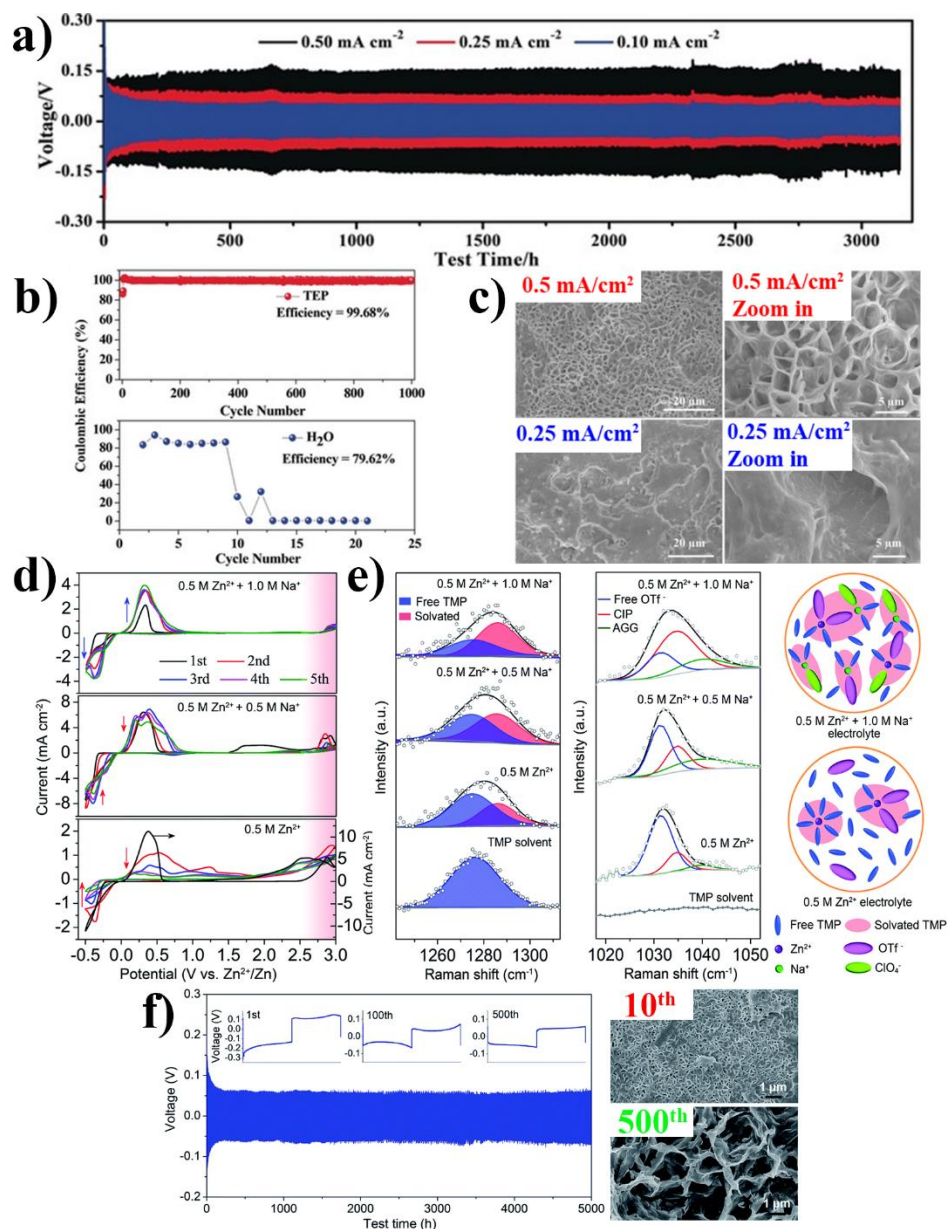
Figure 2.5 Phosphate-based electrolyte in action: a) GCD results of Zn/Zn cell having 0.5 M Zn(OTf)$_2$-TEP at 0.1-0.5 mA/cm^2 b) CE values obtained from GCD test (0.5 mA/cm^2) of SS/Zn cell (0.5 M Zn(OTf)$_2$ in TEP vs. in water) c) SEM images of cycled (2000 h) electrode using 0.5 and 0.25 mA/cm^2 current density. Reproduced with permission [61]. d) Cyclic voltammogram of Ti/Zn cell having 0.5 M Zn(OTf)$_2$/1.0 M NaClO$_4$-TMP, 0.5 M Zn(OTf)$_2$/0.5 M NaClO$_4$-TMP, and 0.5 M Zn(OTf)$_2$-TMP electrolytes, respectively, from top to bottom e) Raman spectra in the region from 1242 to 1313 cm^{-1} (left) and from 1020 to 1050 cm^{-1} (middle), and schematic simulates the solvated

species in electrolyte f) GCD results of Zn/Zn cell having 0.5 M $Zn(OTf)_2$/1.0 M $NaClO_4$-TMP at 0.5 mA/cm^2 and SEM image of cycled electrode after 10th and 500th cycles. Reproduced with permission [64].

2.3.1.5 Ether-based electrolytes

The ether-based solvent such as G2, which contains $Zn(TFSI)_2$, $Zn(OTf)_2$, and $Zn(PF_6)_2$, can provide Zn deposition/dissolution. However, according to Han's work[35], it was found that there was a relatively large trend of additional redox reaction as contributed by the Zn plating/stripping CV test. Only one couple, $Zn(PF_6)_2$-G2 reported 100% CE via the CV test. As yet, to the best of our knowledge, no more reports regarding the use of G2 as an electrolyte for ZIBs have been found.

Tetraethylene glycol dimethyl ether (TEGDME) is viewed as one of the possible solvent choices. However, little is known about TEGDME as an electrolyte for NZIB or for Zn electrodeposition. One example that has been demonstrated is Li's work[60] whereby metallic Zn foil was used as an anode and $K_{1.6}Mn_{1.2}Fe(CN)_6$ was used as a cathode. It was found that the battery can pass 8,500 cycles of full cell-GCD at 200 mA/g of current density: this outcome indicated the high reversibility of Zn in the TEGDME electrolyte. In addition, the cycled Zn electrode was found to be smooth and dendrite-free.

2.3.1.6 Sulfoxide-based electrolytes

One of the possible solvent choices for a Zn battery electrolyte is dimethyl Sulfoxide (DMSO), which possesses several promising properties i.e. high dielectric constant (46.45), high donor number, wide electrochemical window (-2.9 to +1.5 V vs. SCE) and low toxicity. Kao-ian et al. (2021)[31] demonstrated the application of DMSO in NZIB. By conducting CV experiments, it was found that Zn can plate/strip from/into the $Zn(OTf)_2$-DMSO electrolyte . In spite of the low CE achieved through the CV test, the SS/Zn cell having the DMSO electrolyte (0.25 M $Zn(OTf)_2$) exhibited 99.6% according to the GCD cycling test. Furthermore, rate performance proved to be satisfactory via the Zn/Zn cell-GCD test (61, 63, 73, and 93 mV of Zn plating overpotential at 0.1, 0.2, 0.5 and 1.0 mA/cm^2 of current density, respectively). Although

only 100 h of total time was recorded via the Zn/Zn cell-GCD test, the fact that the full cell (Zn/MnO$_2$) cycled up to 1,000 cycles reflects the high reversibility of Zn anode in the DMSO electrolyte.

2.3.1.7 Mixed-solvent electrolyte

Mixing is one approach that can be made in order to enhance the properties of an electrolyte. For example, it is acknowledged that PC has a high dielectric constant, but low Zn(OTf)$_2$ solubility. Qiu et al. (2021) [75] noted that adding a high O-donor solvent such as TEP into a PC electrolyte can increase its Zn(OTf)$_2$ solubility limit (0.08 to >0.5 M), anodic limit (2.42 to 2.8 V) and ionic conductivity (1.2 to max. 9.9 mS/cm for TEP:PC=1:2 sample), and decrease flammability (Fig. 2.6a and c). In addition, it is seen that via the CV test, the TEP/PC electrolyte provided a higher Zn plating/stripping current density than that of the pure TEP and pure PC electrolytes; the TEP:PC=1:2 was found to be the best ratio (Fig. 2.6b). Hence, the Zn/Zn cell passed 2600 h of GCD at 0.5 mA/cm^2 of current density and 0.5 mAh/cm^2 of tested capacity having 0.25 V of voltage polarization. As for SS/Zn cell-GCD test, 97.7% and 99.7% was achieved at current density 0.1 mA/cm^2 and 5 mA /cm^2, respectively. A porous inter-connected Zn was found to be the main Zn morphology formed upon the cycling.

Tetrahydrofuran (THF) is an ether solvent, which has low Zn(TFSI)$_2$ solubility. Nevertheless, it is noted by Genevieve et al. (2021) that adding dimethylamine (DMA) as a cosolvent can increase the Zn(TFSI)$_2$ solubility[76]. Thus, Zn(TFSI)$_2$ solubility, ionic conductivity and deposition/dissolution kinetics of Zn were enhanced (Fig. 2.6d); this improvement occurred as a consequence of the redissociation mechanism. By using 0.3 M Zn(TFSI)$_2$ 2.0 M DMA in THF as an electrolyte, maximum CE (97%) was achieved via the CV test. It is observed that Zn morphology depends on the amount of DMA used (Fig. 2.6e). Platelet and granular structure of Zn was found when 2.0 and 0.5M DMA electrolytes were used: higher DMA content results in higher crystallinity of deposited Zn.

The promising features of the TMP electrolyte can further be enhanced using the cosolvent DMC[73]. When DMC is mixed with TMP in 1:1 volumetric ratio, 0.5 M Zn(OTf)$_2$-TMP:DMC (1:1) is formed. Thus, it is seen that in comparison with the

0.5 M $Zn(OTf)_2$-TMP viscosity was reduced, and ionic conductivity increased (4.58 to 4.90 mS/cm). Furthermore, such an approach can enhance both cycling stability (twice longer than the pristine electrolyte) and rate performance. Besides, the TMP electrolyte can be improved by adding DMF (1:1 by volume), which gives similar results compared to the DMC addition.
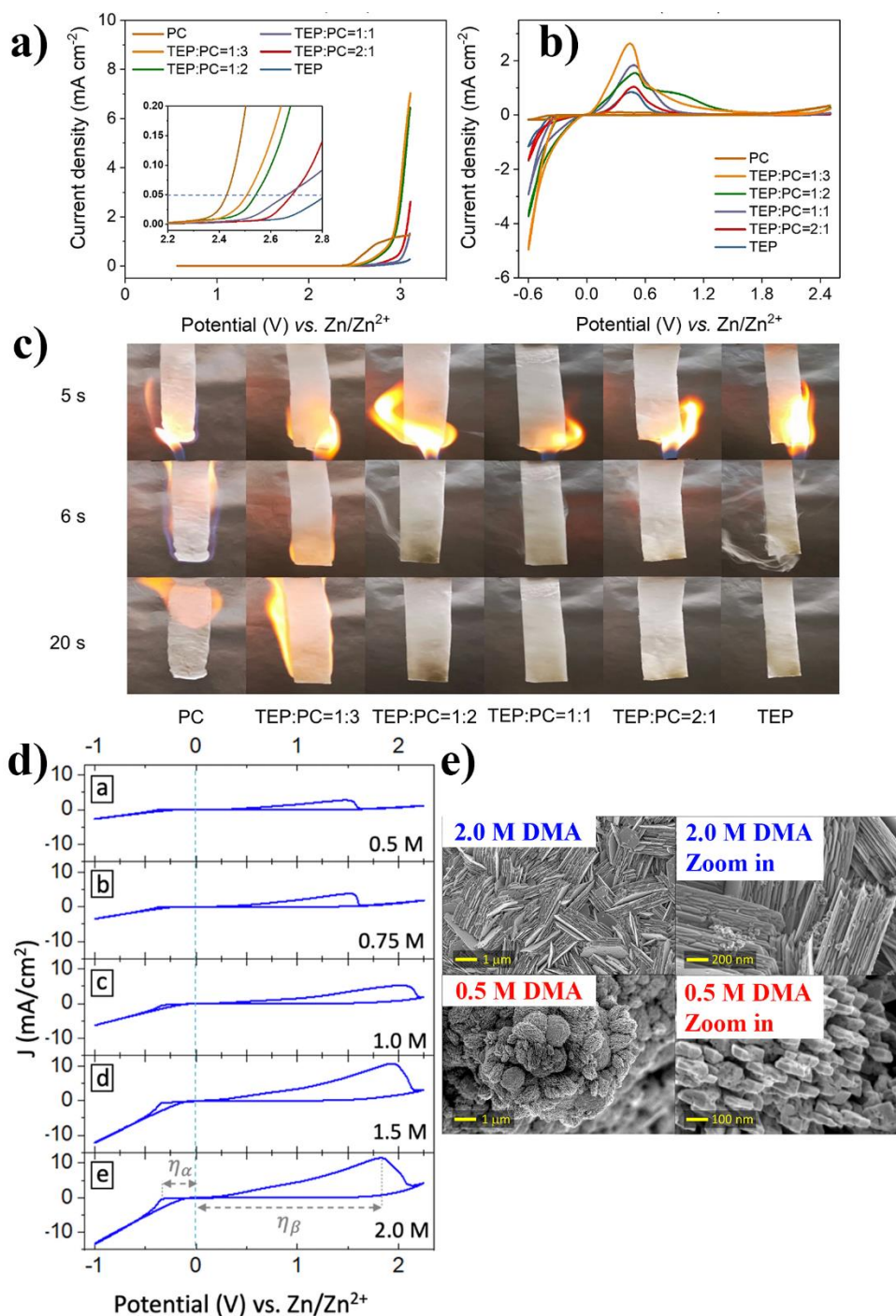
Figure 2.6 a) Stability window of PC, TEP and TEP:PC (1:3, 1:2, 1:1 and 2:1) b) Cyclic voltammograms (1 mV/s) of PC, TEP and TEP:PC (1:3, 1:2, 1:1 and 2:1) which contained $Zn(OTf)_2$ c) Flammability test for PC, TEP and TEP:PC (1:3, 1:2, 1:1 and 2:1). Reproduced with permission [75]. d) Cyclic voltammograms (50 mV/s) of 0.2 M $Zn(TFSI)_2$-THF at different concentrations of DMA (0.5-2.0 M) e) SEM images of plated Zn from 0.2 M $Zn(TFSI)_2$-THF with different concentration of DMA (0.5-2.0 M). Reproduced from Reference [76] (CC BY 4.0).

2.3.2 RTILs and DESs

2.3.2.1 Alkyl imidazolium electrolytes

Alkyl imidazolium i.e. 1-methylimidazolium (mim), 1-ethyl-3-methylimidazolium (C_2mim), 1-ethylimidazolium (eim) is a five-membered N-contained heterocyclic molecule, which carries one positive charge; generally, it appears in the form of salts having one anion e.g. Cl^-, OAc^-, dca, BF_4^-, $TFSI^-$, OTf^- and others. Alkyl Imidazolium salts, which have a melting point lower than room-temperature are classified as RTILs. Due to their heterocyclic structure, imidazolium ILs are found to be thermally and electrochemically stable [78]. According to the literature, several alkyl imidazolium ILs can dissolve Zn salt, having the same anion species i.e. $Zn(OTf)_2$ in [C_2mim]OTf and can provide Zn deposition.

One of the most applied alkyl imidazolium ILs in Zn battery researches is C_2mim. Simons et al. (2012)[79] stated that wet (3 wt.% water) [C_2mim] dca containing $Zn(dca)_2$ is more effective at Zn/Zn cell-GCD cycling than that of the alkyl pyrrolidinium such as [C_4mpyrr]. 95 cycles i.e. 375 h of total cycling time at 0.1 mA/cm^2 current density were achieved using the wet [C_2mim] dca electrolyte whereas the wet [C_4mpyrr] dca sample passed only 15 cycles (0.05 mA/cm^2, ~60 h total). Via CV test of Zn stripping/plating, the wet [C_2mim] dca sample provided superior CE (85%) than that of the wet [C_4mpyrr] dca sample (37%). It was also noted that the Zn deposition within the wet [C_4mpyrr] dca electrolyte required a high overpotential of -0.84 vs. Zn/Zn^{2+}, which is much greater than what it was in the wet [C_2mim] dca electrolyte (-0.23 V vs. Zn/Zn^{2+}). However, the dendrite formation of Zn, which led to the failure at cycling was observed in the wet [C_2mim] dca sample after 375 h of the GCD test. Consequently, in spite of the superior testing results of [C_2mim] dca than that of [C_4mpyrr] dca, the [C_2mim] dca was still not fit enough for use in the practical NZIB. Nevertheless, such an outcome proved that the [C_2mim] ILs were able to provide the Zn recharge.

Another [C_2mim] IL founded in Zn battery application is [C_2mim]OTf [65]. The [C_2mim]OTf containing 0.2 M of $Zn(OTf)_2$ demonstrated 7.3 ms/cm of ionic conductivity, and 2.8 V vs. Zn/Zn^{2+}. However, when $Zn(OTf)_2$ concentration increased, ionic conductivity diminished due to the increase in viscosity. Moreover, the Cu/Zn/Zn

cell-CV test, Cu/Zn cell-GCD test, XRD and EDS reflected that via this electrolyte, Zn deposition/dissolution still existed (Fig. 2.7a-c). Plating and stripping overpotential at 0.4 mA/cm^2 upon GCD was found to be -0.3 V and 0.3 V, respectively. According to the SEM result (Fig. 2.7d) of the cycled electrode (GCD: 10 cycles, Chg time 0.5 h), there was no sign of dendrite formation. However, the long-term cycling stability of Zn in this electrolyte was not evident.

$Zn(BF_4)_2$-[C2mim] BF_4 is one of the most fascinating RTIL electrolytes [30]. Due to its high $Zn(BF_4)_2$ solubility, which is far superior to most of RTILs (at least 2 M), the [C2mim]BF_4 possessed high ionic conductivity (16.9 mS/cm). In addition, it also has a wide anodic limit (2.8 V vs. Zn/Zn^{2+}). As noted by Ma et al. (2020) [30], the Zn/Zn cell having 2 M $Zn(BF_4)_2$-[C2mim] passed 1500 h (3,000 cycles) of GCD test at 2 mA/cm^2 of current density without dendrite formation (Fig. 2.7e). 99.36% CE was achieved via SS/Zn cell-GCD test at current density of 0.5 mA/cm^2 and charging capacity of 0.5 mAh/cm^2. Further, by varying the current density, the CE still attained 98.5% even at very low or very high current densities (0.2 to 10 mA/cm^2) (Fig. 2.7f); this reflected the wide operating range of the Zn anode in the $Zn(BF_4)_2$-[C2mim] electrolyte.

จุฬาลงกรณ์มหาวิทยาลัย

CHULALONGKORN UNIVERSITY
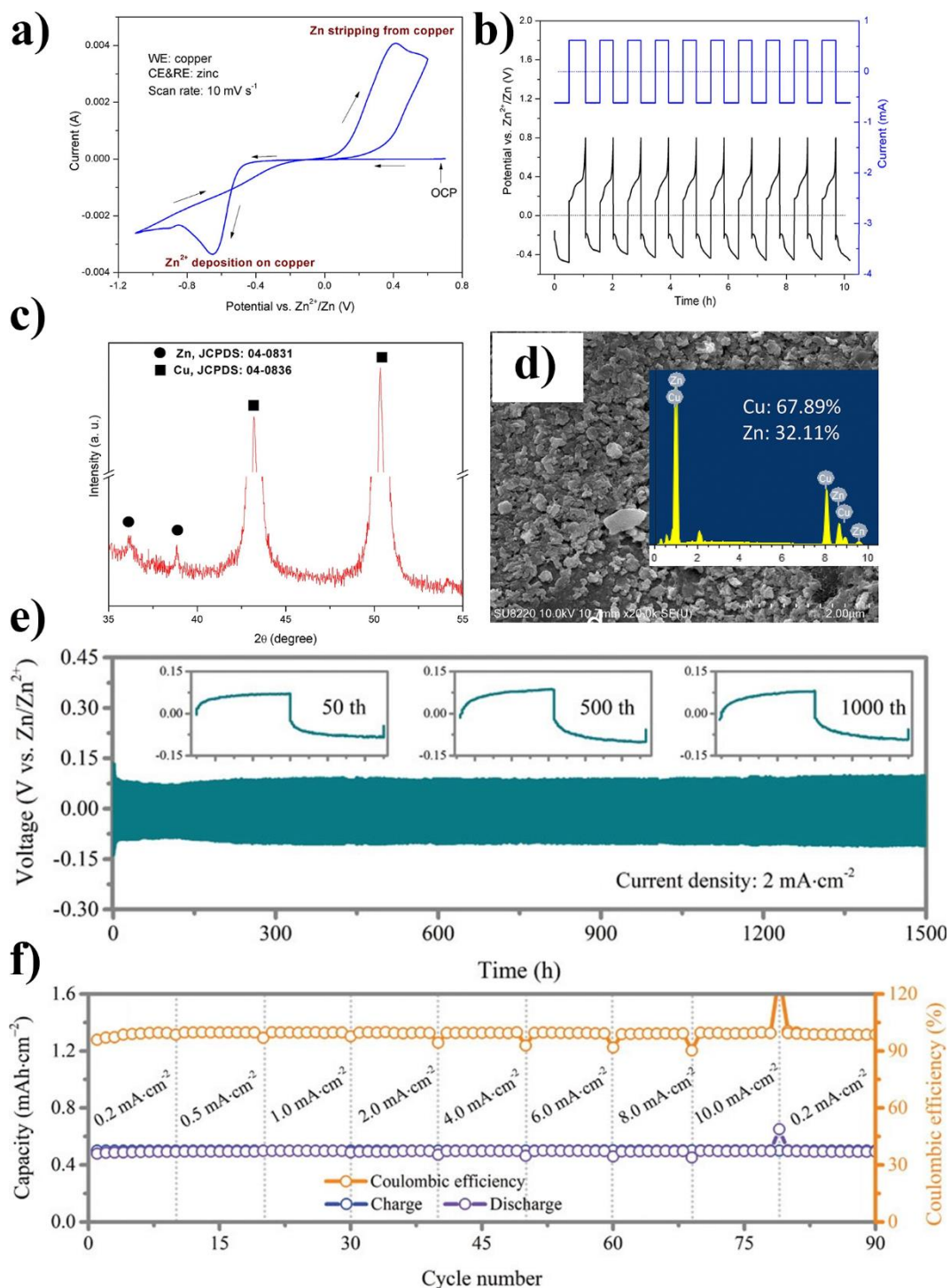
Figure 2.7 a)-d) Anode testing results for 0.2 M of Zn(OTf)$_2$-[C$_2$mim]OTf electrolyte: a) CV curves of Cu/Zn cell at scan rate 10 mV/s b) GCD cycling results of Cu/Zn cell (10 cycles) c) XRD results of cycled electrode d) SEM-EDS result of cycled electrode. Reproduced with permission [65]. e)-f) Anode testing results for 2.0 M Zn(BF$_4$)$_2$-[C2mim]BF$_4$: e) GCD cycling results of Zn/Zn cell at 2 mA/cm^2 f) GCD cycling results of SS/Zn cell upon current density range of 0.2-10.0 mA/cm^2. Reproduced with permission [30].

2.3.2.2 Alkyl pyrrolidinium electrolytes

Alkyl pyrrolidinium ILs are other heterocycles, which have been extensively studied among LIB developers; this is due to several attractive properties such as high reductive stability, low vapor pressure and incombustibility[97]. Data regarding the Zn electrodeposition and the Zn batteries of these ILs, however, are still limited. Deng et al. (2011)[98] was first to apply [C4mpyrr]dca, one of the alkyl pyrrolidinium ILs, in Zn deposition study. The study affirmed that a smooth Zn surface can be produced via the $ZnCl_2$-[C4mpyrr]dca electrolyte. Subsequently, Simon et al. (2014)[79] investigated the [C4mpyrr]dca containing $Zn(dca)_2$. Thus, an attempt at cycling the Zn/Zn cell using 9 mol% $Zn(dca)_2$-/ 3 wt.% water-[C4mpyrr]dca electrolyte was carried out at a current density of 0.05 mA/cm^2 and a charge/discharge time of 2 h. However, only 15 cycles and a large voltage hysteresis (>200 mV) were achieved. Such a poor outcome was thought to be due to short-circuit.

Another alkyl pyrrolidinium IL based electrolyte found in the literature was [C4mpyrr]TFSI. Ji et al. (2020)[87] stated that the [C4mpyrr]TFSI can be used as an electrolyte in a Zn/expanded-graphite dual-ion battery. Both 1 M of $Zn(TFSI)_2$ and 2 wt.% of ethylene sulfite were added into the [C4mpyrr]TFSI to form the electrolyte solution. The mixture had an anodic limit of about 2.6 V; 86% capacity retention and 500 cycles of full cell-GCD (at 2C) were achieved. According to the characterization results of before/after cycling Zn anode, it was found that there was a trace of SEI that formed upon the GCD cycling. The main component of SEI was found to be C, S, F, and O, which attributed to the decomposition of the electrolyte. It is noted that the formed SEI had a role in protecting the electrode from degradation. Besides, the cycled Zn electrode was found to be dense and smooth, and no dendrite detected.

2.3.2.3 Choline-based DES electrolytes

Quaternary ammonium salt, namely, choline chloride (ChCl) is the basic ingredient of choline-based DES. To form the eutectic solvent, ChCl, as an HBA, was mixed with HBD such as urea, ethylene glycol (EG), glycerol, acetamide (Ace) and other HBDs at a specific ratio. The Zn plating/stripping was made using Zn salts (e.g. $ZnCl_2$) and contained DES[84]. The ChCl DES such as ChCl:EG, having 1:2 mole ratio (12CE or

Ethaline 200) and containing $ZnCl_2$, has gained much attention for use as an electrolyte in anti-corrosive coating studies [99-101]. It was found that nano-sized, smooth and less corrosive Zn was achieved using a 12CE electrolyte [102].

In the literature, it is acknowledged that 12CE electrolytes have the following features: high ionic conductivity, low viscosity, stability in air and moisture and a wide-electrochemical window[84]. However, Vieira et al. (2014) found that the Zn deposition process within 12CE electrolytes involved a Zn-ion complex formation step, which provided H_2 as a byproduct [103]. The choice of using 12CE proved unsatisfactory.

Another choline-based DES found in the literature is ChCl:urea having 1:2 molar ratio (12CU). The 12CU possesses the ability to dissolve a variety of metal oxides e.g. ZnO, CuO, MnO_2 etc. Using 12CU containing ZnO or $ZnCl_2$, Zn deposition could be made [102]. According to Yang' research[104], although ZnO-12CU can provide smooth and dense deposited Zn, it is seen that the Zn deposition using ZnO-12CU required high temperature (10-100 $^{\circ}$C) to increase the solubility of ZnO in 12CU; thus, the ZnO-12CU couple did not suit the Zn battery application. However, the 12CU having $ZnCl_2$ was able to deposit Zn at room-temperature. According to Kao-ian et al. (2019)[8], when 0.3 M $ZnCl_2$-12CU electrolyte was used, 98% of charge-transfer ratio, calculated from the area under the CV curve (± 0.5 V vs. OCV.), was obtained, indicating high reversible Zn plating/stripping (Fig. 2.8a). Yet, large plating/stripping overpotential was found upon the rate performance test (57, 89, 146 and 200 mV at 0.1, 0.2, 0.5 and 1.0 mA/cm^2, respectively). Only 40 h of total time on the Zn/Zn cell-GCD test was spent on this work (Fig. 2.8b). The morphology of Zn found after the Zn/Zn cell-GCD cycling was a small sphere-grain ($\sim$100 nm) (Fig. 2.8c). It was noted by Abbott et al. (2011) [99] that due to the fast nucleation of Zn in the $ZnCl_2$-12CU electrolyte, the Zn grains, which evolved on the deposited layer upon deposition were small.
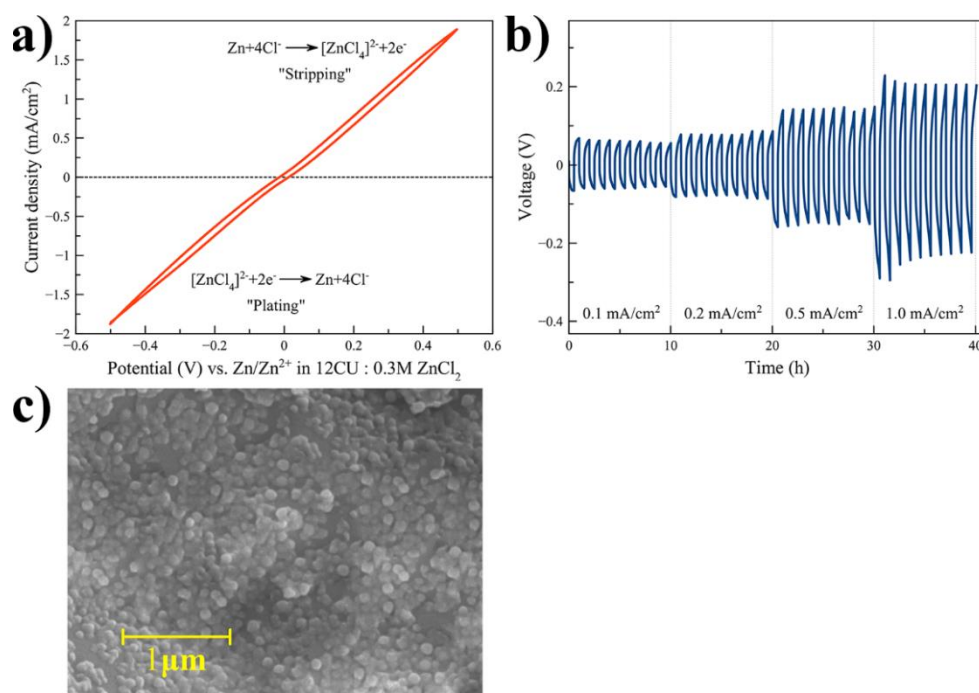
Figure 2.8 Electrochemical performance of Zn anode within 0.3 M ZnCl₂-12CU electrolyte: a) CV curves of Zn/Zn cell at 10 mV/s (±0.5 V vs. OCP.) b) GCD cycling results of Zn/Zn cell at various current densities (0.1-1.0 mA/cm²) c) SEM image of the cycled Zn anode. Reproduced from Reference [8] (CC BY 4.0).

2.3.2.4 Acetamide-based DES electrolytes

An acetamide (Ace) can form eutectic mixtures with some Zn salts, resulting in HBAs such as $Zn(ClO_4)_2$, $Zn(TFSI)_2$ and $ZnCl_2$. Venkata Narayanan et al. (2010) [93] reported the use of $Zn(ClO_4)_2$:Ace as an electrolyte in Zn/MnO_2 battery. Thus, it was found that due to the lower fraction of ion pairs of the 0.2 $Zn(ClO_4)_2$: 0.8 Ace (by mole) mixture than others, as observed via FT-IR and FT-Raman, the 0.2 $Zn(ClO_4)_2$: 0.8 Ace mixture yielded the highest ionic conductivity (6.3 mS/cm), and this fraction was chosen to conduct further tests. By conducting CV on the Zn/Zn cell using 0.2 $Zn(ClO_4)_2$: 0.8, it was noted that Zn plating/stripping was found to exist, and was highly reversible.

Qiu et al. (2019)[34] introduced one of the most promising DES electrolytes for Zn batteries viz. $Zn(TFSI)_2$:Ace (1:4 by mole, called ZES). Subsequently, the electrolyte structure analysis revealed that the solvate structure of Zn in ZES was $[ZnTFSI_m(Ace)_n]^{(2-m)+}$ (where m=1-2, n=1-3) (Fig. 2.9a). This solvate structure provided the formation of anion-derived SEI on the Zn anode upon the plating. It is

acknowledged that SEI played an important role in controlling the shape of deposited Zn (Fig. 2.9b) viz. preventing dendrite and minimizing self-discharge, and finally featuring the high ionic conductivity (2.36×10^{-6} S/cm). Via Zn plating/stripping CV tests, an average CE of 99.7% over 200 cycles was achieved. Furthermore, the Zn/Zn cell steadily cycled up to 2,000 cycles of GCD cycling (at 0.05 mAh/cm^2 of testing capacity and 0.1 mA/cm^2 of current density) (Fig. 2.9c). Upon applying a higher current (1 mA/cm^2) and a capacity of (0.5 mAh/cm^2) GCD cycling, the Zn/Zn cell operated for at least 100 h. In addition, it is noted that SEI can maintain the uniform and dendrite-free Zn deposition even at the higher capacity (2.5-5 mAh/cm^2).
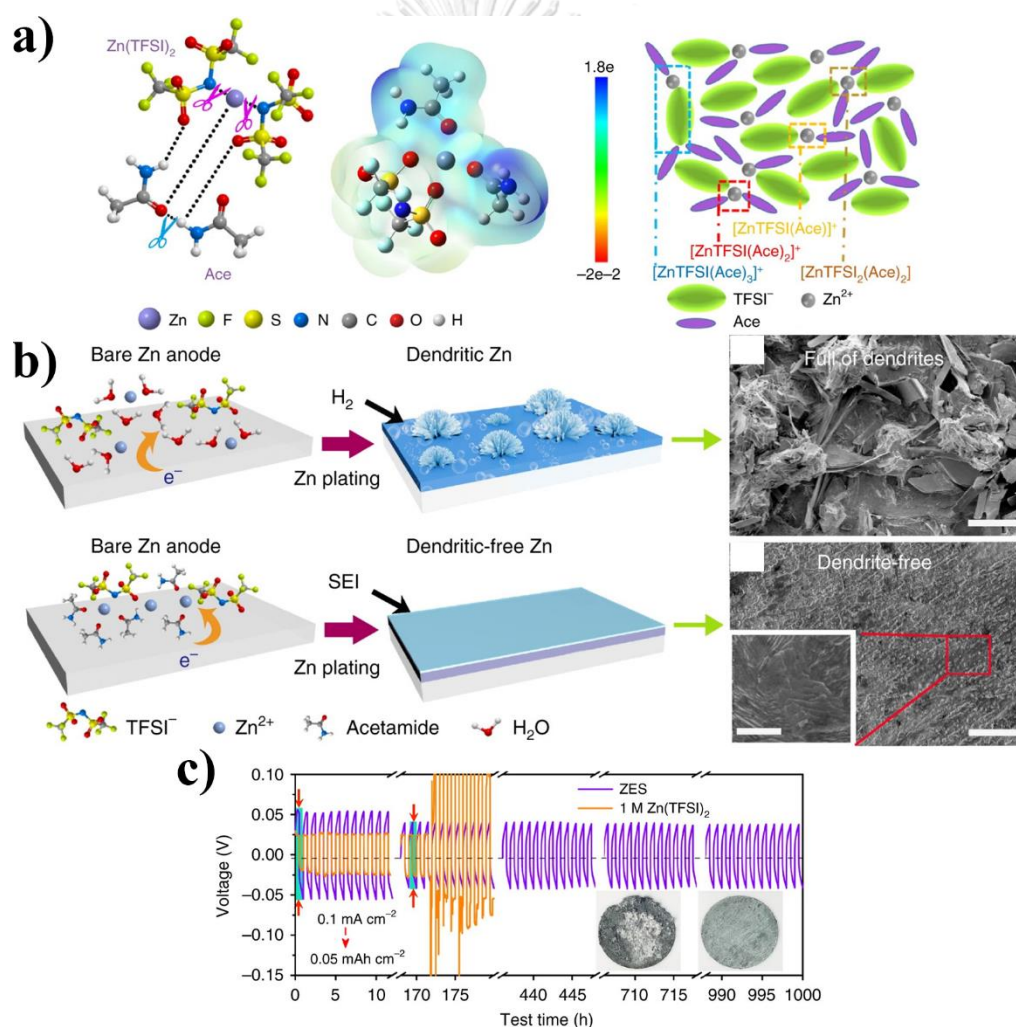
Figure 2.9 a) Schema of the solvated structure of Zn(TFSI)$_2$ and Ace within ZES obtained base on DFT calculation b) Schema of the comparison between water-based electrolyte (1 M Zn(TFSI)$_2$) and ZES upon Zn deposition, and SEM images of the obtained Zn (0.5 mAh/cm^2, 1.0 mA/cm^2) c) GCD cycling results of Zn/Zn cell having ZES electrolyte. Reproduced from Reference [34] (CC BY 4.0).

2.3.2.5 Other eutectic solvent electrolytes

As reported by Zhao et al. (2019)[33], Zn plating/stripping can also be made via LiTFSI:urea DES electrolyte having $Zn(TFSI)_2$. In this research, the fraction of LiTFSI, $Zn(TFSI)_2$, urea and water was optimized to achieve the best electrolyte formula in terms of physicochemical properties. The 1:0.05:3.8:2.0 of LiTFSI:$Zn(TFSI)_2$:urea:water by mole, called LZ-DES/$2H_2O$, was found to be highly ion-conductive (1.85 mS/cm at 30 ℃) and electrochemically stable (above 2.2 V vs Zn/Zn^{2+} of anodic limit, Fig. 2.10a). Via LZ-DES/$2H_2O$ electrolyte, the SS/Zn cell displayed 96.2% of CE upon the GCD test at 0.5 mA/cm^2 of current density. Over 2,400 h total time of GCD test (0.1 mA/cm^2 of current density and 0.74 h of charge/discharge time) was passed using Zn/Zn cell and LZ-DES/$2H_2O$ electrolyte (Fig. 2.10b). In addition, the Zn anode after cycling was found to be dendrite-free (Fig. 2.10c).
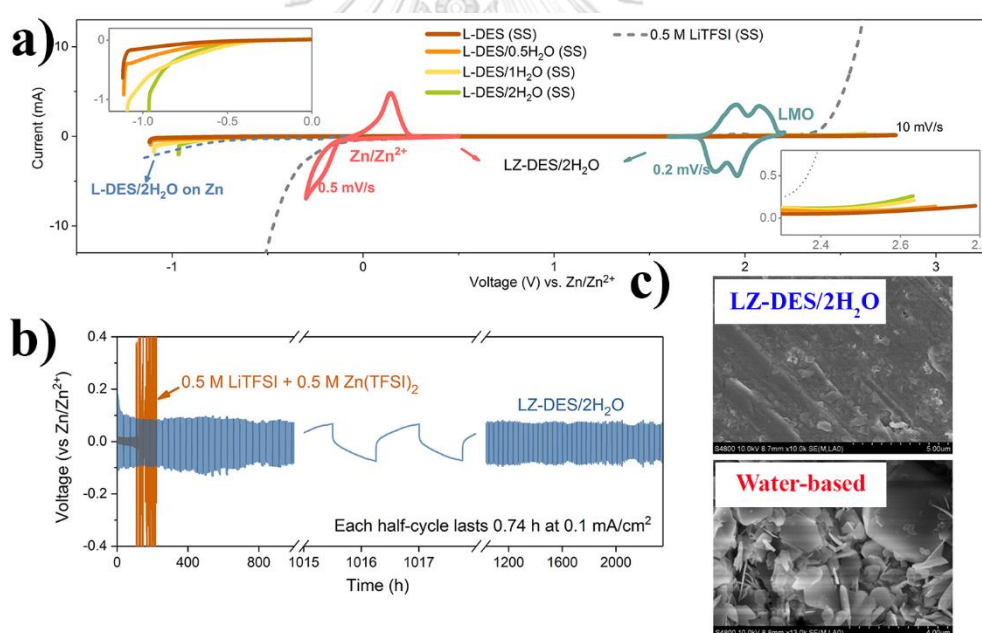
Figure 2.10 a) Electrochemical stability window of LZ-DES/$2H_2O$ in comparison with other electrolytes and the operating window of $Zn/LiMn_2O_4$ b) GCD cycling results of Zn/Zn cell having LZ-DES/$2H_2O$ electrolyte c) cycled Zn anode (LZ-DES/$2H_2O$ vs. 0.5 M Li(TFSI)$_2$/0.5 M Zn (TFSI)$_2$-water). Reproduced with permission [33].

2.4 Cathode material for NZIBs

2.4.1 Manganese-based cathodes

2.4.1.1 Manganese dioxide (MnO₂)

In the development of ZIBs, MnO_2, which possesses high specific capacity and rechargeability, is one of the most studied host materials. The specific capacity of MnO_2 is 616 mAh/g; calculation is based on two-electron redox reactions i.e. Mn (IV) to Mn (II) [105]. However, it is noted that research undertaken cannot get close to such a theoretical value [2, 106]. In general, Zn/MnO_2 batteries, having aqueous electrolytes i.e. aqueous $ZnSO_4$, aqueous $ZnCl_2$, aqueous $Zn(OTf)_2$ and other aqueous electrolytes, exhibit >200 mAh/g of specific capacity and ~1.3 V of average voltage, which is high enough for practical application. [1, 106]

Different phases of MnO_2 (α-, β-, γ-, and δ-, Fig. 2.11a) and different nanostructure shapes provide quite different characteristics and unequal performance [107-109]. For example, it is seen that the 2x2 tunnels host such as α-MnO_2 and the aqueous $ZnSO_4$ electrolyte, two reactions viz. intercalation of Zn^{2+} and intercalation of H^+ are involved in the charge-storage mechanism, while there is only the intercalation of Zn^{2+} when the layered-type δ-MnO_2 is used as host material [2]. In addition, other factors e.g. Zn salt choices as well as supporting electrolyte additives play an important role in determining the performance of the MnO_2 cathode[1].

Most MnO_2 based ZIB researches have been conducted using aqueous electrolytes. Yet, since the severe H_2 production issue in aqueous systems was revealed, attempts have been made to use nonaqueous electrolytes instead. In fact, Venkata Narayanan et al. (2010) [93] first reported the NZIB based on the MnO_2 cathode. The γ-MnO_2 having $Zn(ClO_4)_2$:Ace DES electrolyte yielded a first discharge capacity of 190 mAh/g and the stabilized discharge capacity (after 10 cycles passed) of 90 mAh/g (Fig. 2.11b). A trace of Zn in the discharged γ-MnO2 cathode was revealed using the EDAX technique (Fig. 2.11c), thus indicating that the Zn intercalation into the γ-MnO_2 is the main charge-storage reaction within the $Zn(ClO_4)_2$:Ace/γ-MnO_2 system.

Han et al. (2017)[69] investigated the intercalation mechanism of Zn into δ-MnO_2 within $Zn(TFSI)_2$-AN electrolyte. In the study, it is seen that the source of

δ-MnO$_2$ cathode capacity in Zn(TFSI)$_2$-AN arose from the ~0.6 oxidation change of Mn atom (from 3.8+ at charged state to 3.2+ at discharged state). It was also found that there was no significant structural or phase transformation of δ-MnO$_2$ cathode upon the Zn^{2+} insertion; the only change noticed was the change in the unit cell volume. Thus, the intercalation reaction within AN electrolyte could be more reversible than that of an aqueous system, which has the spinel ZnMn$_2$O$_4$ as a main discharge product (δ-MnO$_2 \leftrightarrow$ spinel ZnMn$_2$O$_4$). However, only 123 mAh/g of maximum discharge capacity (at 12.3 mA/g), poor rate capability and low voltage (more than a half of discharge profile < 1 V, Fig. 2.11d) were achieved from the Zn/δ-MnO$_2$ cell having Zn(TFSI)$_2$-AN electrolyte. In addition, electrochemical characterization results revealed the formation of a passivation layer on the cathode upon cycling, which led to poor capacity retention. As reported by Kao-ian et al. (2021) [31], the Zn/δ-MnO$_2$ cell having Zn(OTf)$_2$-DMSO electrolyte attained higher performance (1.15 V of nominal voltage and 159 mAh/g of specific capacity at 50 mA/g, Fig. 2.11e) and cyclability (1,000 cycles, 60% capacity retention, Fig. 2.11f). Corpuz et al. (2020)[74] recorded the use of α-MnO2 in NZIB. Thus, it was found that Zn/α-MnO$_2$ having Zn(OTf)$_2$-DMSO exhibited only 60 mAh/g of specific capacity at 100 mA/g, but, in terms of stability, this battery can cycle up to 2,000 cycles.
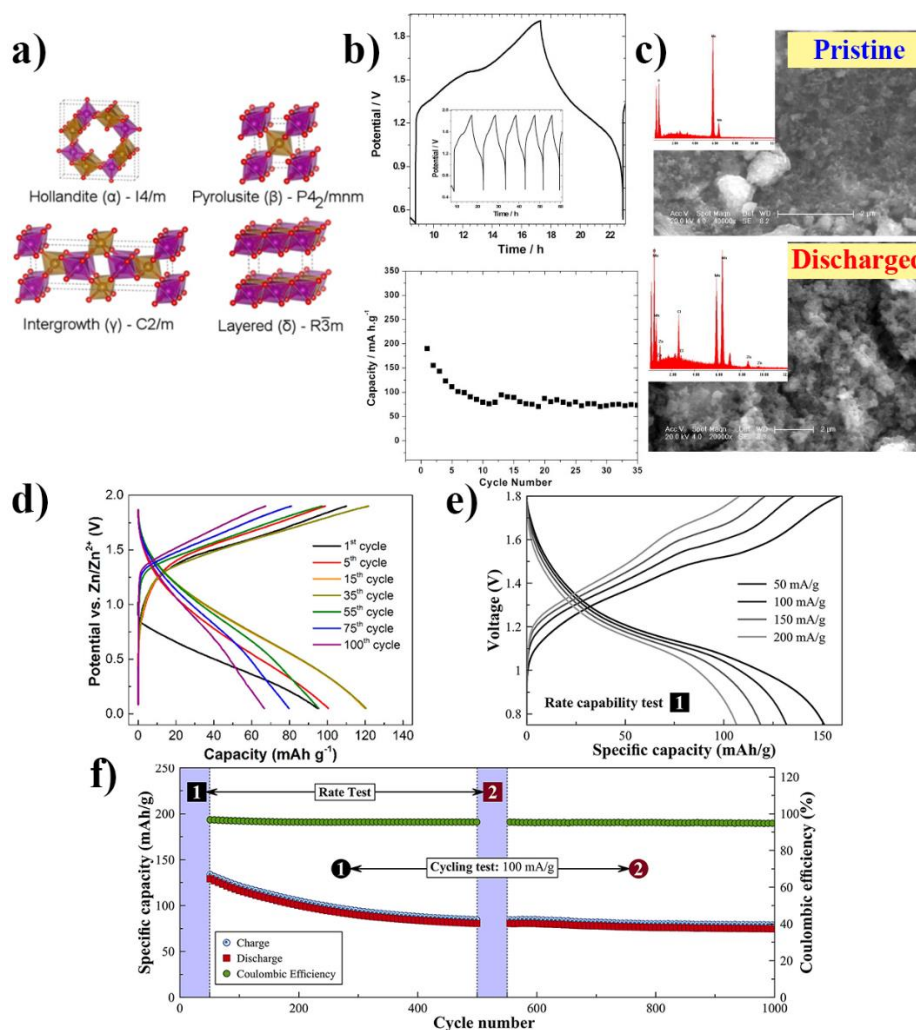
Figure 2.11 a) Schema of the crystal structure of α-, β-, γ-, and δ-MnO$_2$. Reproduced from Reference [110] (CC BY 3.0). b) GCD cycling results of Zn/γ-MnO$_2$ having Zn(ClO$_4$)$_2$:Ace DES electrolyte (100 μA/cm^2, MnO$_2$ loading: 4.5 mg/cm^2) c) SEM images (EDAX included) of pristine and discharged electrodes. Reproduced with permission [93]. d) GCD cycling results of Zn/δ-MnO$_2$ having 0.5 M Zn(TFSI)$_2$-AN electrolyte at 12.3 mA/g. Reproduced with permission [69]. Copyright, 2017 American Chemical Society. e)-f) GCD cycling results of Zn/δ-MnO$_2$ having 0.25 M Zn(OTf)$_2$-DMSO electrolyte. Reproduced from Reference [31] (CC BY-NC-ND 4.0).

2.4.1.2 LiMn$_2$O$_4$ spinel

Another manganese oxide host used in Zn batteries using nonaqueous media is the cubic spinel LiMn$_2$O$_4$ (Fig. 2.12a). LiMn$_2$O$_4$ allows reversible Li$^+$ intercalation within a range of $1 < x < 2$ (Li$_x$Mn$_2$O$_4$) yielding a theoretical capacity of 148 mAh/g [111]. Within this range, LiMn$_2$O$_4$ can maintain its cubic structure, and there is only 6.5 % of volume

change found at full-intercalation (discharged). The application of $LiMn_2O_4$ in a Zn battery can be made using a Zn^{2+}/Li^+ contained electrolyte. Upon the battery discharging, Li^+ is intercalated at the cathode whereas Zn is stripped from the anode [33]. Consequently, the $Zn/LiMn_2O_4$ cell having LZ-DES/$2H_2O$ electrolyte delivered 117 mAh/g of initial capacity (0.06C) and ~1.92 V discharge voltage (Fig. 2.12b). The cell retained 70% capacity at a higher rate (1C). Upon the cyclability test, 82.7% capacity retention was achieved after 600 cycles (Fig. 2.12c). In this system, the high content of water (~30 mol%) of LZ-DES/$2H_2O$ may be the source of the facile Li^+ intercalation kinetics [112]. However, it is noted that the $Zn/LiMn_2O_4$ system cannot run perfectly under the aqueous electrolyte: this is due to the high terminal charging voltage of the $Zn/LiMn_2O_4$ cell (>2 V), which is higher than the stability limit of the aqueous electrolyte (~2 V, Fig. 2.12d).
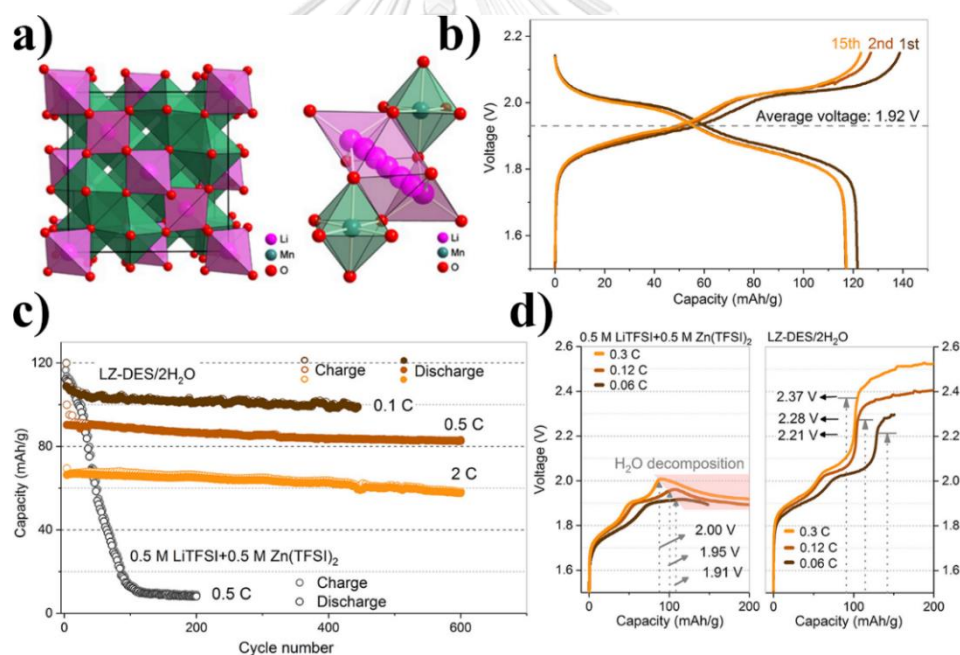
Figure 2.12 a) Crystal structure of $LiMn_2O_4$. Reproduced from Reference [113] (CC BY-NC-ND 3.0). b) GCD discharge profile of $Zn/LiMn_2O_4$ cell (LZ-DES/$2H_2O$) during first few cycles c) GCD cycling performance of $Zn/LiMn_2O_4$ cell at various current rate d) Charging limits of $Zn/LiMn_2O_4$ cell having water-based (left) and LZ-DES/$2H_2O$ (right) electrolyte. Reproduced with permission [33].

2.4.2 Vanadium-based cathodes

2.4.2.1 Vanadium oxide

Due to their large-inter spacing and high specific capacity, vanadium oxides i.e. V_2O_5, $V_2O_5 \cdot nH_2O$, $V_3O_7 \cdot H_2O$ and XV_2O_5, where X = Zn, Na, Ca…, which are constructed from the VO_5 pyramid or the VO_6 octahedra, are attractive host material for ZIBs [1, 114]. According to the literature, the Zn^{2+} intercalation capacities of vanadium oxides in aqueous media range from 224 to 470 mAh/g, and originate from the V^{5+} to V^{4+} or even to V^{3+} of the oxidation state changes of vanadium atoms [115, 116]. Several reports state that most of the vanadium oxide cathodes provide exceptional rate capability: this is due to the large inter-space of the vanadium oxides, which can further be enhanced by adding water molecules or cations into their layers [2]. However, the main disadvantage of vanadium oxides is the low discharge voltage (~0.8-1 V). As for the nonaqueous media, vanadium oxides are found to be compatible with $Zn(TFSI)_2$-AN, $Zn(OTf)_2$ and ZES [34, 46, 71].

Senguttuvan et al. (2016) [71] stated that an average voltage of 0.85 V on a specific capacity of 170 mAh/g was achieved from a Zn/V_2O_5 cell having $Zn(TFSI)_2$-AN electrolyte . It is noted that the cell exhibited excellent rate capability and was able to cycle at least 120 cycles with negligible capacity loss (Fig. 2.13a). Qiu et al. (2019) [34] proposed the use of ZES as an electrolyte for a Zn/V_2O_5 cell. Accordingly, it was found that ~150 mAh/g capacity (80 mA/g), ~0.9 V discharge voltage (80 mA/g) and 92.8% capacity retention after 800 cycles (at 600 mA/g) were achieved (Fig. 2.13b and c). It is significant that all the Zn/V_2O_5 cells conducted in the nonaqueous media provided lower capacity than in the aqueous electrolyte. Kundu et al. (2018)[46] reported on the phenomena behind such outcomes. In Kundu's study, it was seen that a similar charge-storage mechanism between aqueous and nonaqueous systems was found (according to the XRD and XPS analysis) whereby the $V_3O_7 \cdot H_2O$ cathode provided 375 mAh/g at 1C and 275 mAh/g at 8C in the aqueous $ZnSO_4$ electrolyte; such a good performance, however, was not afforded by $Zn(OTf)_2$-AN (~59 mAh/g at 5 mA/g). It was found that desolvation was the main process that determined the rate performance of the battery: the desolvation energy required in nonaqueous systems is

much higher than that in aqueous systems. Thus, the performance of the nonaqueous battery was tremendously reduced.
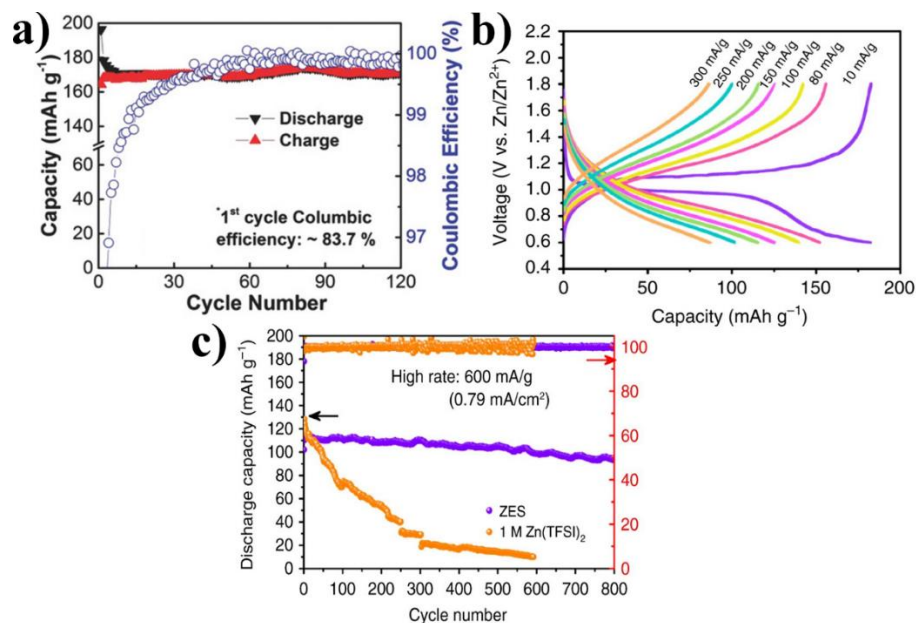
Figure 2.13 Electrochemical performance of nonaqueous Zn/V_2O_5 batteries: a) GCD cycling results of Zn/V_2O_5 cell having 0.5 $Zn(TFSI)_2$-AN at C/10 (14.4 mA/g). Reproduced with permission [71]. b) GCD voltage profile of Zn/V_2O_5 cell having ZES electrolyte at various current densities (10-300 mA/g) c) Cyclability results of Zn/V_2O_5 cell having ZES at 600 mA/g (ZES vs. aqueous). Reproduced from Reference [34] (CC BY 4.0).

2.4.2.2 Vanadium Sulfide

It is found that reversible Zn^{2+} intercalation can be made using layered vanadium sulfide (VS_2). He et al. (2017) [117] stated that via the V^{4+}/V^{3+} oxidation change, the Zn/VS_2 having an aqueous $ZnSO_4$ electrolyte can provide 190.3 mAh/g of specific capacity (50 mA/g) and ~0.6 V discharge voltage. Further, according to Naveed et al. (2019), Zn/VS_2 can run under TMP–DMC electrolyte achieving 94.38% capacity retention after 500 cycles [73]. However, both low capacity (maximum 146.6 mAh/g) and the low voltage (~0.45 V) were recorded.

2.4.2.3 Vanadium-based polyanionic compounds

Another state-of-art of the vanadium-based electrode is the polyanionic compound. Li et al. (2016) [118] introduced polyanionic cathodes having NASICON structure such

as $Na_3V_2(PO_4)_3$ (NPV) for use in ZIBs. The NASICON structure of NPV allows fast Na^+ diffusion and further results in fast intercalation kinetics. The study also reported that the first charging resulted in Na^+ extraction from the NPV (V^{3+}), thus forming $NaV_2(PO_4)_3(V^{4+})$. Subsequently, Zn^{2+} intercalation/deintercalation took place. Thus, the Zn/NPV cell having aqueous $Zn(CH_3COO)_2$ electrolyte provided 97 mAh/g specific capacity (0.5C) and ~1.1 V discharge voltage. Guo et al. (2017) [119] next surveyed the development of polyanionic cathodes. It is noted that O^{2-} and F^- had high electronegativity, which was able to enhance the voltage of the cathode. Consequently, a $Na_3V_2(PO_4)_2O_2F$ (NVPOF) cathode was introduced for use in a Na-ion battery. Dong et al. (2020) [64] put forward the use of NVPOF in ZIBs. Consequently, having 0.5 M/1.0 M of $Zn(OTf)_2$/$NaClO_4$-TMP electrolyte, the Zn/NVPOF cell (Fig. 2.14a) provided a high specific capacity of 113 mAh/g and an average discharge voltage of 1.8 V (Fig. 2.14b). In addition, 83.5% capacity retention was achieved upon 1,000 cycles (Fig. 2.14c). The charging voltage cut-off of this battery was 2.2 V; thus, the use of the aqueous electrolyte proved infeasible. Different from what it was in the aqueous Zn/NPV system, Na^+ intercalation took place in the Zn/NVPOF having 0.5 M/1.0 M of $Zn(OTf)_2$/$NaClO_4$-TMP electrolyte instead of Zn^{2+} intercalation: this may be the cause of the improved stability of the Zn/NVPOF system.

Another polyanionic cathode found in nonaqueous Zn battery researches is the layered $VOPO_4$, which was further enhanced by adding a preintercalated polypyrrole (PPy) into $VOPO_4$ interspace [68]. The PPy addition was found to reduce the interspacing size and improved the electronic conductivity of $VOPO_4$. The Zn/PPy-$VOPO_4$, cell having water, containing $Zn(OTf)_2$-AN electrolyte exhibited 1.1 V average voltage and maximum capacity of 86 mAh/g. Besides, the cell passed at least 350 cycles at a current density of 100 mA/g.
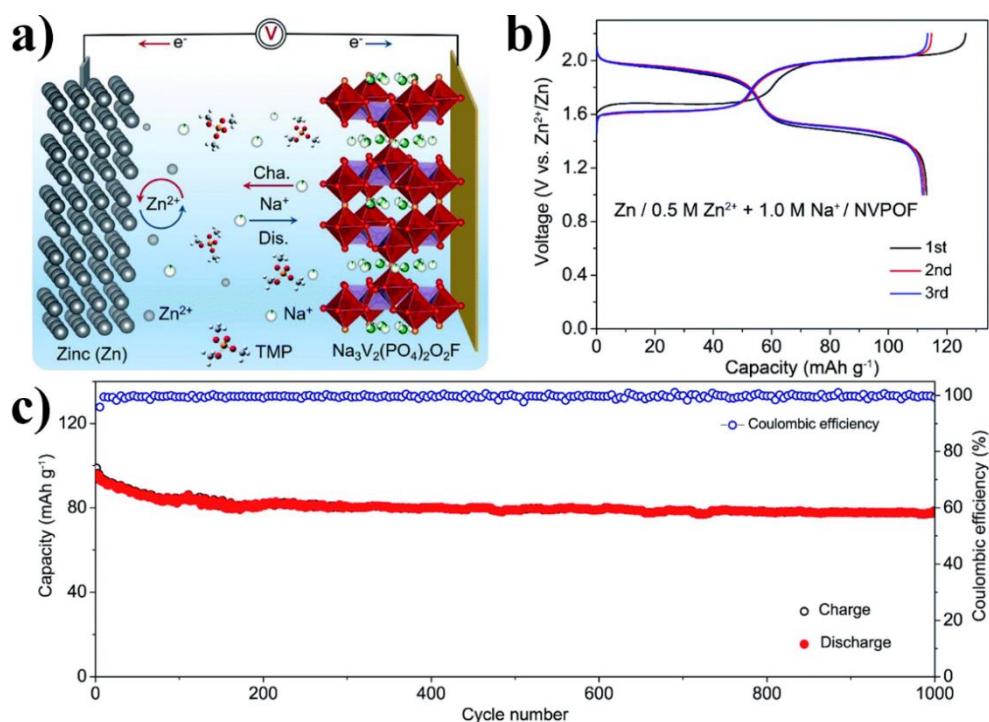
Figure 2.14 a) Schema of the Zn/NVPOF dual-ion battery b) GCD discharge profiles of Zn/NVPOF cell having 0.5 M/1.0 M of $Zn(OTf)_2$/$NaClO_4$-TMP electrolyte at 0.2C c) GCD cycling results of Zn/NVPOF cell at 1.0C. Reproduced with permission [64].

2.4.3 Cobalt based cathodes

The cobalt oxide e.g. $LiCoO_2$ is a traditional host material, which has been used in LIBs for more than a decade[120]. The intercalation fraction (x) of Li^+ to Li_xCoO_2 ranges from x=0 (Co^{4+}) to x=1 (Co^{3+}) having 274 mAh/g theoretical capacity. Due to their large capacity, 3D-tunnel structure and high voltage, attempts have been made to apply the CoO_2 framework to ZIBs. Pan et al. (2017) [62] first proposed the use of CoO_2 framework ($ZnCo_2O_4$ form) in ZIBs. To compensate for the instability issue of the spinel $ZnCo_2O_4$ caused by oxygen evolution, Al was doped in $ZnCo_2O_4$ to form the more stable $ZnAl_xCo_{2-x}O_4$ (Fig. 2.15a). Material characterizations highlight the fact that there was a reversible change in the Co oxidation state upon discharging/charging ($Co^{4+} \leftrightarrow Co^{3+}$). CV results revealed that the best electrochemical performance was achieved at x=0.67 ($ZnAl_{0.67}Co_{1.33}O_4$). The Zn/$ZnAl_{0.67}Co_{1.33}O_4$ cell having $Zn(OTf)_2$-AN electrolyte provided 134 mAh/g (~84% of theoretical capacity) of initial discharge capacity and ~1.7 V discharge voltage at 0.1C (16 mA/g) (Fig. 2.15b). At

1C, capacity retained only 70% of its initial capacity (Fig. 2.15c); this outcome indicates the limitation of this system in terms of rate capability.

The CoO_2 framework for ZIBs was further developed by the same group work. Pan et al. (2018)[63] noted that the inadequate Zn^{2+} diffusion rate was the cause of the deficient performance of the Al-doped $ZnCo_2O_4$ cathode; it was found that Zn^{2+} in the cathode was not fully extracted during the charging process. To improve capacity and structural stability, $ZnNi_xMn_xCo_{2-2x}O_4$, containing Ni and Mn, was introduced. According to the GCD test, the optimized formula of $ZnNi_xMn_xCo_{2-2x}O_4$ was found to be $ZnNi_{1/2}Mn_{1/2}CoO_4$. The $Zn/ZnNi_{1/2}Mn_{1/2}CoO_4$ cell having $Zn(OTf)_2$-AN electrolyte possessed a high capacity of 180 mAh/g (0.1C ≈ 21 mA/g) and provided excellent cyclability (> 200 cycles at 0.2C) (Fig. 2.15e). The enhanced capacity arose from the additional redox sources i.e. Mn^{4+}/Mn^{3+} and $Ni^{4+}/Ni^{3+}/Ni^{2+}$ (Fig. 2.15d) instead of only Co^{4+}/Co^{3+} as in the case of $ZnAl_xCo_{2-x}O_4$. Besides, there was an improved rate capability compared to the $ZnAl_xCo_{2-x}O_4$; at 1 C the capacity retained 80% of its initial capacity (Fig. 2.15f).
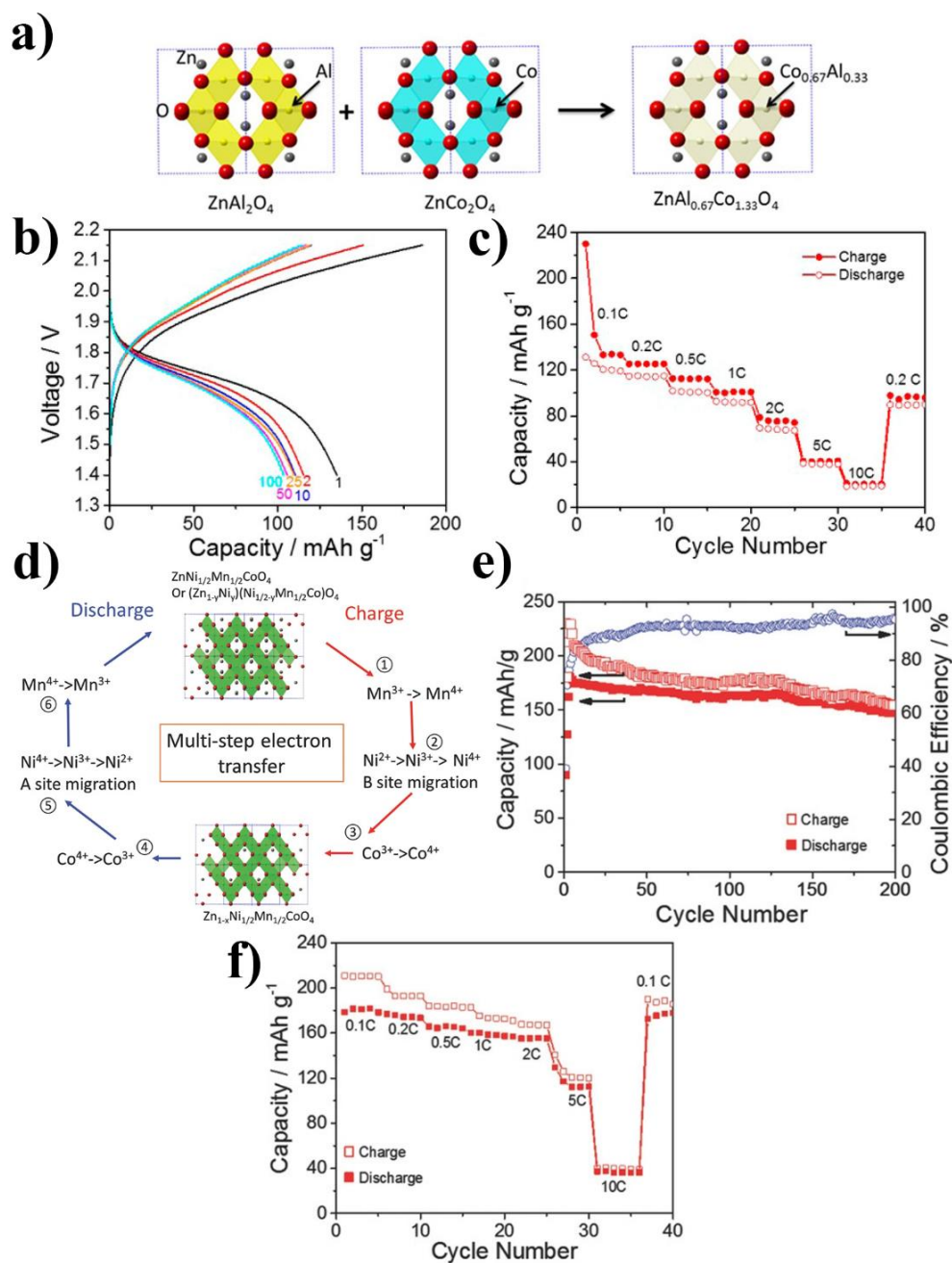
Figure 2.15 a) Schema of the crystal structure of $ZnAl_{0.67}Co_{1.33}O_4$ b) GCD discharge (0.2 C) profile of $Zn/ZnAl_{0.67}Co_{1.33}O_4$ cell ($Zn(OTf)_2$-AN electrolyte) at various cycling position c) Rate capability results of $Zn/ZnAl_{0.67}Co_{1.33}O_4$ cell. Reproduced with permission [62]. Copyright 2017, American Chemical Society. d) Schema of charge-charge storage reactions of $ZnNi_xMn_xCo_{2-2x}O_4$ cathode e) Cyclability results of $Zn/ZnNi_xMn_xCo_{2-2x}O_4$ cell ($Zn(OTf)_2$-AN electrolyte) at 0.2 C f) Rate capability results of $Zn/ZnNi_xMn_xCo_{2-2x}O_4$ cell. Reproduced with permission [63].

2.4.4 Prussian blue-based cathodes

Prussian blue analogue (PBA) is a high voltage host material, which is constructed following the MFe(CN)$_6$ formula where M = Zn, Cu, Ni, Mn, Co and other transition metals, MHCf [2]. PBAs always appear in cubic or monoclinic forms. Nonaqueous electrolytes are required for the ZIBs having PBA cathodes to avoid electrolyte decomposition upon charging. The specific capacity of PBA in nonaqueous media ranges from 50 to 190 mAh/g, depending on the type of M species. Munseok et al. (2017) reported the use of KNiHCf having the formula K$_{0.86}$Ni[Fe(CN)$_6$]$_{0.954}$(H2O)$_{0.766}$ as cathode material for NZIB [70]. Via Zn(ClO$_4$)$_2$-AN electrolyte, Zn/KNiHCf cell exhibited a first discharge capacity of 55.6 mAh/g (0.2C $\approx$ 11.2 mA/g), which is about 67% of the theoretical capacity. XRD and EDX results confirmed the insertion/extraction of Zn^{2+} (Fig. 2.16a). However, poor rate capability was noted; capacity decreased progressively as the current increased (Fig. 2.16b).

Naveed et al. (2019) [61] set up KCuFe(CN)$_6$ (KCuHCf) for use in a NZIB. In the Zn(OTf)$_2$-TEP electrolyte, the Zn/KCuHCf cell failed at cycling; capacity decreased progressively during the first 5 cycles. It is evident that water should have been added to the electrolyte to drive the Zn^{2+} intercalation. The Zn/KCuHCf having Zn(OTf)$_2$-TEP:water (7:3 by volume) electrolyte passed 1,000 cycles of GCD test at 1C (~73.3 mA/g), yielding 74% capacity retention (Fig. 2.16c). The cell provided 73.3 mAh/g of initial capacity and ~1.6 V of discharge voltage at 0.5C. In addition, superior rate performance was obtained; a slight decrease in capacity occurred when the cell cycled at 0.5C to 2C (Fig. 2.16d).

As presented by Li et al. (2020) [60], the K$_{1.6}$Mn$_{1.2}$Fe(CN)$_6$ (KMnHCf) cathode is viewed as one of the most promising cathodes for NZIBs displaying a reversible change between cubic monoclinic (discharge) and (charged) structure upon Zn^{2+} interaction/deintercalation. Thus, the Zn/KMnHCf in Zn(ClO$_4$)$_2$–TEGDME exhibited a high discharge voltage (1.6 V), a high specific capacity (65.5 mAh/g at 50 mA/g), a good rate capability (65, 52, 48, and 45 mAh/g capacity at 50 to 100, 150 and 200 mA/g current density, respectively) and excellent cyclability (94% capacity retention at 8,500 cycles (200 mA/g)). The cell also revealed negligible self-discharge (3% capacity loss) upon one week rest period (Fig. 2.16e).

Another PBA cathode found in NZIB researches is CoHCf [30]. According to Ma et al. (2020), a CoHCf nanocube cathode, having $Zn(BF_4)_2$-[C2mim]BF_4 electrolyte, delivered an extremely high capacity of 187.3 mAh/g at 250 mA/g current density, which is superior to all PBA cathodes that have ever been recorded in the literature. The Zn/CoHCf cell also attained a very wide current range of operation (0.25-6 A/g) (Fig. 2.16f); at 6 A/g, capacity still retained 135.6 mAh/g. In addition, the cell passed 40,000 cycles (2 A/g), yielding 95% capacity retention (Fig. 2.16g). It is noted that the contribution of both Co ($Co^{3+} \leftrightarrow Co^{2+}$) and Fe ($Fe^{3+} \leftrightarrow Fe^{2+}$) resulted in two-electron charge-storage reactions, which provided the source of the high capacity of the CoHCf cathode.
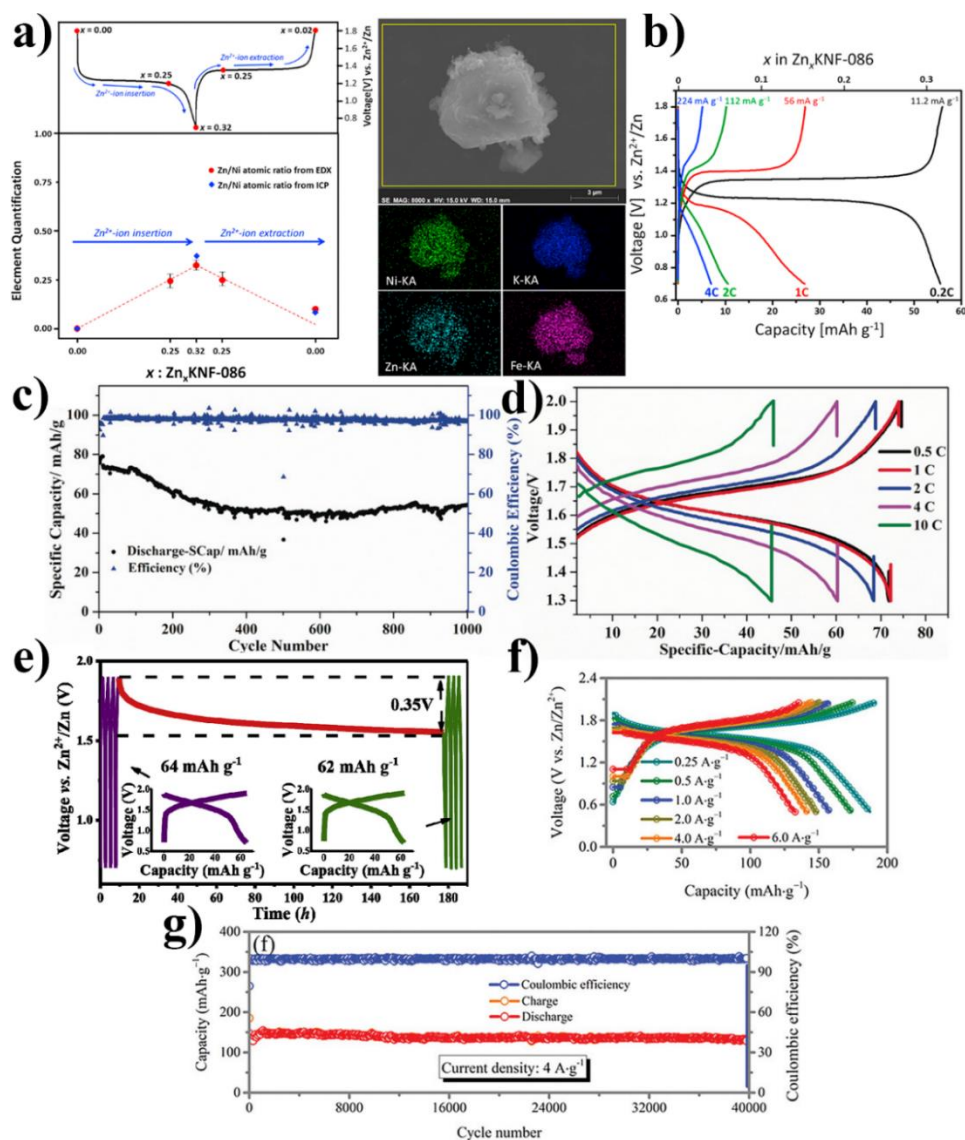
Figure 2.16 a)-b) Zn/KNiHCf system (Zn(ClO$_4$)$_2$-AN): a) voltage vs. intercalation fraction (left) and SEM-EDX image of discharged cathode b) Rate capability results of Zn/KNiHCf cell. Reproduced with permission [70]. c)-d) Zn/KCuHCf system (Zn(OTf)$_2$-TEP:water): c) cyclability result of Zn/KCuHCf cell at 1 C d) Rate capability results of Zn/KCuHCf cell. Reproduced with permission [61]. e) Self-discharge test of Zn/KMnHCf cell (Zn(ClO$_4$)$_2$–TEGDME). Reproduced with permission [60]. f)-g) Zn/CoHCf system (Zn(BF4)$_2$-[C2mim]BF$_4$): f) Rate capability results of Zn/CoHCf cell g) Cyclability results of Zn/CoHCf cell at 4 A/g. Reproduced with permission [30].

2.4.5 Organic based cathodes

Polyaniline (PANi), a conducting polymer, is one of the organic based cathodes, which can be used in NZIBs. The charge-storage process of PANi relies on the reaction between anions i.e. Cl$^-$, TFSI$^-$ and OTf$^-$ and the nitrogen (imine group) on PANi

molecule to form salts: upon charging, the electron on the nitrogen will be removed; accordingly, the association with anions occurs[121]. Guerfi et al. (2014)[72] recommended the Zn/PANi battery based on a nonaqueous electrolyte. The Zn/PANi having $Zn(TFSI)_2$-PC demonstrated maximum capacity of 148 mAh/g and an average discharge voltage of ~0.85 V at 0.5C, and passed at least 1,700 cycles of GCD cycling.

A phenanthrenequinone macrocyclic trimer (PQ-MCT) is also one of the organic based cathodes being used in NZIBs [59]. PQ-MCT can store Zn^{2+} on its C=O groups via coordination reaction (Fig. 2.17a), and has a theoretical capacity of 257.74 mAh/g. Wang et al. (2020) [59] put forward a nonaqueous Zn/PQ-MCT battery using $Zn(OTf)_2$-DMF electrolyte. At 1 A/g, the cell was found to be extremely stable at cycling: over 20,000 cycles were achieved having negligible capacity fading (Fig. 2.17b). The PQ-MCT cathodes exhibited 145 mAh/g of specific capacity and ~0.75 V vs. Zn/Zn^{2+} of average discharge voltage at 0.05 A/g. In addition, the cell was able to run at 50 A/g yielding 60 mAh/g discharging capacity (Fig. 2.17c), and operated normally at extreme temperature conditions (-70 ℃ and 150 ℃).

Another organic based cathode for nonaqueous Zn batteries found in the literature is the polytriphenylamine composite (PTPAn) [75]. The charge-storage mechanism of PTPAn is very close to that of PANi. Upon charging, the C-N groups on PTPAn are seen to lose electrons. Then, the situation changed into the positive-charged C=N+, which bonded with the guest anions i.e. $TFSI^-$ (Fig. 2.17d). Qiu et al. (2021) [75] studied the application of PTPAn in NZIBs. At 2 mg/cm^2 of PTPAn loading, the Zn/PTPAn cell having $Zn(OTf)_2$-TEP:PC (1:2) electrolyte delivered maximum capacity of 85 mAh/g and average discharge voltage of ~1.5 V at 0.1 A/g. Further, at high PTPAn loading (8 mg/cm^2) and high current density (1 A/g), the cell perfectly retained capacity, which lasted for 4,000 cycles.
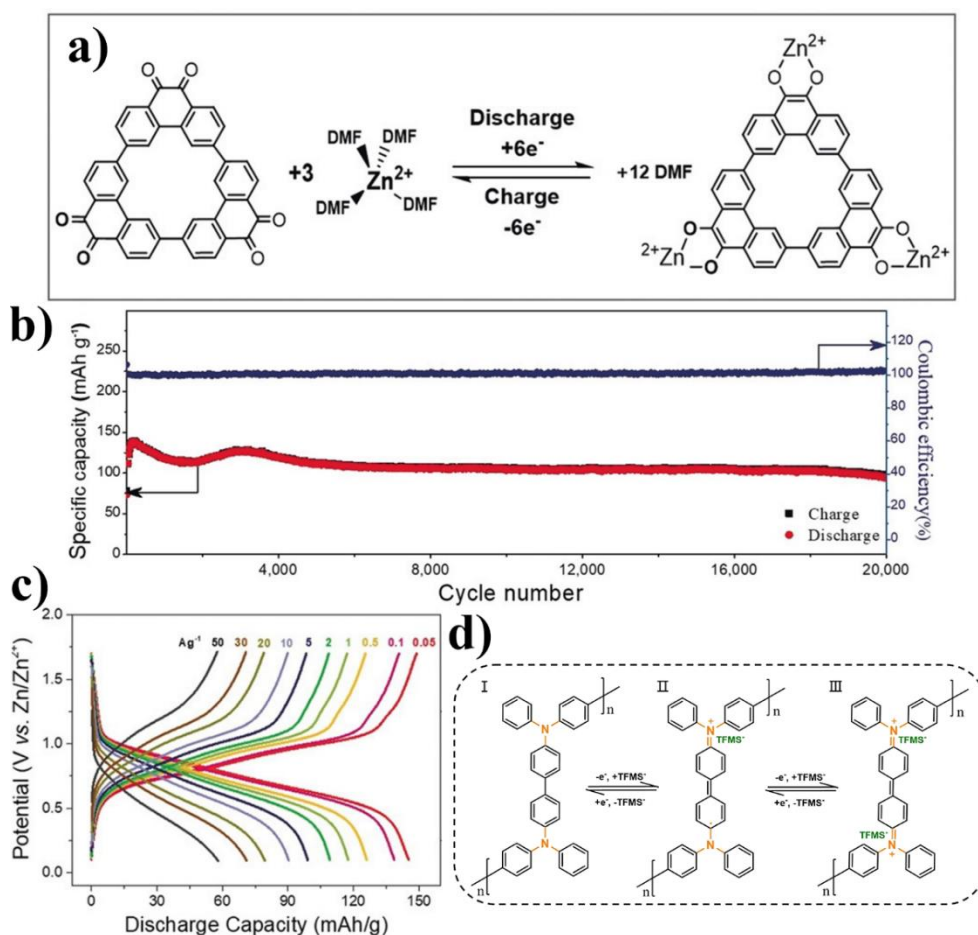
Figure 2.17 a)-c) Zn/PQ-MCT battery (Zn(OTf)$_2$-DMF): a) Schema of the charge-storage mechanisms of PQ-MCT cathode b) Cyclability results of Zn/PQ-MCT cell at 1 A/g c) Rate capability results of Zn/PQ-MCT cell. Reproduced with permission [59]. d) Schema of the charge-storage mechanisms of PTPAn cathode. Reproduced with permission [75].

2.4.6 Graphite cathodes

The charge-storage mechanism of a graphite cathode in a dual-ion battery relies on the intercalation (charging)/deintercalation (discharging) of the anion i.e. PF$_6^-$, TFSI$^-$ and OTf$^-$ [65, 66, 87]. Accordingly, the graphite cathode having anion intercalation exhibited very high voltage (> 2.0 V vs. Zn/Zn^{2+}); thus, high stability electrolytes such as organic electrolytes and RTIL electrolytes are required. Fan et al. (2019) [65] put forward a Zn/graphite cell having Zn(OTf)$_2$-[EMIm]OTf electrolyte. Via 0.2 M Zn(OTf)$_2$ electrolyte, maximum capacity and discharge voltage was found to be 33.7 mAh/g and 2.0 V (0.2 mA/cm^2 ≈ 154 mA/g), respectively. At 0.5 mA/cm^2 (~385 mA/g),

capacity dropped to 22.4 mAh/g. The cell was seen to run for at least 100 cycles. However, a clear capacity drop was observed upon cycling at 0.2 mA/cm^2.

Zhang et al. (2019)[66] introduced the use of Zn(TFSI)$_2$-AN on a Zn/graphite cell (Fig. 2.18a). After 10 cycles passed (50 mA/g), the capacity stabilized at 47.5 mAh/g, yielding the average discharge voltage of 2.2 V. The cell also exhibited excellent cyclability (82% capacity retention after 4,000 cycles at 1.0 A/g) and superior rate capability (Fig. 2.18b and c); there was only a negligible capacity drop upon the current density range of 0.1 A/g to 1.5 A/g.

As proposed by Ji et al. (2020)[87], another Zn/graphite cell was carried out using Zn(TFSI)$_2$-[C4mpyrr]TFSI electrolyte. Thus, it was found that the reversible discharge capacity and the average discharge voltage was 57 mAh/g and 1.6 V (at 2C ≈ 200 mA/g), respectively. The cell displayed 86% capacity retention after passing 500 cycles.
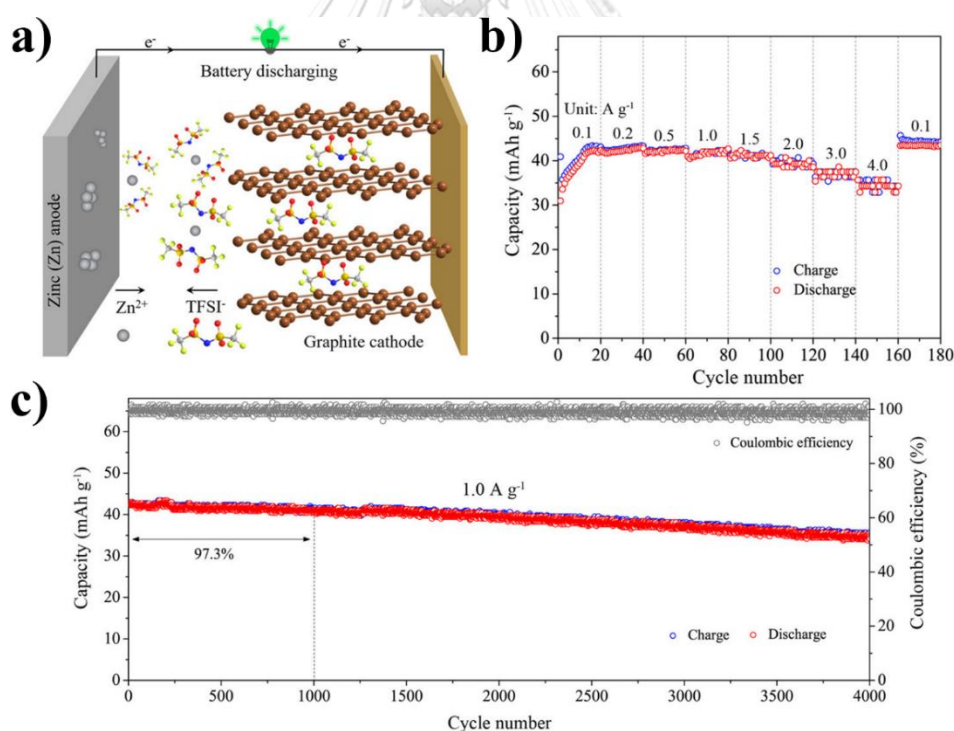
Figure 2.18 Electrochemical performance of Zn/graphite cell having Zn(TFSI)$_2$-AN electrolyte: a) Schema of the charge-storage reaction of Zn/graphite cell b) Rate capability results of Zn/graphite cell c) Cyclability results of Zn/graphite cell at 1 A/g. Reproduced with permission [66] Copyright, 2019 American Chemical Society.

2.5 Perspective and Summary

This review highlights the application of nonaqueous electrolytes i.e. organic electrolytes, RTIL electrolytes and DES electrolytes in rechargeable ZIBs. The main reason for using nonaqueous electrolytes in improving ZIBs is due to their high electrochemical stability and gas production inhibition e.g. H_2 evolution and Zn self-corrosion, which allows the use of high voltage cathode (>2 V vs. Zn/Zn^{2+} upon charging) such as spinel $LiMn_2O_4$, polyanionic compound, cobalt oxide, Prussian blue and graphite, demonstrating little degradation upon cycling. In addition, it is noted that most nonaqueous electrolytes can significantly suppress dendrite formation on the Zn anode which is one of the most critical issues in ZIB development and can provide long-life Zn anode cycling. At this point, nonaqueous electrolytes appear to be an ideal choice for ZIB electrolytes. Nevertheless, there are several issues that need resolving for nonaqueous electrolytes to be applied on a practical scale.

In Fig. 2.19, the plots of specific power versus specific energy of cathode materials conducted in nonaqueous media are illustrated. Herein, it is seen that published cathode-electrolyte systems cover a wide range of operations, and have a specific energy range (lower than 100 Wh/kg to higher than 300 Wh/kg). Of all cathode materials, $ZnNi_{1/2}Mn_{1/2}CoO_4$ and the CoHCf demonstrate the highest energy density (>300 Wh/kg). However, most of the systems provide the best performance (both in terms of power and energy) at around 1C discharging rate, which indicates the moderate intercalation kinetics of NZIBs. Although high voltage cathodes are now available for ZIBs, they are quite slow in terms of rate capability compared to AZIBs. It is acknowledged that the ionic conductivity of nonaqueous electrolytes such as organic electrolytes are in the range of 10^{-3} to 10^{-2} S/cm, which are not much different from aqueous electrolytes.

In order to improve the performance of NZIBs, the rational design of the electrolyte or fine-tuning via cosolvents can minimize the effect of anion-cation pairing. Another viable approach is to tune the surface chemistry of the host material to support the solvation of guest ions. To date, the most straightforward approach to improve NZIB performance is the addition of water; the addition of water not only enhances the ionic conductivity, but also increases the rate performance of the battery. Water added

to the electrolyte acts like a "lubricant" to drive the insertion reaction. However, complete understanding regarding the intrinsic role of water has yet to be elucidated.
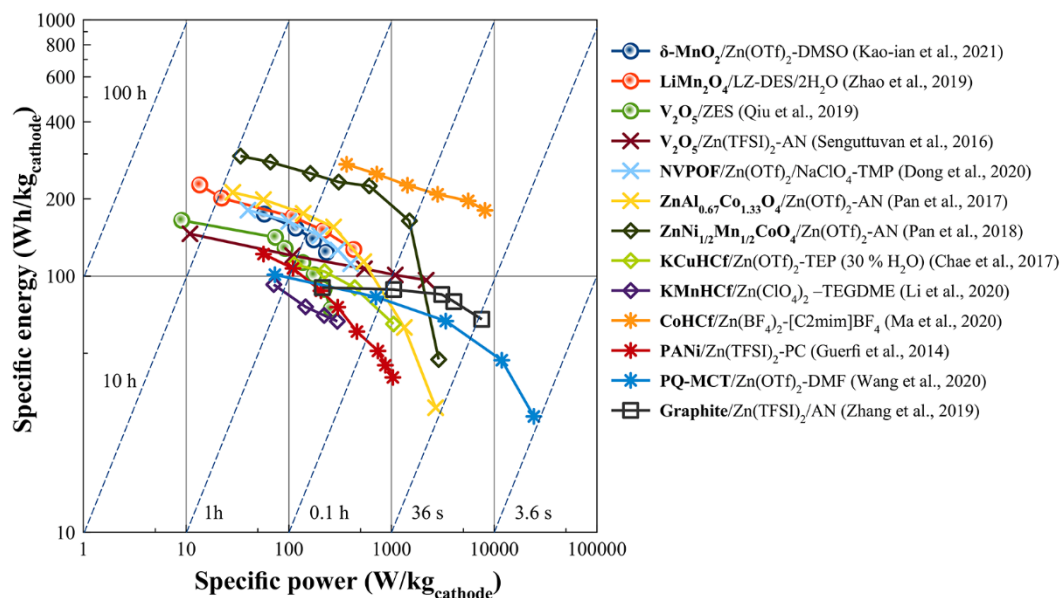
Figure 2.19 Ragone plots of NZIBs (normalized by weight of cathode material) [30, 31, 33, 34, 59, 60, 62-64, 66, 70-72].

Several research groups have demonstrated satisfactory results when Zn anodes have been applied using nonaqueous electrolytes. However, more substantiation is required to ensure their practical application. Ma et al. (2020) [7] stated that an ideal target for Zn anode towards commercialization is 5 mAh/cm^2 areal capacity having 100% CE, which can last for 2,000 cycles; the Zn anode should be capable enough to hold against the high charging rate (2C, 10 mA/cm^2). To achieve such a goal, it is important to recognize the current status of the Zn anode within nonaqueous ZIB research. In Table 2.3, the data regarding Zn anode rechargeability in nonaqueous media gathered from this review is shown. It is seen that there are only two systems viz. Zn(OTf)$_2$-TEP and Zn(OTf)$_2$-TMP that can meet the target of 5 mAh/cm^2 areal capacity. Yet neither of these can operate at high current of 10 mA/cm^2. In section 3 of this review, the Zn(OTf)$_2$/Zn(TFSI)$_2$-AN and Zn(BF$_4$)$_2$-[C2mim]BF$_4$ can hit 10 mA/cm^2 current density, but only 0.4 and 0.5 mAh testing capacity was used, respectively. Overall, it is evident that there are limits in terms of the plating/stripping kinetics of Zn in nonaqueous media, and as such require further improvement. Possible

strategies that can be undertaken to surpass this goal include 1) the development of the solid electrolyte interface (SEI) that can reduce energy loss due to the desolvation penalty and 2) the electrolyte design to reduce the effect of anion-cation pairing.

In terms of CE, most Zn-nonaqueous systems provide positively good results (> 99%). Such results are due to the stability of nonaqueous electrolytes. However, it is found that none of the works presented herein can perform higher than 10% depth of discharge (DOD). This means that more than 90% of unused Zn still existed in the cell. This excessive amount of Zn may well lead to the low energy density of the full cell. Thus, the effects of DOD should be further investigated.

Table 2.3 Zn anode performance evaluated using GCD tests

Electrolytes	CE (CC/Zn cell)	Maximum cycling time (Zn/Zn cell)	Testing capacity	Anode type	DOD (each cycle)	Ref.
0.5 M Zn(TFSI)$_2$-AN	99.80%	~300 h (1.25 mA/cm^2)	0.408 mAh/cm^2	Zn foil (thickness:0.25 mm, ~146.2 mAh/cm^2)	0.28%	[67]
0.5 M Zn(OTf)$_2$-AN	99.90%	~400 h (1.25 mA/cm^2)	0.408 mAh/cm^2	Zn foil (thickness:0.25 mm, ~146.2 mAh/cm^2)	0.28%	[67]
1 M Zn(TFSI)$_2$-AN	99.50%	1000 h (0.5 mA/cm^2)	0.25 mAh/cm^2	Zn foil	N/A	[66]
0.5 M Zn(TFSI)$_2$-PC	99.1% **	9 cycles (0.5 mA cm^2)**	1 mAh/cm^2 **	Zn on Cu: 5 mAh/cm^2**	N/A	[95]
0.5 M Zn(OTf)$_2$-DMF	99.8%	2800 h (1.0 mA/cm^2)	1 mAh/cm^2	Zn foil (t:0.03 mm, ~17.5 mAh/cm^2)	5.71%	[59]
0.5 Zn(OTf)$_2$-TEP	99.86%	3000 h (0.1-0.5 mA/cm^2)	0.1-0.5 mAh/cm^2	Zn foil (t:0.25 mm, ~146.2 mAh/cm^2)	0.07-0.34%	[61]
		2000 h (0.5 mA/cm^2)	5 mAh/cm^2	Zn foil (t:0.25 mm, ~146.2 mAh/cm^2)	3.42%	
0.5 M Zn(OTf)$_2$-TMP	99.57%	>2300 h (0.1-1.0 mA/cm^2)	0.1-0.5 mAh/cm^2	Zn foil	N/A	[73]
		1000 h (0.5-1 mA/cm^2)	5-10 mAh/cm^2	Zn foil (t:0.25 mm, ~146.2 mAh/cm^2)	3.42-6.84%	
0.5 M/1.0 M of Zn(OTf)$_2$/NaClO$_4$-TMP	99.80%	5000 h (0.5 mA/cm^2)	0.25 mAh/cm^2	Zn foil	N/A	[64]

0.25 M Zn(OTf)2-DMSO	99.60%	>100 h (0.1-1.0 mA/cm²)	0.025-0.25 mAh/cm²	Zn foil (t:0.10 mm, 58.5 mAh/cm²)	0.04-0.43%	[31]
0.5 Zn(OTf)$_2$-TEP:PC	99.70%	2600 h (0.5 mA/cm²)	0.5 mAh/cm²	Zn foil (t:0.03 mm, ~17.5 mAh/cm²)	2.86%	[75]
0.5 M Zn(OTf)$_2$-TMP:DMC	99.15%	>5000 h (1.0 mA/cm²)	1 mAh/cm²	Zn foil	N/A	[73]
9 mol% Zn(dca)$_2$-[C2mim] dca (3 wt.% water)	85%	375 h (0.1 mA/cm²)	0.2 mAh/cm²	Zn foil	N/A	[79]
2M Zn(BF$_4$)$_2$-[C2mim]BF$_4$	99.36%	1500 h (2 mA/cm²)	0.5 mAh/cm²	Zn foil	N/A	[30]
9 mol% Zn(dca)$_2$-[C4mpyrr] dca (3 wt.% water)	37%	60 h (0.05 mA/cm²)	0.05 mAh/cm²	Zn foil	N/A	[79]
ZES	99.70%	2000 h (0.1 mA/cm²)	0.05 mAh/cm²	Zn foil (11.7 mAh/cm²)	0.43%	[34]
		100 h (0.1 mA/cm²)	0.5 mAh/cm²	Zn foil (11.7 mAh/cm²)	4.27%	
LZ-DES/2H$_2$O	96.20%	2400 h (0.1 mA/cm²)	0.074 mA/cm²	Zn foil (11.2 mAh/cm²)	0.66%	[33]

จุฬาลงกรณ์มหาวิทยาลัย

CHULALONGKORN UNIVERSITY

CHAPTER 3

CHOLINE CHLORIDE-UREA ELECTROLYTE

Article: Rechargeable Zinc-Ion Battery Based on Choline Chloride-Urea Deep Eutectic Solvent

Author Names: Wathanyu Kao-ian[1], Rojana Pornprasertsuk[2,3], Patchanita Thamyongkit[4], Thandavarayan Maiyalagan[5], Soorathep Kheawhom[1,3,*,z]

Affiliation(s):
[1]Department of Chemical Engineering, Faculty of Engineering, Chulalongkorn University, Bangkok 10330, Thailand
[2]Department of Material Science, Faculty of Science, Chulalongkorn University, Bangkok 10330, Thailand
[3]Research Unit of Advanced Materials for Energy Storage, Chulalongkorn University, Bangkok 10330, Thailand
[4]Department of Chemistry, Faculty of Science, Chulalongkorn University, Bangkok 10330, Thailand
[5]Department of Chemistry, SRM Institute of Science and Technology, Kattankulathur, 603203, Chennai, Tamilnadu, India

[z]Corresponding Author E-mail Address: soorathep.k@chula.ac.th

*Electrochemical Society Member

Abstract

Recently, because of their cost effectiveness, high safety and environmental friendliness, zinc-ion batteries (ZIBs) are receiving enormous attention. Until now, aqueous-based ZIBs have been the focus of attention. However, the issues regarding hydrogen evolution, and zinc electrode passivation as well as dendrite formation limit their practical application. In this work, a biocompatible, stable and low-cost choline chloride/ urea (ChCl/urea) deep eutectic solvent is reported as an alternative electrolyte for rechargeable ZIBs based on delta-type manganese oxide (δ-MnO_2) intercalation electrode. The behavior of the zinc electrode on stripping and deposition in ChCl/urea electrolyte was examined. Besides, the charge storage and charge-transfer characteristics of the battery was studied. The results showed that there was no sign of dendrite formation on the zinc electrode during long-term cycling. Consequently, the fabricated battery exhibited good electrochemical performance with the maximum specific capacity of 170 mAh/g and good cyclability. In addition, the system showed reversible plating/stripping of zinc (Zn) without dendrite formation and no passivation layer on the zinc electrode. Hence, the results confirmed the reversible intercalation of Zn from the deep eutectic solvent ChCl/urea into the δ-MnO_2 electrode. Overall, the proposed electrolyte shows good promise for Zn/δ-MnO_2 battery system.

3.1 Introduction

It is noted that the development of clean, safe and low-cost electrical energy storage systems (ESSs), particularly batteries, has attracted much attention. This is due to an increase in the degree of electrification in various applications, namely portable electronic devices, electric appliances and electric vehicles [122-124]. Although many batteries, such as the lithium-ion battery (LIB), lead-acid battery and nickel–metal hydride battery (Ni-MH), have been commercialized already, they are still expensive. Besides, there are concerns regarding toxic and safety issues and raw material supply [125, 126]. Thus, the challenge for battery development is to find a battery system that meets both economic and environmental demands. Presently, a rechargeable zinc-ion battery (ZIB) using a manganese oxide (MnO_2) intercalation electrode is regarded as the most promising system [127]. This battery can be fabricated via LIB manufacturing process but uses a much cheaper raw material [128].

Compared with other electrode materials, both zinc (Zn) and MnO_2 are abundant, environmentally benign and relatively cheap [129]. Zn also provides a very high specific capacity of 820 mAh/g. In recent years, aqueous-based ZIBs have been the focus of attention. This system exhibits a specific capacity above 200 mAh/g with a nominal voltage around 1.1 - 1.3 V [20]. Besides, ZIBs with aqueous electrolytes have a number of advantages i.e. high-energy density, high-safety and good stability over a large number of cycles and are environmentally friendly. Nevertheless, they suffer from other issues, such as hydrogen evolution, electrolyte decomposition due to low voltage window of aqueous solution (~1.23 V) and Zn electrode passivation which reduces battery performance [130-132]. Therefore, ZIBs using non-aqueous electrolytes, exhibiting a wide operating voltage window and high reversibility of Zn deposition and dissolution, have been proposed to address these issues [133].

A polar-aprotic electrolyte, such as acetonitrile (AN), is one of the most extensively studied [62, 70]. It provides a wide electrochemical window (up to ~3.8 V) and when combined with $Zn(CF_3SO_3)_2$ or $Zn(TFSI)_2$, it offers efficient plating and stripping of Zn (columbic efficiency > 99%) [35]. Sang-Don et Al. (2017) investigated ZIBs using δ-MnO_2 electrode and AN with $Zn(TFSI)_2$ electrolyte [69]. This system delivered a maximum specific capacity of 123 mAh/g and more than 99% of columbic efficiency. However, despite its good performance, it was noted that there was significant capacity fading caused by passivation at the electrode surface. Furthermore, there was a report of using AN with other ZIB systems: e.g. $Zn/ZnAl_xCo_{2-x}O_4$ [62], $Zn/V_3O_7 \cdot H_2O$ [46] and Zn/PBA [70]. Nonetheless, AN was found to be flammable, toxic and very volatile which decreased the overall stability of the batteries.

Another viable alternative electrolyte was to use a room temperature ionic liquid (RTIL) electrolyte which consisted of cations and anions. Over the past decades, RTIL, as an electrolyte, proved to be extremely interesting for the electroplating of metals [134]. RTIL had several attractive properties, such as high ionic conductivity, high electrical stability and low vapor pressure [93]. Traditional RTIL, imidazolium-based ionic liquid, demonstrated a great performance of Zn electrodeposition and an outstanding electrochemical window (above 4 V) [135]. Therefore, it seemed to be a good choice for battery applications. Nevertheless, it proved to be costly and highly sensitive to moisture, making batteries using RTIL infeasible to produce on a large-

scale [136]. There are only a few reports of imidazolium-based RTIL applications as regards ZIBs [137-139].

An alternative class of RTIL, namely a deep eutectic solvent (DES), was formed from a mixture of quaternary ammonium salts i.e. choline chloride (ChCl) and a hydrogen-bond donor. This combination was found to be both air and moisture stable. DES provided many advantages over traditional RTIL since DES was of low toxicity, low-cost and biodegradable [140]. Due to its large metal-salts solubility, ChCl/urea is one of the most promising DES systems which is crucial for efficient platting and stripping of metals and provides a wide electrochemical window (up to ~2.54 V for dry solvent) [92]. Several studies have reported the use of ChCl/urea combined with anhydrous $ZnCl_2$ for the Zn electrodeposition to obtain the nano-porous structure of Zn; some focus on its deposition mechanism [84, 136]. However, the real mechanism of Zn electrodeposition in this system has not been clearly described. The most precious conclusion reached was that the nucleation of Zn during the deposition strongly depended upon the structure of an electrical double layer in the liquid caused by the presence of $ZnCl_2$ [99]. Besides, to the best of our knowledge, the application of DESs in ZIBs has never been reported.

Herein, this study focuses on investigating the performance and feasibility of using ChCl/urea DES as the electrolyte for ZIB with MnO_2 intercalation electrode. In an effort to maximize the performance, delta-type manganese oxide (δ-MnO_2) was chosen for this work due to the crystallographic water inside the δ-MnO_2 structure which has a crucial role in reducing the desolvation energy of intercalation reaction [35]. Furthermore, the stripping and deposition behavior of Zn electrode in ChCl/urea electrolyte was examined. Galvanostatic cycling (charge-discharge), cyclic voltammetry (CV) and electrochemical impedance spectroscopy (EIS) techniques were applied to investigate the charge storage and charge-transfer characteristic of the batteries.

3.2 Experimental

3.2.1 Materials

Choline Chloride ($HOC_2H_4N(CH_3)_3^+Cl^-$, ChCl, 98.0%) was purchased from Sigma-Aldrich. Potassium permanganate ($KMnO_4$, 99.0%), Urea (CH_4N_2O, 98.0%),

zinc sulphate heptahydrate ($ZnSO_4.7H_2O$, 99.0%) and zinc chloride ($ZnCl_2$, 98.0%) were purchased from Ajax Finechem. Dimethylformamide (DMF, 98.0%) was purchased from Sigma-Aldrich. Conductive carbon black (BP2000) was purchased from Carbot Corp. *Manganese(II) sulphate monohydrate (*$MnSO_4.H_2O$, 99.0%) was purchased from QReC. Poly(vinylidene fluoride) (PVDF, MW ~180,000) was purchased from Sigma-Aldrich. Ni-foam (0.5 mm thick, 100 PPI) was purchased from Qijing Trading Co., Ltd. Glass microfiber (Whatman 1822-047 GF/C, 1.2μm) was purchased from Whatman PLC. Carbon cloth (0.35 mm thick) was purchased from SGL Group. Zn sheet (99.99%) was purchased from Sirikul Engineering Ltd., Part.

3.2.2 Electrolyte preparation

The ChCl/urea based deep eutectic solvent was formed by ChCl with urea, at the eutectic composition, in a ratio of 1:2 by moles under controlled temperature of 70 ℃, until it all melted together. The preparation was conducted inside a nitrogen filled glove box (< 0.5 ppm H_2O) to prevent the contamination of moisture from the ambient air. Then, $ZnCl_2$ was added at 0.3 M concentration. The resultant solution was a clear, medium viscous liquid. Herein, the prepared electrolyte is referred as 12CU: 0.3M $ZnCl_2$.

3.2.3 Delta-type MnO_2 preparation

A delta-type manganese oxide (δ-MnO_2) nanosheet was synthesized by a simple hydrothermal method [141]. 0.948 g $KMnO_4$ was dissolved in 35 mL of deionized (DI) water and vigorously stirred. Then, 0.169 g $MnSO_4.H_2O$ was added to the solution and left for 30 min; again, the solution was vigorously stirred. Next, the solution was loaded into a Teflon-lined stainless-steel autoclave and heated at 160 ℃ for 24 h. Subsequently, the product was filtered, washed many times with DI water and then dried overnight at 70 ℃ under vacuum. X-Ray Diffraction (XRD) analysis was used to confirm that the synthesized sample was δ-MnO_2.

3.2.4 Electrode preparation and cell fabrication

δ-MnO_2 electrodes (discharge cathodes) were prepared by slurry mixing of synthesized δ-MnO_2, conductive carbon black, PVDF in a ratio of 7:2:1 by weight in DMF. Then, the slurry was coated onto carbon cloth by a lab coating machine (AOT-FCM-250, AOT Electronic Technology Co., LTD) and dried at 70 ℃ under vacuum. The dry weight of loading material was around 3 mg/cm^2. Zn electrodes (discharge

anodes) were prepared by electrodeposition of Zn from 1 M $ZnSO_4$ aqueous solution onto Ni-foam using Zn sheet as a counter electrode at the current density of 50 mA/cm^2. The weight of zinc loaded was 20 mg/cm^2. Both electrodes were punched into a 15 mm diameter disk. A glass microfiber was punched into a 19 mm disk and used as the separator. Then, 0.3 mL of electrolyte was added to the cell. The testing cells were fabricated as a coin cell (CR2032). The structure of the cell is shown in Fig. 3.1a. During discharge, the Zn electrode serves as the anode whilst MnO_2 electrode functions as the cathode (Fig. 3.1b). Consequently, electrochemical dissolution of the Zn electrode (oxidation of Zn) in ChCl/urea DES occurs; insertion of Zn^{2+} species from the electrolyte takes place at the MnO_2 cathode. In comparison, during recharge, the Zn electrode and MnO_2 electrode function as the cathode and anode, respectively (Fig. 3.1c). Both the extraction of Zn^{2+} species from the MnO_2 electrode as well as the deposition of Zn (reduction of Zn) onto Zn electrode take place simultaneously. Therefore, Zn/Zn^{2+} deposition/stripping on Zn electrode and insertion/extraction on MnO_2 electrode enables the battery to repeatedly store/deliver electrical energy.
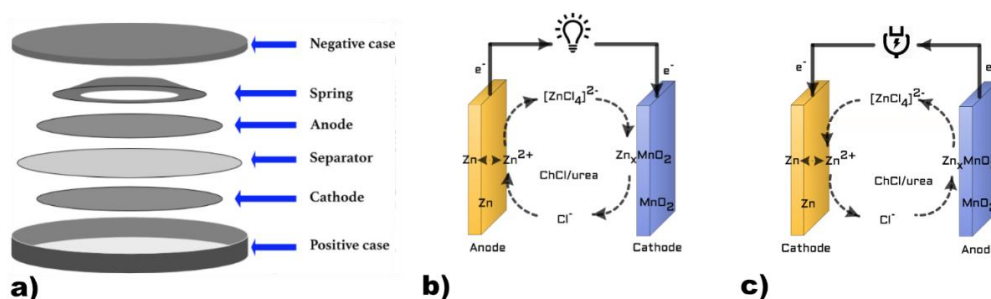
Figure 3.1 Schematic diagram of the battery: a) CR2032 coin cell configuration, b) battery during discharge (Zn anode and MnO_2 cathode), and c) battery during recharge (Zn cathode and MnO_2 anode).

3.2.5 Electrochemical and material characterization

Cyclic voltammetry (CV) and electrochemical impedance spectroscopy (EIS) were performed via a potentiostat/galvanostat with an impedance measurement unit (AMETEK, PAR VersaSTAT 3A). Galvanostatic cycling of the battery was carried out by a battery analyzer (NEWARE BTS-4000 series). The structure and morphology of the electrodes were investigated using a scanning electron microscope (SEM; JEOL, JSM-5800LV). X-ray diffraction analysis was carried out using an X-ray diffractometer (XRD; Bruker, D2 PHA- SER) with Cu Kα radiation at 2θ from 10 to 70˚. To

characterize the electrode after use, the electrodes were disassembled from the cell and washed with DI water repeatedly to remove the electrolyte. Then, the electrode was dried overnight at 70 °C under vacuum.

3.3 Results and Discussions

3.3.1 Zinc plating and stripping

The reversible plating/stripping of Zn is one of the most important aspects of the Zn electrode for ZIBs. The electrolyte ChCl/urea deep eutectic solvent with $ZnCl_2$ contains chlorozincate ($[ZnCl_4]^{2-}$) as a Zn containing species. This species has an important role in the double-layer structure during the Zn deposition process. According to the work of Abbott et.al. (2011) [142], critical concentration of $ZnCl_2$ is required for the deposition of Zn from this mixture. Hence, 0.3 M $ZnCl_2$, which is above the critical concentration, was chosen for our study. The long-term cycling behavior of the Zn electrode was examined using a Zn|electrolyte|Zn cell, where the prepared Zn electrodes were used as both positive and negative electrodes. The cell was cycled for 10 cycles at 0.1, 0.2, 0.5, and 1.0 mA/cm² for 30 min at each current density. The results are displayed in Fig. 3.2a. During cycling, at each current density, the polarization voltage at each current density was bounded by the maximum and minimum voltages. Also, the maximum voltages did not increase upon the cycling indicating that no passivation layer takes place on the Zn surface. In addition, the CV experiment of the Zn electrode was performed using the two-electrode configuration at a scan rate of 10 mV/s and potential range of -0.5 to +0.5 V (vs. Zn/Zn^{2+} in 12CU: 0.3M $ZnCl_2$) using the Zn|electrolyte|Zn cell. In this configuration, the prepared Zn electrodes were used as the working and counter electrodes. Also, the counter electrode was used as the reference electrode. The cyclic voltammogram of Zn plating/striping is shown in Fig. 3.2b. The charge-transfer ratio of plating/stripping between the testing range was calculated to be 0.98, indicating that the deposition and dissolution process is highly reversible. We further investigated the behavior of the long-term cycling behavior of the Zn electrode. The cell was cycled for 150 cycles at 1.0 mA/cm² for 30 min. Fig. 3.2c shows the morphology of Zn deposited after the 150th cycle. The grain size was found to be ~100 nm. This small grain size corresponds to the fast rate of nucleation

whereas the bulk growth was slow [102]. Besides, there was no sign of dendrite formation on the Zn electrode during a long-term cycling.
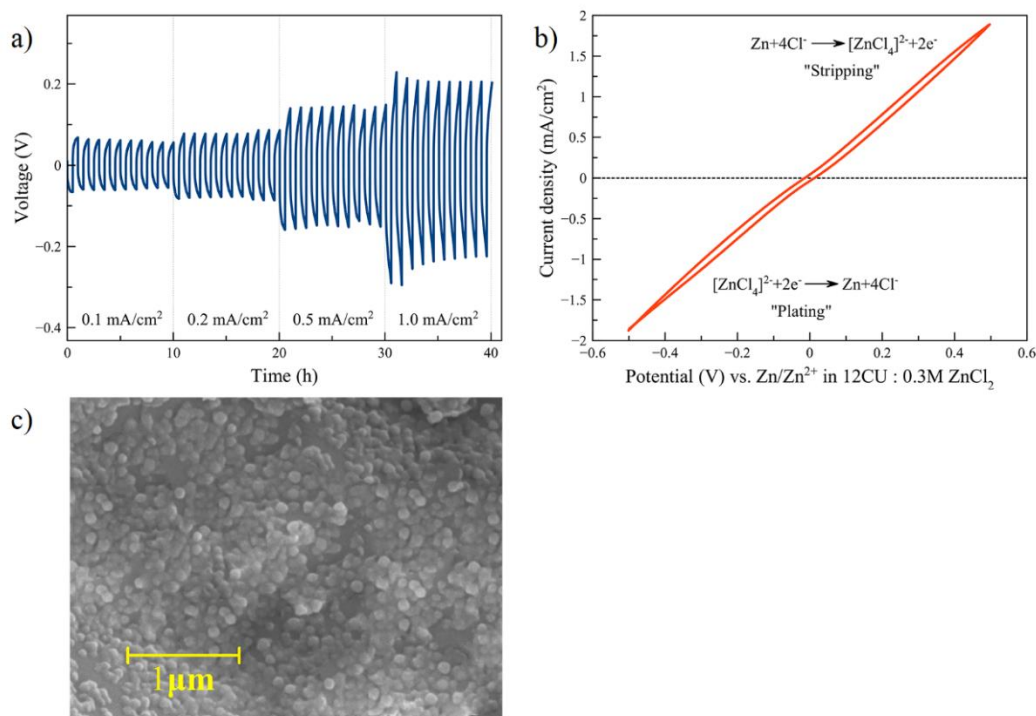
Figure 3.2 Electrochemical performance of Zn stripping and plating (Zn|electrolyte|Zn cell): a) galvanostatic charge-discharge at 0.1, 0.2, 0.5, and 1.0 mA/cm^2, b) CV at a scan rate of 10 mV/s from -0.5 to +0.5 V, and c) SEM image of Zn electrode deposited after the 150th cycle.

3.3.2 Battery performance

A galvanostatic (constant-current) cycling test of the battery was performed using a Zn|electrolyte|δ-MnO$_2$ cell. In this cell, the prepared Zn electrode was used as the negative electrode whilst the prepared δ-MnO$_2$ was used as the positive electrode. The battery exhibited an open-circuit voltage of ~1.5 V as-prepared. The rate performance test was conducted by discharging the battery until it reached the lower cut-off voltage of 0.4 V. Then, charging continued until it reached a higher cut-off voltage of 1.9 V. The cell was tested at various current densities of 50, 100, 150, and 200 mA/g of δ-MnO$_2$ for 10 cycles at each current density. Fig. 3.3a illustrates the rate performance of the battery from the 1st cycle to the 50th cycle. The cell exhibited an initial discharge capacity of 170 mAh/g while the capacity at the 2nd, 3rd, 4th and 5th

were 133, 114, 99 and 92 mAh/g, respectively. Thus, in the 10th cycle, the capacity reached a stable plateau at ~90 mAh/g. The large capacity, fading in the first five cycles may be due to the high solubility of δ-MnO$_2$ in the electrolyte (493 ppm at 60°C) [143]. Unfortunately, there is no reported of such a value at ambient temperature. However, the dissolution of cathode materials could change the surface structure and the surface properties by forming SEI layer which lead to the less reversibility of the cathode reaction [144]. In comparison to other Zn|δ-MnO$_2$ cells previously reported, the proposed ChCl/urea system exhibited the maximum specific capacity of 170 mAh/g which was found to be significantly higher than that of the non-aqueous AN/Zn(TFSI)$_2$ system (123 mAh/g, 0.05-1.9V) [69]. However, it was lower than that of the aqueous-based system (252 mAh/g, 1.0-1.8V) [145]. The higher capacity of the aqueous-based system was due to the conversion reaction of Zn^{2+} with MnO$_2$ to form Mn(III) species, such as ZnMn$_2$O$_4$ which has poor reversibility. Moreover, the operating voltage of aqueous-based system is astride the water voltage window (~1.23V) [131], thus the charge transfer of this system may contribute with water decomposition, these have led to the significant degradation of the cell upon the cycling.

The capacity, observed at different current densities, was 72 mAh/g at 100 mA/g, 63 mAh/g at 150 mA/g and 51 mAh/g at 200 mA/g. Subsequently, the current density was switched back to 50 mA/g. Thus, the capacity was found to be 85 mAh/g which was slightly lower than the value observed at the 10th cycle.

Fig. 3.3b shows the cycling behavior of the cell at the current density of 100 mA/g. During cycling, a slight decrease in the capacity was observed. The fading rate was calculated to be 0.7% per cycle. This capacity loss may correspond to the change in the contact surface between the δ-MnO$_2$ electrode materials and the current collector after a long-term cycling. Compare with such systems in aqueous ZnSO$_4$ and AN/Zn(TFSI)$_2$, the fading rate of ChCl/urea system is close to both aqueous and AN. Nevertheless, the primary cause of the capacity fading was reported with different reason, in aqueous ZnSO$_4$ system, the capacity fading occurred from the formation of irreversible ZnMn$_2$O$_4$ at the cathode [145]. While the AN/Zn(TFSI)$_2$ system, ZnMn$_2$O$_4$ was detected, but it was found to be reversible, the fading occurred from the formation of ZnO on the cathode surface [69].

Fig. 3.3c shows the cyclic voltammogram of the δ-MnO$_2$ electrode. The CV experiment was conducted on the same battery at the 10th cycle with the potential range from 0.4 to 1.9 V and a scan rate of 0.5 mV/s in order to observe the charge-transfer characteristic of the δ-MnO$_2$ electrode. Also, the CV experiment was carried out using the two-electrode configuration where the positive (δ-MnO$_2$) electrode and the negative (Zn) electrode were connected as the working and the counter electrodes, respectively. Besides, the counter electrode was used as the reference electrode. The reduction reaction started from the open-circuit potential of 1.69 V and reached the peak at 0.97 V; this may be attributed to the insertion of Zn^{2+} into the MnO$_2$ host material. Subsequently, the oxidation peak occurred at 1.51 V which refers to the Zn^{2+} extraction from the δ-MnO$_2$ host material. In addition, the high background current may correspond to the high capacitance effect during the charge-transfer reaction. This characteristic is consistent with the results, as observed in Fig. 3.3d. At low current density, the cell behaved like a typical metal-ion intercalation battery, while at high current density, the voltage is linearly proportional to the capacity (capacitor-like behavior) [146]. This hybrid behavior of the latter corresponds to the electrolyte structure. As an ionic liquid contains various cations and anions, the adsorption of unreacted-species onto the electrode surface resulted in the high capacitance current. The polarization of voltage, with respect to the specific capacity, was observed to be steeper as compared with the aqueous-based system. This was due to higher overpotential when the reaction occurred and corresponds to the lower ionic conductivity in contrast to the aqueous electrolyte.

Also, as shown above in Fig. 3.3d, only one discharge plateau is depicted, indicating that there was just one reaction occurring on the δ-MnO$_2$ electrode, similar to that observed in the AN/Zn(TFSI)$_2$ system. In comparison, the aqueous-based system involved two discharge plateaus [145]. The first one was Zn intercalation which formed a layered Zn$_x$MnO$_2$. The second one was the conversion reaction which produced ZnMn$_2$O$_4$.
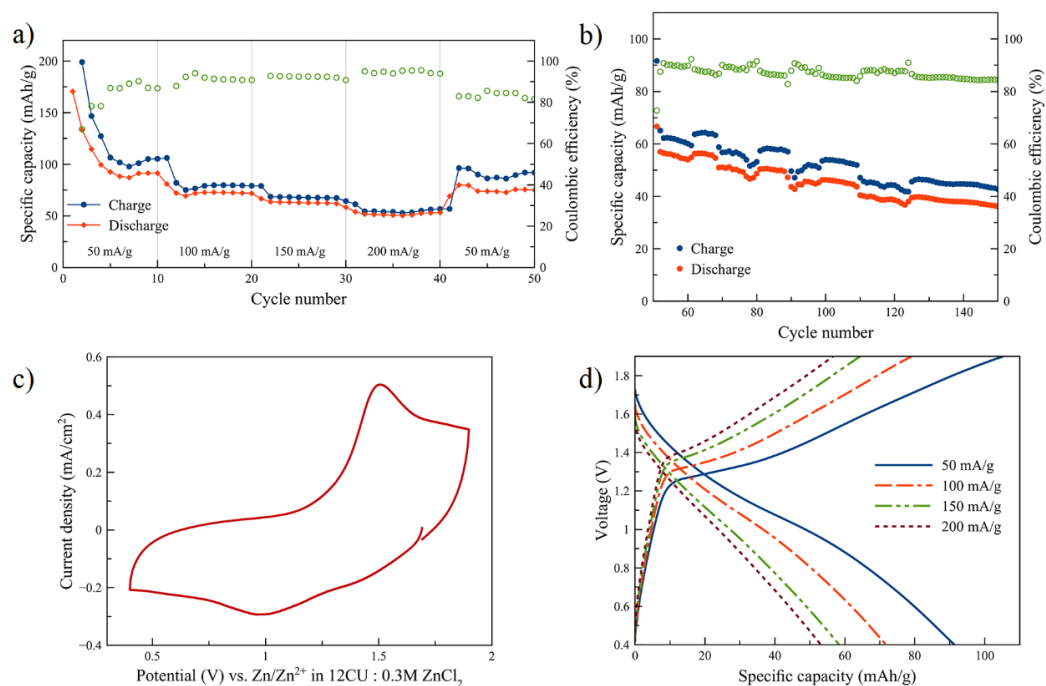
Figure 3.3 Electrochemical performance of the battery (Zn|electrolyte| δ-MnO$_2$ cell): a) rate performance of the battery at 50, 100, 150, and 200 mA/g, b) cycling behavior at current density of 100 mA/g from 51st to 150th cycle, c) CV at a scan rate of 0.5 mV/s from 0.4 to 1.9 V, and d) charge-discharge profile at 50, 100, 150, and 200 mA/g.

To further investigate the change in the charge-transfer characteristic of the battery, EIS technique was performed using the two-electrode configuration with potentiostatic EIS mode. The EIS experiments were carried out at the as-prepared, at the 1st cycle, and at the 130th cycle of the galvanostatic test, in the frequency range of 100 kHz to 10 mHz and amplitude potential of 10 mV. Fig. 3.4a shows the equivalent-circuit model describing the charge-transfer characteristic of the cell. In this model, the first horizontal-axis intercept (R$_0$), the high-frequency semicircle (R$_1$, CPE-1), the low-frequency semicircle (R$_2$, CPE-2) and the 45° inclined-straight line (W) can be assigned to: the internal resistance, the reaction at negative electrode, the reaction at positive electrode and the diffusion of Zn species in the δ-MnO$_2$ electrode materials, respectively [147]. As shown in Fig. 3.4b, it is important to note that the size of R$_1$ and R$_2$ refers to the charge-transfer resistance of the negative and positive electrode. Besides, the size of W (Warburg coefficient) is inversely proportional to the square root of guest-species diffusivity in the host materials. The interested parameters which included R$_0$, R$_1$, R$_2$ and W were determined via ZSimpWin version 3.20. The modeling

results are shown in Table 3.1. According to the impedance spectra shown in Fig. 3.4c and the parameters presented in Table 3.1, after the first cycle, the diameters of the low-frequency semicircle (or R_2) and W decreased. It implies that there was a lowering in activation energy of Zn insertion caused by better mass transport in the δ-MnO_2 electrode, while R_0 and R_1 were almost the same. After the 130th cycle, all parameters were observed to be higher than those of the 1st cycle. The increase in R_0 related to the change in electronic contact, such as the deterioration of the polymeric binder which binds the active materials and the current collector together. The change in R_1 may correspond to the change in the morphology of Zn surface after the long cycling. However, the increase in R_2 and W may be due to the fact that some part of the intercalated electrode was not reversed back when charging. Therefore, the amount of the available site for the intercalation of Zn^{2+} species was degraded. Further EIS experiments of the cell at fully charged and discharged state were conducted. The results are as shown in Fig. 3.4d. At discharge state, the low-frequency semicircle increased in size more than those at fully charged state. Moreover, the length of the inclined-straight line was found to be longer, indicating that the charge-transfer resistance R_2 increased while the diffusivity decreased when the intercalated electrode took place. Thus, it is deduced that the irreversible intercalated part had an important role in the increase of R_2, resulting in the capacity fading upon cycling.

Table 3.1 EIS parameters obtained by fitting the data to equivalent circuit models.

Conditions	R_0 (10^{-1} Ω)	R_1 (Ω)	R_2 (10^{-2} Ω)	W (10^{-2})
As prepared	1.699	8.065	1.430	1.113
Fully charged (1st)	1.795	7.217	0.319	0.743
Fully charged (130th)	2.635	10.270	1.081	1.745
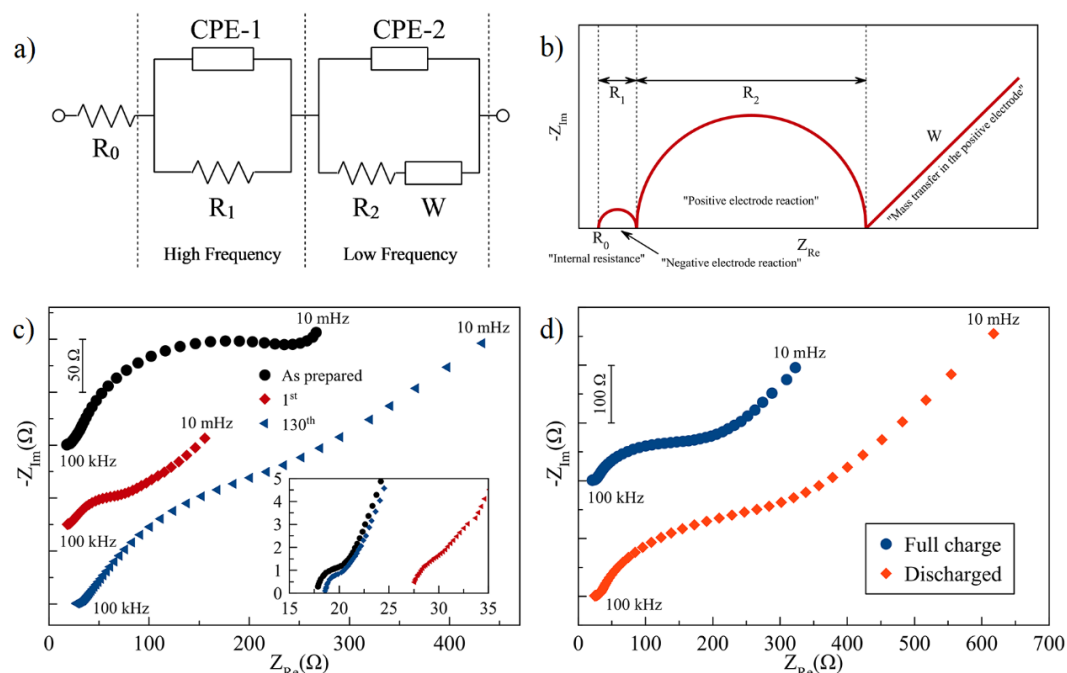
Figure 3.4 Potentiostatic impedance spectra of the δ-MnO$_2$ electrode with testing frequency range of 100 kHz to 10 mHz and amplitude of 10mV: a) equivalent circuit used to simulate the impedance spectra, b) schematic diagram describing the component of impedance spectra, c) EIS of the before/cycled electrode, and d) EIS of the fully charged and discharged electrode at the 10th cycle.

For supporting the hypothesis that we have made on EIS investigation, SEM was used to investigate the change of the δ-MnO$_2$ electrodes surface after for 5th and 150th cycle, the results shown in Fig. 3.5a and Fig. 3.5b, respectively. After long cycling, the cracks are clearly seen which can indicate to the destruction of polymer binder upon the cycling, while the nanostructure of the cathode materials are not significantly change. It means the change in the charge storage performance of battery may resulting from the cracking of the binding materials rather than the structural change of the δ-MnO$_2$ particles. The cracking of cathode affects the electronic conductivity of the cell which results in the increase of overpotential, hence, while the cut-off voltage of the Galvanostatic tests are remain constant. There was some part of the cathode materials that not reverse back after charging process, this may lead to the significant fading of the capacity after long cycling. The summing-up of this section is consistent with such on the EIS investigation.
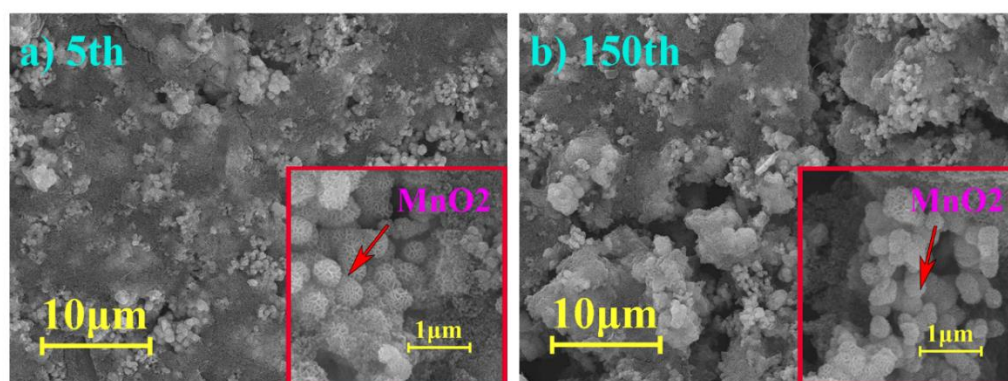
Figure 3.5 SEM image of δ-MnO$_2$ electrodes at a) 5th cycle and b) 150th cycle.

Fig. 3.6a shows the XRD pattern of the prepared δ-MnO$_2$ nanosheet. The characteristic peaks i.e. (001), (002), (11-1) and (31-2), observed at 2θ, were namely, 12.5°, 25°, 36.5° and 65.3°, suggesting the sample is δ-MnO$_2$ [141]. Furthermore, the as-prepared electrode was characterized. The observed additional peaks at 26° and 43° are ascribed as the characteristic peaks of the current collector, such as carbon cloth [148]. The δ-MnO$_2$ electrodes were collected from the cell at fully charged and discharged state of the 10th cycle, for the ex-situ XRD experiments in order to observe the structure changing upon the discharging. According to Fig. 3.6b, after discharge, the intensity of the characteristic peaks of δ-MnO$_2$ at (001) and (002) decreased significantly. In addition, a small shift back of the peak (11-1) was observed. This may correspond to the change in the unit cell parameters. Nonetheless, the overall structure is still almost the layered structure. Besides, the peaks of ZnMn$_2$O$_4$ were not observed. Thus, the behavior of Zn intercalation on the MnO$_2$ electrode was similar to that of AN/Zn(TFSI)$_2$ system reported by Sang-Don et al. (2017) [69]. Consequently, the existence of the layered Zn$_x$MnO$_2$ was confirmed. Besides, the main reactions of the proposed battery system can be expressed as:

Negative electrode reaction: $x\text{Zn} + 4x\text{Cl}^- \leftrightarrow x[\text{ZnCl}_4]^{2-} + 2xe^-$

Positive electrode reaction: $x[\text{ZnCl}_4]^{2-} + \text{MnO}_2 + 2xe^- \leftrightarrow \text{Zn}_x\text{MnO}_2 + 4x\text{Cl}^-$

Overall reaction: $x\text{Zn} + \text{MnO}_2 \leftrightarrow \text{Zn}_x\text{MnO}_2$
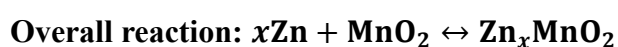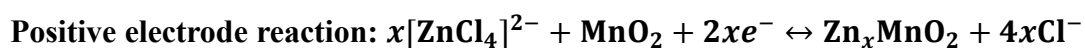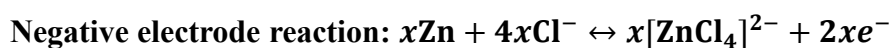
In the proposed system, during discharge, Zn dissolution occurs at the negative electrode. Then, Zn^{2+} coordinates with chloride anion (Cl$^-$) to form [ZnCl$_4$]$^{2-}$, acting as

a charge-transfer species and carrying Zn^{2+} to the positive electrode. Thus, Zn^{2+} at the positive electrode intercalates into the δ-MnO_2 structure and forms Zn_xMnO_2. During recharge, extraction of Zn^{2+} from Zn_xMnO_2 takes place at the positive electrode and forms $[ZnCl_4]^{2-}$. Further, $[ZnCl_4]^{2-}$ transfers across the cell to the negative electrode. At the same time, the deposition of Zn from $[ZnCl_4]^{2-}$ occurs onto the negative electrode. The reaction mechanism is similar to what was reported in AN/Zn[TFSI]$_2$ electrolyte system [35].
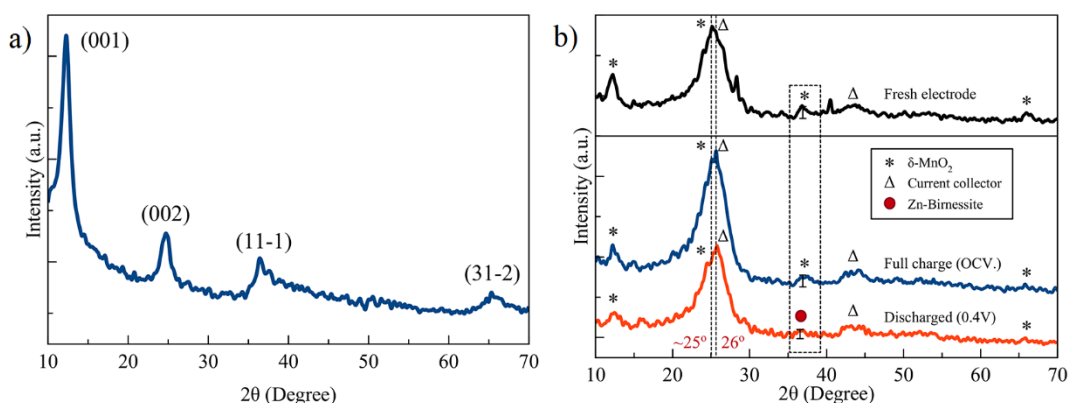
Figure 3.6 The XRD patterns of the positive electrode: a) as-prepared δ-MnO_2 nanosheet, and b) as-prepared electrode, fully charged electrode and discharged electrode.

3.4 Conclusions

In this study, a biocompatible, stable and low-cost ChCl/urea deep eutectic solvent has been reported as an alternative electrolyte for rechargeable zinc-ion batteries based on a δ-MnO_2 intercalation electrode. Herein, the work demonstrated that intercalation of Zn^{2+} from the deep eutectic solvent ChCl/urea into the δ-MnO_2 electrode is reversible. Besides, the formation of the irreversible product $ZnMn_2O_4$, on the δ-MnO_2 electrode during discharging was not observed. Consequently, the fabricated battery exhibited good electrochemical performance, including high specific capacity and good cyclability. In addition, this system showed the reversible plating/stripping of Zn without a sign of dendrite formation and passivation on the zinc electrode. The results indicated that the ChCl/urea electrolyte is promising for the Zn/δ-MnO_2 battery system.

CHAPTER 4

DIMETHYL SULFOXIDE ELECTROLYTE

Article: Highly Stable Rechargeable Zinc-ion Battery using Dimethyl Sulfoxide Electrolyte

Author Names: Wathanyu Kao-ian[1], Mai Thanh Nguyen[2], Tetsu Yonezawa[2,3], Rojana Pornprasertsuk[4,5,6], Jiaqian Qin[6,7], Siwaruk Siwamogsatham[8] and Soorathep Kheawhom[1,6,*]

Affiliations:
[1] Department of Chemical Engineering, Faculty of Engineering, Chulalongkorn University, Bangkok 10330, Thailand; wathanyu.k@student.chula.ac.th (W.K.-i.)
[2] Division of Materials Science and Engineering, Faculty of Engineering, Hokkaido University, Hokkaido 060-8628, Japan; mai_nt@eng.hokudai.ac.jp (M.T.N.); tetsu@eng.hokudai.ac.jp (T.Y.)
[3] Institute for the Promotion of Business-Regional Collaboration, Hokkaido University, Sapporo, Japan
[4] Department of Materials Science, Faculty of Science, Chulalongkorn University, Bangkok 10330, Thailand; rojana.p@chula.ac.th (R.P.)
[5] Center of Excellence in Petrochemical and Materials Technology, Chulalongkorn University, Bangkok 10330, Thailand
[6] Research Unit of Advanced Materials for Energy Storage, Chulalongkorn University, Bangkok 10330, Thailand
[7] Metallurgy and Materials Science Research Institute, Chulalongkorn University, Bangkok 10330, Thailand; Jiaqian.Q@chula.ac.th (J.Q.)
[8] National Science and Technology Development Agency, Pathumthani 12120, Thailand; siwaruk.siw@nstda.or.th (S.S.)

* Correspondence: soorathep.k@chula.ac.th (S.K.)

Abstract

Due to their high safety, low-cost, eco-friendliness and impressive electrochemical performance, rechargeable zinc-ion batteries (ZIBs) show great potential as electrical energy storage devices for large-scale application. Nonetheless, recently developed ZIBs still suffer from low cycling stability and high capacity fading. Such shortcomings are caused by the reversibility of both zinc (Zn) and the cathode host material as well as hydrogen evolution in aqueous electrolytes, which are naturally protic solvent. Herein, dimethyl sulfoxide (DMSO), a polar aprotic solvent, is examined as an electrolyte for a ZIB. Zn stripping/plating in DMSO-based electrolytes shows excellent reversibility and dendrite-free morphology. During charging and resting modes, hydrogen evolution is effectively inhibited. Insertion/extraction of Zn ions in DMSO-based electrolytes into delta-type manganese dioxide (δ-MnO$_2$) demonstrates high stability, achieving a decent initial capacity of 159 mAh/g at 50 mA/g and a nominal discharge voltage of 1.15 V. At 100 mA/g charge/discharge cycling, the ZIB, having the DMSO-based electrolyte, can pass 1000 cycles, displaying a capacity retention of 60%. Overall, improved performance of ZIBs can be attained using DMSO-based electrolytes. Results pave the way towards the practical application of ZIBs.

Keywords: zinc-ion battery; dimethyl sulfoxide; stability; zinc trifluoromethanesulfonate; manganese oxide

4.1 Introduction

Following the increasing trend for renewable energy production and utilization, rechargeable Zn-based batteries are the most promising candidates for a large-scale storage system [149-151]. Zn is cost-effective, non-toxic and abundant [46, 152-155]. Furthermore, Zn exhibits a very high volumetric capacity (5854 mAh/cm^3), which allows a more compact battery design [114]. There are several types of rechargeable Zn-based batteries e.g. Zn-nickel, Zn-air, Zn-bromine and ZIBs [106, 156-158]. Recently, ZIBs using intercalation-type host material, such as vanadium oxide (V$_2$O$_5$) and manganese dioxide (MnO$_2$), have received much attention, after the discovery of the reversible intercalation of Zn-ions from aqueous electrolytes into the tunnel structure of α-MnO$_2$ [20, 159]. ZIBs having MnO$_2$ electrodes demonstrate high specific

capacity (~300 mAh/g) owing to the co-insertion of Zn-ions and protons [160-162]. Furthermore, MnO_2 is abundant and cheap just like Zn, and it increases the feasibility of producing a battery based on Zn/MnO_2, on a commercial scale [163]. Nevertheless, the stability of such a system, with regard to the long-term charge-discharge cycling, remains suspicious [145, 164].

As for aqueous ZIBs, several issues must be addressed. These issues include: (1) the production of gas from the self-corrosion of Zn (2) water decomposition upon charging, and (3) loss of capacity from the irreversible charge-storage reaction of proton insertion [70, 165]. These problems occur due to the acidity of dissolved Zn salts in water, as water is a protic solvent, which can dissociate and provide protons [166]. Most researchers focus on the use of electrolyte additives or coating materials in order to inhibit hydrogen evolution reaction (HER) and suppress dendrite growth in aqueous-based ZIBs [14, 166-168]. Self-corrosion of Zn is one of the most crucial issues, which has not been entirely eliminated [169, 170]. Even a small rate of Zn corrosion can cause serious damage to the battery packaging and can reduce the overall performance of the battery long-term [30, 166].

A viable solution for solving these problems could be achieved through the use of a non-hydrogen donor substance, as a solvent for electrolytes, to prevent the existence of protons in the system [70, 74]. In the literature, however, implementation of this idea is hard to find. Little research has been carried out using non-hydrogen donor solvents i.e. room temperature ionic liquids (RTILs) and polar-aprotic solvents in Zn intercalation batteries [37]. In this field, more work needs to be done. Nevertheless, one example of an RTIL electrolyte, having been used in ZIBs, refers to a choline chloride/urea deep eutectic solvent (DES) having Zn chloride. The system exhibited good reversibility of Zn deposition/dissolution without the problem of dendrite formation and Zn oxide passivation. When compared with other ZIB systems, full-cell performance proved to be deficient due to the low ionic conductivity of this electrolyte [8]. Another RTIL application focused on acetamide and Zn perchlorate room temperature molten electrolytes, which provided high capacity and high thermal stability. The high charge-transfer resistance of the Zn electrode within this system resulted in the inferior rate capability of the battery. [93].

Compared with RTIL, polar-aprotic solvents are more accepted in battery applications. Several researchers have proposed the use of polar-aprotic solvents, instead of aprotic solvents, to avoid the production of hydrogen from both self-corrosion of Zn and HER [2, 37]. A well-known solvent acetonitrile (AN), in combination with various uncommon Zn salts viz. Zn perchlorate ($Zn(ClO_4)_2$), Zn trifluoromethanesulfonate ($Zn(OTf)_2$), and Zn bis(trifluoromethylsulfonyl)imide ($Zn(TFSI)_2$), has been used as a ZIB electrolyte [62, 66, 70]. All the solutions mentioned above have been utilized along with several intercalation host materials as follows: MnO_2, $ZnAl_xCo_{2-x}O_4$, $V_3O_7·H_2O$ and potassium nickel hexacyanoferrate ($K_{0.86}Ni[Fe(CN)_6]_{0.954}(H_2O)_{0.766}$) [62, 69, 70].

Despite the widely compatible, dendrite free Zn after cycling and complete hydrogen inhibition, the electrolyte based on AN has several disadvantages, being highly volatile, non-eco-friendly and highly toxic [171]. In addition, its large overpotential and inferior rate capability are also the signature of nonaqueous batteries when compared with aqueous-based batteries. This is a consequence of the large activation energy of intercalation reaction due to the large desolvation penalty of the solvated Zn species in nonaqueous electrolytes [1, 46]. The performance of intercalation electrodes in nonaqueous electrolytes strongly depends on its interfacial properties which results in the increase or decrease of the desolvation penalty. It has been reported that the water molecule inside the delta-type MnO_2 (δ-MnO_2) structure could reduce the desolvation energy of a very strong electrostatic forced magnesium solvated species upon the intercalation reaction in aqueous and even in wetted nonaqueous electrolytes [172]. Thus, δ-MnO_2 is an interesting choice for nonaqueous ZIBs. This concept has also been applied in a ZIB having a $Zn(TFSI)_2$/AN electrolyte [69]. However, it attained only 123 mAh/g of maximum capacity and exhibited modest cycling stability due to the formation of a passivation layer on the cathode material.

The strong polarity aprotic solvent: namely, dimethyl sulfoxide (DMSO) is a promising candidate for use as an electrolyte. This is because of its high dielectric constant (46.45), higher than 35.95 of AN at 20 °C, its high donor number, wide electrochemical window (-2.9 to +1.5) V, high boiling point (189 °C at 1 atm) and low toxicity in comparison with other solvents [173]. DMSO has been applied in several

works regarding battery development. The use of DMSO, as an additive, in an alkaline electrolyte of a rechargeable Zn-air battery (ZAB) demonstrates that it can improve performance and cyclability of a ZAB, by inhibiting Zn oxide passivation and HER [174]. DMSO has also been applied in a lithium-air battery (LAB), as an electrolyte, and exhibited excellent electrochemical performance and great stability [175].

Only a few works have been found regarding other intercalation electrodes [176, 177]. In a study of Zn intercalation on $Zn_xMo_{2.5+y}VO_{9+z}$ from the DMSO/propylene carbonate electrolyte, it is seen that this couple provided a large specific capacity due to a highly open tunnel structure of $Zn_xMo_{2.5+y}VO_{9+z}$ [178]. Yet, the low voltage and inferior rate capability limit their real scale application. Ryan et al. (2020) reported the use of DMSO combined with Zn trifluoromethanesulfonate ($Zn(OTf)_2$) in a Zn/α-MnO_2 battery [74]. According to this report, the battery having a DMSO-based electrolyte was found to be more stable than that of an aqueous electrolyte. Nonetheless, more proof is required as to the feasibility of using it in a ZIB system.

In this paper, the application of a DMSO-based electrolyte in ZIBs, using a MnO_2 cathode, is duly investigated. Despite its superior features as a main solvent and additive for several works, no true application of DMSO in a ZIB, based on MnO_2 cathode, has been substantiated previously. Herein, our work is new and authentic. Our current findings expand upon prior work of which there is scant evidence. Stripping and deposition behaviors of Zn, at the anode, within the DMSO-based electrolyte as well as its electrochemical performance of a symmetrical-Zn cell, are examined. Consequently, reactions at the cathode (δ-MnO_2), which focus on several aspects, including electrochemical behavior, crystallography and electrochemical performance, are studied. Different techniques for battery testing and characterization, such as galvanostatic test (charge-discharge), cyclic voltammetry (CV), electrochemical impedance spectroscopy (EIS), X-ray diffraction spectroscopy (XRD) and scanning electron microscopy (SEM) are applied. All experimental procedures are given in the supplementary information (Appendix A). Results suggest high reversibility of Zn stripping/plating and insertion/extraction of Zn-ions into/from the MnO_2 structure in DMSO. It is evident that DMSO-based electrolytes can enhance battery performance and stability.

4.2 Results and Discussion

4.2.1 Electrochemical behavior of Zn anode

CV was carried out using different vertex potentials to determine the onset potential of Zn deposition on a platinum (Pt) working electrode. In Fig. A3a, the cell configuration is shown. The vertex potentials examined were within the stability window of DMSO, which was reported as (-2.9 ~1.5) V vs. saturated calomel electrode (SCE) or (-2.85~1.55) V vs. silver/silver chloride (Ag/AgCl) reference electrode. From this potential range, the starting point and the ending point were set at 1.55 V vs. Ag/AgCl. As the standard electrode potential of Zn is -0.957 V vs. Ag/AgCl, the vertex potentials were arbitrary set at (-1.25, -1.50, -2.00, -2.50 and -2.85) V vs Ag/AgCl.

As shown in Fig. 4.1a, the CVs of the 0.25 M $Zn(OTf)_2$/DMSO system, having different vertex potentials, are displayed. Thus, it is clear that the size and position of the peaks changed. Besides, by proceeding to more negative vertex potentials, both processes of reduction and oxidation were enhanced. The reduction of Zn started at the onset potential i.e. -1.17 V vs. Ag/AgCl, in the negative current region; thus, the current grew continuously until it reached the vertex point. Then, the current returned to the end point via the smaller slope. As for the vertex points of (-1.25 and -1.50) V vs. Ag/AgCl, the growing rate of the current hovered around constant, within the range between onset and vertex point. At the vertex points of (-2.0, -2.5 and -2.85) V vs. Ag/AgCl, during the inclined curve at -1.74 V vs. Ag/AgCl, small peaks appeared. As for the oxidation reaction, it started at -1.03 V vs. Ag/AgCl and rose up constantly within the positive current region to the peak; then, it suddenly dropped.

In the oxidation and reduction region (Fig. 4.1a), the ratios of charge transfer were found to be 0.99, 0.97, 0.61, 0.56 and 0.57 corresponding to the vertex points of (-1.25, -1.50, -2.00, -2.50 and -2.85) V vs. Ag/AgCl, respectively. These ratios represent the contribution of other competitive reactions, such as the decomposition of the electrolyte in the system when a more negative vertex point was applied. The inclined curve that appeared at -1.74 V vs. Ag/AgCl may be ascribed as the starting point of the competitive reactions. During the CV test, there was no sign of bubbling or the production of gas.

In Fig. 4.1b and 4.1c, the CVs under the effects of scan rate and $Zn(OTf)_2$ concentration are shown. Results showed that the scan rate did not strongly affect the recorded CVs, indicating that in the potential window of (-2.85~1.55) V vs. Ag/AgCl, the rate of reaction was found to be dominated by the surface-reaction mechanisms. Moreover, when concentration of $Zn(OTf)_2$ increased, both peaks of oxidation and reduction were enhanced. Hence, results indicated that the main reaction, regarding the deposition/dissolution of Zn, was kinetically controlled. Moreover, the peaks observed, on the oxidation side, were attributed to the depletion of Zn, on the working electrode.

As shown in Fig. 4.1d, the CV test was performed once again, using pure DMSO as an electrolyte. Hence, the CV curve of the pure DMSO was found to be very small in intensity compared with the electrolyte containing $Zn(OTf)_2$; but, within the testing range, it was found to be very broad. When this behavior was compared with the aqueous based electrolyte, it proved to be totally different. This was because the current of the aqueous electrolyte grew exponentially when it reached the onset potential of HER and oxygen evolution, yet remained at zero before the onset [37]. From the results, the CV curve of 0.25 M $Zn(OTf)_2$/DMSO exhibited the ratio of the charge transfer as being only 0.27, indicating that the competitive reactions, e.g. the reduction of the solvent molecules, were greater than the reversible Zn stripping/plating reactions. Thus, this indicated that an excessive amount of $Zn(OTf)_2$ leads to a higher rate of competitive reactions even at low potential. Furthermore, it is seen that the electrolyte started to oxidize at about 1.4 V vs. Ag/AgCl. In practice, the potential of Zn anode in a battery, during charging, does not change much from its open-circuit. [179]. To estimate the feasibility of using this electrolyte in the Zn-based battery, a real battery testing method is required.
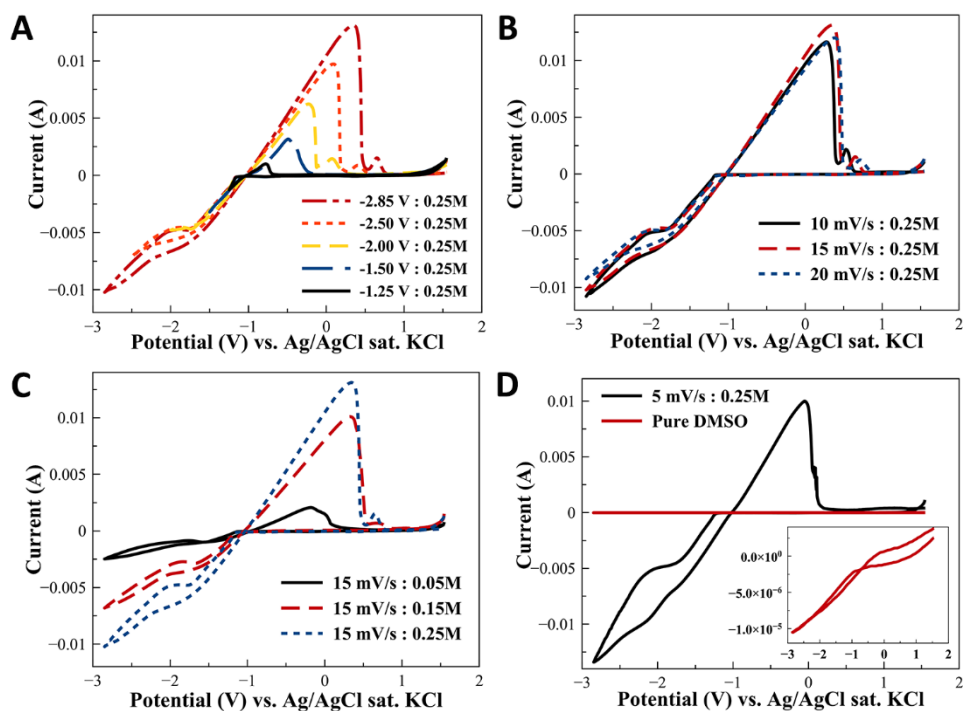
Figure 4.1 Electrochemical data of Zn half-cell. (a-d) The cyclic voltammogram of Pt/Pt cell in which: (a) different vertex potentials were applied within 0.25 M $Zn(OTf)_2$/DMSO electrolyte at a scan rate of 15 mV/s (b) different scan rates were applied within 0.25 M $Zn(OTf)_2$/DMSO electrolyte having a voltage range of (-2.85 to +1.55) V (c) different concentrations of $Zn(OTf)_2$/DMSO were applied at a scan rate of 15 mV/s from (-2.85 to +1.55) V, and (d) pure DMSO and 0.25M $Zn(OTf)_2$/DMSO were used as electrolytes, at a scan rate of 5 mV/s from (-2.85 to +1.55) V.

To observe the cycling behavior and morphology of Zn, for use in a DMSO based electrolyte, a galvanostatic cycling test of a Zn electrode was conducted. Four levels of current densities were applied: (0.1, 0.2, 0.5 and 1.0) mA/cm^2 to the Zn-symmetrical cell (Fig. A3b). Cycling comprised of 15 min charging and 15 min discharging, and was repeated 50 times per current density. At the first cycle (Fig. 4.2a), it was found that the size of the deposition/dissolution voltage, for each DMSO sample, was relatively high: 0.5 V for 0.15 M $Zn(OTf)_2$ and 0.3 V for 0.25 M $Zn(OTf)_2$, compared to the aqueous 2 M $ZnSO_4$ sample (0.1 V). Then, the voltage of the DMSO samples decreased continuously until a stable plateau was reached, close to that of the aqueous sample, around the 30th cycle. This change denotes the change in Zn morphology from the flat surface (Fig. A1c) to the rough surface (Fig. 4.2b and 4.2c), which has a higher surface area. Hence, the energy requirement for the redox reaction

of Zn would be lower than that of the flat surface [180]. This behavior was also found in the Zn deposition/dissolution in $Zn(OTf)_2$/Triethyl phosphate (TEP) [61]. In terms of cycling stability, after 30th cycle, both the DMSO-based electrolyte and the aqueous-based electrolyte were found to be very stable. This stable trend continued for at least 200 cycles. Subsequently, when the deposition/dissolution voltage of the aqueous sample was compared with the DMSO-based sample, at the current density of (0.5 and 1.0) mA/cm^2, a clear gap was found. This was owing to the slower kinetic reaction of the Zn surface within the organic solvent. Nevertheless, this difference could be compensated by increasing the concentration of $Zn(OTf)_2$ in DMSO, which resulted in the lower deposition/dissolution voltage (Fig. 4.2a); wherein the concentration of $Zn(OTf)_2$ was 0.25 M.

As presented in Fig. 4.2, the morphology of Zn, which evolved during the cycling test (at 1.0 mA/cm^2) was examined by SEM. Thus, the morphology of Zn was found to be a large boulder ($>20\mu m$) having several hexagonal-like structures. It is noted that these structures (Fig. 4.2b and 4.2c) proved to be similar to those obtained in the $ZnSO_4$ aqueous system, at high current density: (20-40) mA/cm^2 [132]. Results confirmed that no Zn dendrite growth took place. The Zn obtained from $Zn(OTf)_2$/DMSO was different from the Zn nanolines obtained via $Zn(TFSI)_2$/AN, a cage-like porous Zn from $Zn(OTf)_2$/TEP and a nanosphere from the $ZnCl_2$/ChCl-Urea DES in terms of morphology [35, 61, 69]. Interestingly, all morphologies of Zn, which are formed from nonaqueous electrolytes, have no dendrite formation. When the voltage is similar, the current density obtained during deposition/dissolution from nonaqueous electrolytes is lower than that of aqueous electrolytes due to their higher charge-transfer resistance [1]. Besides, at the same current density, the Zn deposited from the aqueous $ZnSO_4$ ends up as small loose hexagonal grain ($< 5\mu m$), which has a high surface area (Fig. 4.2d). Nonetheless, when the grain is very loose, the Zn can fall off from the bulk electrode (dead Zn); and as a result, there is a severe loss of capacity [170].

Having a good deposition/dissolution voltage and no dendrite formed during plating are important requirements for the Zn as an anode. Using the galvanostatic method, the plating efficiency of Zn in DMSO electrolyte was also investigated; details

of the test and results are given in the supplementary file (Appendix A, Fig. A6). Besides, the promising solvent for nonaqueous Zn-based batteries such as TEP was tested along with DMSO, at the same $Zn(OTf)_2$ concentration (0.25 M). In Fig. A6a, it was found that the plating efficiency i.e. Zn utilization percentage of the DMSO sample, first cycle, reached 71.0% As for the TEP sample, it was found to be 55.9% It is seen that both samples, DMSO and TEP, were growing continuously and reached a stable plateau around the 80th cycle. Thus, the average plating efficiency of the two samples at the stable plateau was 99.6% and 99.4%, respectively. Such high results reveal the compatibility of the DMSO with that of TEP.

In Fig. A6b and A6c, it is observed that the charge –discharge voltage of both DMSO and TEP sample evolved along with the cycle number. Thus, after charging for 300 s, the voltage gap between zero-line and the charging profile of DMSO and TEP sample proved to be 51 and 296 mV. This huge difference in voltage gap between the two samples indicates the lower plating energy of Zn in DMSO electrolyte than that of TEP. Such an outcome may result from the difference in their ionic conductivity. Fig. A5b reveals that the ionic conductivity of DMSO i.e. 0.25 M $Zn(OTf)_2$ is more than twice that of TEP.

During charging and resting modes, the production of hydrogen was studied; details of the test are given in the supplementary file (Appendix A). As shown in Fig. 4.2f, it is clear that no hydrogen was produced during the Zn deposition and dissolution in the DMSO-based electrolyte. As seen in Fig. 4.2h, the hydrogen produced from the self-corrosion of Zn was effectively eliminated in this electrolyte system. These results confirmed the advantages of this electrolyte over the aqueous-based electrolyte, by improving the stability of the Zn electrode.
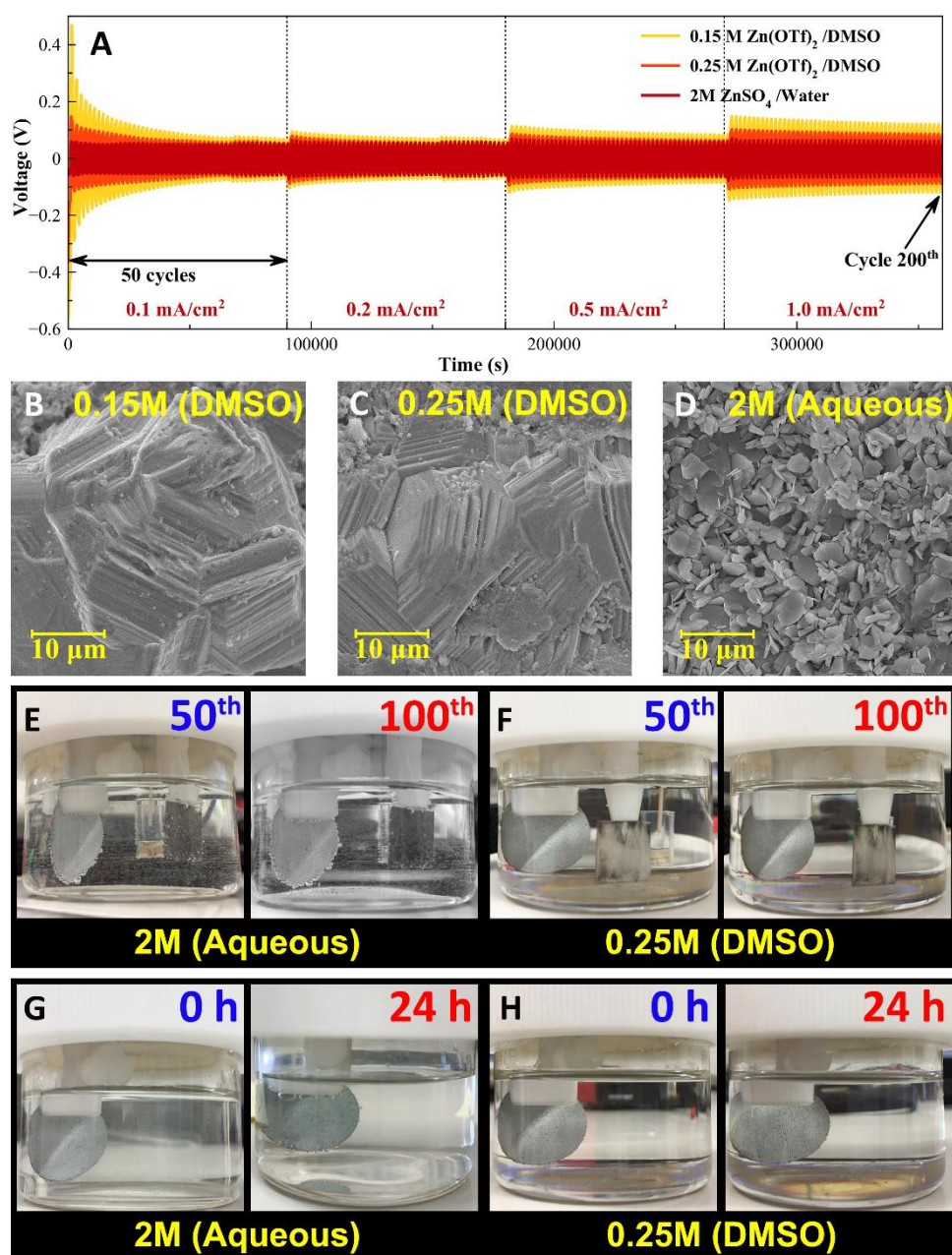
Figure 4.2 Galvanostatic cycling results of symmetrical-Zn cells and their SEM images. (a) The galvanostatic charge-discharge profile of all electrolytes at 0.1, 0.2, 0.5, and 1.0 mA/cm^2. (b-d) SEM image of cycled electrode (1 mA/cm^2) when the electrolyte was: (b) 0.15 M Zn(OTf)$_2$/DMSO (c) 0.25 M Zn(OTf)$_2$/DMSO, and (d) aqueous 2M ZnSO$_4$. (e-f) The picture of three-electrode cell during multiple CV test ($\pm$0.2 V vs. OCV, 15 mV/s) at 50th and 100th cycle, when the electrolyte was: (e) 2 M ZnSO$_4$/Water and (f) 0.25 M Zn(OTf)$_2$/DMSO. (g-h) The picture of Zn electrode soaking in electrolyte at 0 h and 24 h, when the electrolyte was: (g) 2 M ZnSO$_4$/Water and (h) 0.25 M Zn(OTf)$_2$/DMSO.

4.2.2 Electrochemical behavior of δ-MnO₂ cathode

The electrochemical investigation for the δ-MnO₂ cathode reaction was carried out via CV technique (two-electrode setup) at three scan rates: (0.2, 0.3 and 0.5) mV/s within the potential range of (0.75 to 1.8) V. The cell for this test was fabricated by the configuration, as shown in Fig. A3b. In this experiment, the δ-MnO₂ cathode (δ-MnO₂ electrode) was assigned as a working electrode, while the counter-reference paired electrode was a Zn electrode. The electrodeposited Zn on the nickel/copper cloth was used as an anode, instead of Zn foil, in order to lower the voltage polarization effect from the reaction of Zn, as it had a much higher surface area due to its 3-dimensional structure. As observed in Fig. A8a, two anodic peaks (ID.1 and ID.2) can be seen as well as one cathodic peak (ID.3). These peaks correspond to the charge-storage reaction of δ-MnO₂ (working electrode). In general, the reaction mechanism of the wet-electrochemical system is diffusion-controlled reaction, capacitive reaction or the combination of these two [181]. Fig. A8b depicts the plot of log i versus log v and the calculated b-value. It was found that for peaks ID.1, 2 and 3, the corresponding b-values were 0.7347, 0.4682 and 0.6339, respectively. It is seen that the b-value of peaks ID.1 and ID.3 were greater than the value (0.50), which means they are a mixture of diffusion-controlled and capacitive processes. Furthermore, this implies that reactions, which correspond to these peaks, occurred at the solid-liquid interphase, as they have the contribution of the capacitive process in their resulting current. Peak ID.2 is pure diffusion-controlled ($b \approx 0.5$) which indicates that this process was free from the effect of a capacitive-double layer. Hence, this reaction may occur in the solid phase.

In Fig. A8c and A8d, results are shown. It was found that at a scan rate of (0.2, 0.3 and 0.5) mV/s, the percentages of capacitive contribution were 76, 82 and 94, respectively. In comparison with those in the aqueous ZnSO₄ system, these values are relatively high [109, 182]. This indicated slower diffusion-controlled reaction of the δ-MnO₂ cathode in the DMSO-based electrolyte compared with the aqueous-based system [183]. Thus, when there is a high rate of discharging and charging, the charge-storage process within the DMSO-based cell is dominated by capacitance reaction, at a higher ratio than what it would be in the aqueous-based system. When the applied current density is increased, it may also result in higher capacity polarization.

Next, the Zn/δ-MnO$_2$ cell, having the 0.25 M Zn(OTf)$_2$/DMSO electrolyte, was further tested, using the galvanostatic cycling method in order to determine its performance and stability. This test was comprised of four steps: rate capability test round 1 (RC1), cyclability test round 1(C1), rate capability test round 2 (RC2) and cyclability test round 2 (C2), respectively. The rate capability tests employed a current density of (50, 100, 150, 200 and 100) mA/g in series (each current density ran for 10 cycles: 50 cycles in total). As for the cyclability tests, current density was 100 mA/g (450 cycles for each cyclability test). All tests were carried out within the voltage range of (0.75-1.8) V. In Fig. 4.3, results are shown. The initial discharge capacity during RC1 was found to be 159 mAh/g. During the first 10 cycles (50 mA/g), it was almost stable at 151 mAh/g. It was noted that the discharge capacity of this system at the first cycle (159 mAh/g at 50 mA/g) was lower than that of Zn/δ-MnO$_2$, in the aqueous ZnSO$_4$ system (>200 mAh/g), as well as the other nonaqueous ZIBs based on MnO$_2$ (Table A2) [108, 145, 184, 185]. This outcome may be due to the lack of proton contribution in the charge-storage reaction at the δ-MnO$_2$ cathode, which occurred as a result of the proton-free electrolyte. Besides, the single plateau of the discharging voltage profile as well as the single reduction peak of δ-MnO$_2$ in the CV test confirmed that only one reaction was involved in the discharging process. Subsequently, discharge capacity changed and was found to be stable at (132, 118, 108 and 131) mAh/g corresponding to the current density of (100, 150, 200 and 100) mA/g, respectively. In Fig. 4.3b, the voltage polarization profiles, for each current elevation, are shown. On account of this rate performance, the battery demonstrated high-power density and high energy density among the nonaqueous Zn intercalation batteries (Fig. A12).

As seen in Fig. 4.3a, when the first step of C1 was reached, specific capacity was found to be 128 mAh/g. Then, it slowly decreased until it reached 81 mAh/g at the 500th cycle (63 % of C1 initial). Next, as seen in Fig. 4.3d, specific capacity was found to be (93, 78, 63, 50 and 83) mAh/g at (50, 100, 150, 200 and 100) mA/g. Thus, it was clear that specific capacity dropped in comparison with the results as seen in RC1. These results point to the degradation of the battery performance after long-term cycling. During C2, as seen in Fig. 4.3e, it was observed that capacity fading was relatively low in comparison with C1. Eventually, at the end of C2 (1000th cycle),

capacity reached 77 mAh/g (60 % of C1 initial). At this point, the fading rate was calculated to be approximately 0.047% per cycle. This proved that the battery demonstrated far greater stability than most of the AN-based and RTIL-based ZIBs (Table A2).

According to Fig. 4.3a, A11a and A11b, the average coulombic efficiency, during RC1, was (96.1, 97.6, 98.4 and 99.0) % at a current density of (50, 100, 150 and 200) mA/g, respectively. During C1, it was 95.6%. Then, when 500th cycle was reached, upon RC2, it was (86.0, 96.4, 98.6 and 100.0) % at (50, 100, 150 and 200) mA/g. Finally, after 551st cycle up to 1000th cycle, during C2, it was 95.1%. The break-even coulombic efficiency at low current density may arise from the high fraction of the solid-liquid capacitive process during charging, which was confirmed by the capacitive contribution result from CV test. This high fraction can lead to loss of capacity during the long period of discharging as a result of self-discharge [186, 187].
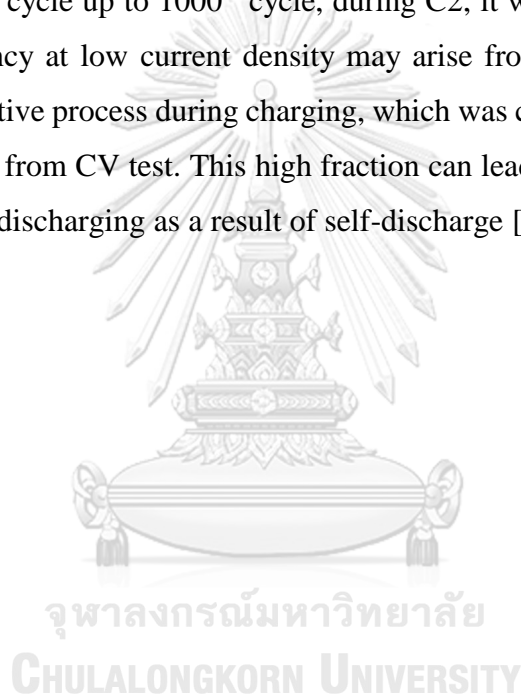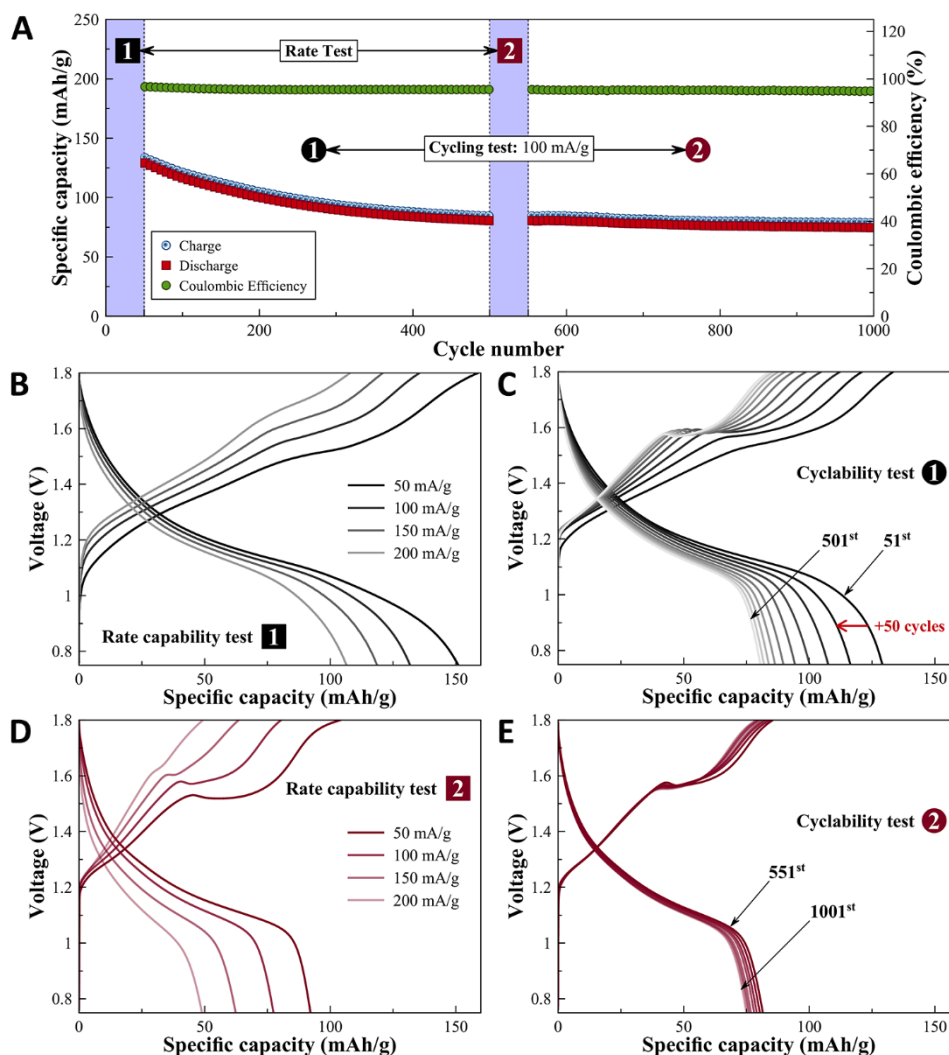
Figure 4.3 The appearance performance of Zn|0.25 M Zn(OTf)$_2$/DMSO |δ-MnO$_2$ cell: (a) specific capacity versus number of cycles (b) voltage polarization at different current densities during rate capability test 1 (RC1) (c) voltage polarization during cyclability test 1 (C1) (d) voltage polarization at different current densities during rate capability test 2 (RC2), and (e) voltage polarization during cyclability test 2 (C2).

4.2.3 Battery investigation

Despite the impressive performance and stability of the battery based on this electrolyte system, as seen in the cell testing, it is also crucial to find out the real reaction mechanism of the battery as well as the cause of degradation within this system. As determined by the galvanostatic test, capacity fading materialized during the long cycling. In general, the fading problem mostly occurred from degradation of the δ-MnO$_2$ cathode [179]. Thus, the change in the δ-MnO$_2$ electrode was inspected via ex-

situ XRD and SEM, at different cycling positions viz. as-prepared, 5th cycle and 200th cycle. Furthermore, in order to identify the reaction type of the δ-MnO$_2$ in this electrolyte system, XRD was also performed at different states of the battery (Full charge and Discharged).

As shown in Fig. 4.4a, the bare electrode curve contains characteristic peaks of the δ-MnO$_2$ nanosheet: namely, (001), (002), (11-1) and (31-2) corresponding to 2θ of (12.5, 25.0, 36.5 and 65.3) degree, respectively [145]. Peaks at 2θ of (18.2, 26.7, 29.5, 31.5, 36.0, 39.5, 43.3, 47.6, 48.6, 54.8, 57.5, 61.1, 64.8, 65.8 and 69.5) degree were also observed, which corresponded to the carbon paper (current collector). After being preconditioned and cycled for 5 cycles, all peaks still existed in the XRD curve. Nevertheless, changes in intensity of the δ-MnO$_2$ peaks were observed i.e. (001), (002) and (11-1), which significantly dropped when compared with the bare electrode, while the others remained about the same. This occurred due to the dissolution of δ-MnO$_2$ in the DMSO-based electrolyte. Generally, MnO$_2$ does not dissolve in anhydrous DMSO [188]. It is possible that water in the δ-MnO$_2$ structure plays an important role in such phenomena. At the 200th cycle, it is apparent that the intensity of several peaks of the carbon paper decreased quite severely and some peaks totally disappeared. The peaks that disappeared were calcite peaks; calcite is a binder for the carbon paper (Fig. A1a). Thus, after long term utilization, overall electronic resistivity of the δ-MnO$_2$ electrode increased. Such an outcome can lead to the disconnection of some active material from the electron-transfer pathway, which results in significant capacity fading due to the accumulation of the reacted active material. As seen in Fig. 4.4b and 4.4c, even though there was a huge change in the crystallography of the electrode, there was no clear difference in terms of the morphology between the electrode surface of the bare electrode and the 200th cycle. However, underneath the electrode surface major changes occurred.

In Fig. 4.4d, it was found that all components with regard to δ-MnO$_2$, within the XRD spectra of the discharged electrode, were relatively the same, as at full charge state. As shown in Fig. 4.4e and 4.4f, two differences can be seen. The first was the shortening of the (001) peak, and the second was the small shift of the broad (11-1) peak. Such behavior indicated change in the volume of the unit cell viz. of the active

material after discharging, while the overall structure remained the same, as at full charge state [69]. This characteristic is similar to what occurred in the $Zn(TFSI)_2$/ACN and $ZnCl_2$/ChCl-Urea electrolytes, denoting that the reversible reaction of δ-MnO_2 in the $Zn(OTf)_2$/DMSO electrolyte is an intercalation of Zn, when the discharge product is birnessite-like Zn_xMnO_2 [8]. Besides, the other irreversible byproducts, such as spinel- $ZnMn_2O_4$ and MnOOH, were not observed [145]. This implies that the Zn intercalation reaction within this system is totally reversible.
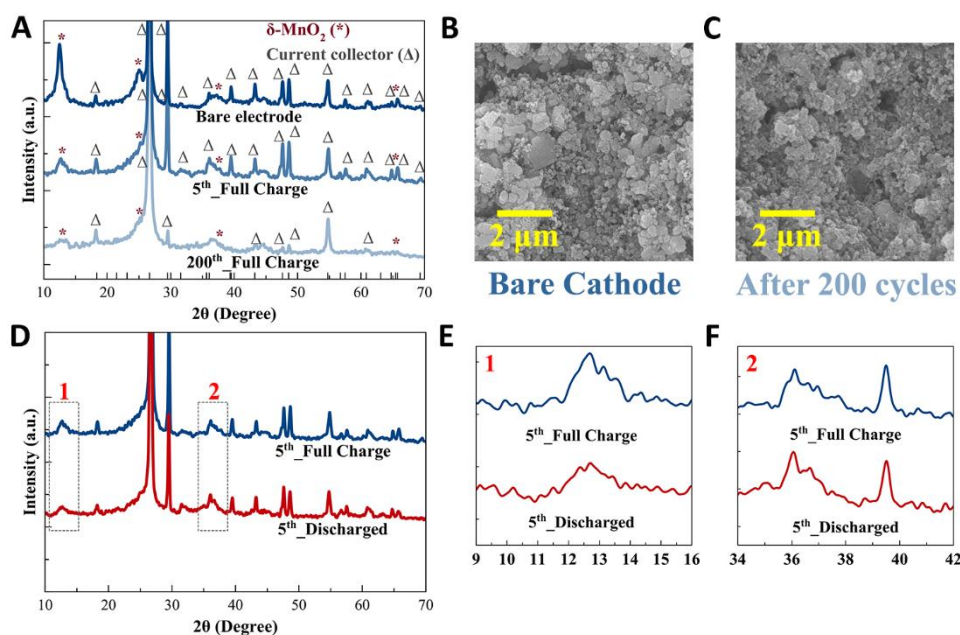
Figure 4.4 Material characterization results of δ-MnO_2 electrode. (a) XRD spectra of the δ-MnO_2 electrode at different cycling positions. (b-c) SEM image of the δ-MnO_2 electrode: initial and 200th cycle (b) bare electrode and (c) after cycling for 200 cycles. (d-f) XRD spectra of the δ-MnO_2 electrode at different discharging states: (d) Overall profile (e) Zoom in during a 2θ of 9 to 16 degree, and (f) Zoom in during a 2θ of 34 to 42 degree.

Due to the fact that δ-MnO_2 contains water molecules in its interlayer, it is interesting to examine these water molecules upon cycling [69, 189]. Thus, in Fig. A10, amount of water in the δ-MnO_2 was analyzed using thermogravimetric analysis (TGA). According to Fig. A10, it is seen that the weight of δ-MnO_2 decreased as temperature increased. In the temperature range: 30-170 ℃, the mass loss of 9.6 wt.% is seen to correspond to the evaporation of surface water. The further loss of 4.9 wt. % in the temperature range: 170-470 ℃, corresponds to the evaporation of interlayer water

[189]. The total amount of water, therefore, δ-MnO_2 powder is approximately 14.5 wt. % As for the bare and cycled electrode (25th cycle), the exact amount of water cannot be measured as the electrode contains other materials i.e. conductive carbon and binder. In the temperature range: 30-170 ℃, the weight loss of the bare electrode sample was found to be higher than that of the cycled electrode sample. This implied that the amount of water on the bare electrode surface is higher than that of the cycled electrode. The high surface water is attributed to the high hygroscopic property of conductive carbon. Upon cycling by the DMSO, the water was removed from the surface. As shown in Table A1, the water content of electrolyte increased significantly after 25th cycle. In the temperature range: 170-470 ℃, the weight loss of both samples reduced dramatically due to the combination of interlayer water evaporation and decomposition of other electrode components.

Herein, further investigation was conducted in order to strengthen the hypothesis that was stated in the section on material characterization, regarding the change in electronic resistivity and its consequence. For this purpose, the potentiostatic EIS technique was used to investigate the change in its charge-transfer components, using the frequency range of 200 kHz to 100 mHz at 0 V versus open-circuit voltage (OCV). EIS was carried out at the same cycling position, as observed in Fig. 4.4a. In Fig. 4.5, results are shown. In general, the EIS spectra of the battery are comprised of at least four major components within the Nyquist plot curve i.e. the high frequency zero-intercept, the semicircle-like curve at high frequency, the semicircle-like curve between medium to low frequency and the inclined-straight line at low frequency. All of these components represent the ohmic ion/electron conduction, the reaction of a faster electrode, the reaction of a slower electrode and the solid phase ion diffusion, respectively [190]. Nevertheless, it is important to identify which Nyquist components they belong to, as well as which electrodes and which processes. According to Fig. 4.5a, the first semicircle (inset figure), during (~3.5 to 4.5) Ω, did not change much corresponding to the state of the battery; due to the excess Zn capacity that was prepared for the δ-MnO_2 cathode test. Thus, this curve can be attributed to the reaction of the Zn electrode, since it appeared at the high frequency range (80-4 kHz). Hence, the second semicircle, at moderate to low frequency (4 kHz – 2.5 Hz), is easily assigned as an

intercalation of Zn ions into the δ-MnO$_2$ structure. When the cell is discharged, the semicircle gets larger in diameter. This change points to the higher energy requirement of the δ-MnO$_2$ electrode, due to the lowering of the available active sites for the insertion of Zn ions upon discharging [191]. It is noted that, after discharge, the inclined line increased in length, highlighting the poorer diffusivity of Zn ions in the solid phase, when δ-MnO$_2$ was converted into Zn$_x$MnO$_2$ [8].

As shown in Fig. 4.5b, a change in the Nyquist curve was observed, when the number of cycles changed. Firstly, at the 5th cycle, the size of the Zn electrode semicircle (inset figure) was found to be smaller than the as-prepared. This may indicate the change in the Zn surface upon preconditioning and after the first few cycles. Between the 5th cycle and 200th cycle, no difference in the diameter of the semicircle was found. Such a result highlights the great stability of the Zn electrode under the Zn(OTf)$_2$/DMSO electrolyte. When compared with the as-prepared sample, a huge change in the size of the Zn ion/δ-MnO$_2$ intercalation semicircle at the 5th cycle was observed. This was a consequence of the repeated insert/extract of Zn ions after a few cycles. Accordingly, the kinetic reaction of the active materials improved due to the higher active surface area of δ-MnO$_2$, as a result of electrochemical grinding [69]. However, at the 200th cycle, the diameter of the Zn ion/δ-MnO$_2$ intercalation semicircle was found to be larger than at the 5th cycle. This may be due to the accumulation of irreversible Zn$_x$MnO$_2$ within the δ-MnO$_2$ cathode, after the long cycling, which led to the significant decrease in Zn ion diffusivity of the δ-MnO$_2$ electrode. A higher amount of Zn$_x$MnO$_2$ in the electrode might be the cause of lower diffusivity of the bulk electrode after long cycling. The accumulation of irreversible Zn$_x$MnO$_2$ may arise from the deterioration of CaCO$_3$ in the carbon paper and results in the disconnection of some active materials from the electron-transfer pathway. Besides, this deterioration also reduced the overall electronic resistivity of the electrode, which can be observed from the right-shift of the zero-interception point, within the Nyquist plot at high frequency (3.5 to 4.3 Ω).
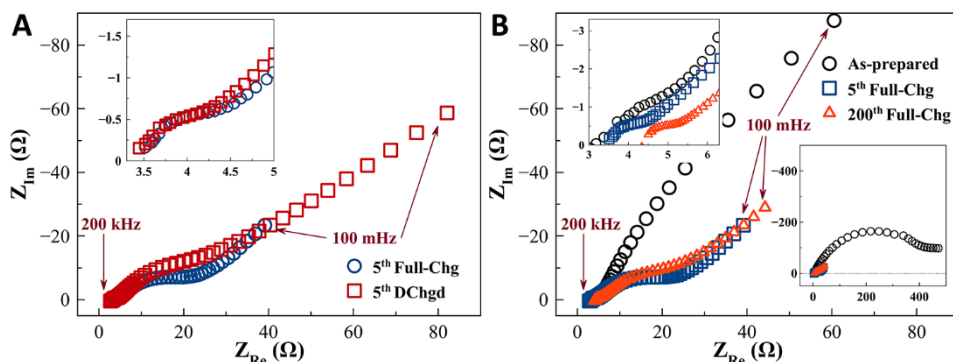
Figure 4.5 Inspection results of Zn|0.25 M Zn(OTf)$_2$/DMSO |δ-MnO$_2$ cell via EIS technique. (a-b) EIS spectra of the Zn|0.25 M Zn(OTf)$_2$/DMSO |δ-MnO$_2$ cell: (a) at different states (Full charge/Discharged) and (b) at different cycles (Full charge state).

In a summary of this section, it was found that reversible Zn ions/δ-MnO$_2$ intercalation is the main charge-storage reaction within this system where the product of this reaction is Zn$_x$MnO$_2$. Irreversible products, for instance, spinel-ZnMn$_2$O$_4$ and MnOOH were not found on the δ-MnO$_2$ electrode. In addition, EIS results substantiated that the Zn electrode is highly stable even after long charge-discharge cycles. The main cause of capacity fading arose from the degradation of the current collector, but not from direct deterioration of active materials such as Zn and δ-MnO$_2$.

4.3 Conclusion

Zn(OTf)$_2$/DMSO electrolyte shows excellent application in MnO$_2$-based ZIBs. The reversibility of Zn stripping/plating in DMSO-based electrolytes is excellent. The resulted morphology of Zn anode after cycling is dendrite-free. The reversible stripping/plating of Zn demonstrates excellent electrochemical performance. Initially, the battery delivers a high specific capacity of 159 mAh/g at 50 mA/g. Furthermore, in the cyclability test at a current density of 100 mA/g, capacity retention recorded 60% after 1000 cycles, which is superior to several previous reports regarding nonaqueous ZIBs using various types of intercalation host material [8, 46, 61, 62, 69, 70, 93, 178]. Thus, it was found that DMSO-based electrolytes can effectively inhibit hydrogen production, during both charging and resting modes. This work opens up new directions in the search for non-aqueous and safe electrolytes for ZIBs.

CHAPTER 5

CONCLUSIONS AND SUGGESTIONS

5.1 Conclusions

In this dissertation, published articles involving topics of Zn plating/stripping in nonaqueous media as well as topics related to NZIBs have been reviewed. It is evident that nonaqueous electrolytes viz. cyanomethane-base, carbonate-based, amide-based, phosphate-based, ether-based, sulfoxide-based, alkyl imidazolium, alkyl pyrrolidinium, choline-based DES and acetamide-based DES electrolytes provided the reversible Zn plating/stripping. Most of the above-mentioned electrolytes exhibited >99 % CE upon GCD cycling and yielded dendrite-free Zn. It is significant that such outcomes reflect the promising features of nonaqueous electrolytes in enhancing the stability of Zn anode. However, none of the proposed works can fulfill the commercialized criterion i.e. 5 mAh/cm^2 of areal capacity, the ability to run at 2C, and last for 2,000 cycles. To improve Zn anode performance in nonaqueous media, therefore, the following approach is necessary: 1) develop SEI that can reduce the effect of the desolvation penalty 2) fine-tune the solvated structure of the Zn species to diminish the effect of anion-cation pairing. In addition, a standard testing protocol in determining performance of Zn anode should be established.

In general, full cell NZIBs offer acceptable energy density (~100 to ~300 Wh/kg). Nevertheless, the rate performance of NZIBs has been found to be relatively low (~1C) in comparison with that of AZIBs. Such a result reveals their limitation in terms of the reaction kinetics of an intercalation cathode in nonaqueous media. Thus, to enhance the full cell performance of NZIBs, the design of electrodes that can reduce the effect of anion-cation pairing together with the tuning of surface chemistry that supports the solvation process needs to be improved.

It is seen that nonaqueous electrolytes allow the use of high voltage cathodes (> 2 V vs. Zn/Zn^{2+}) and exhibit stable Zn anode cycling without dendrite and H$_2$ production issues. The highest level of concern that requires further development is the "speed" of the redox reaction in both anode and cathode. A one-stop solution to enhance

the performance of NZIBs may lie in the development of an electrolyte that has the capability to provide faster desolvation.

According to the NZIB systems proposed in this work, the Zn/MnO_2 based on the biocompatible ChCl/urea DES ($ZnCl_2$) electrolyte demonstrated reversible smooth-nanosized Zn upon cycling and a large initial discharge capacity of 170 mAh/g (50 mA/g). In contrast, Zn/MnO_2 based on the polar-aprotic DMSO ($Zn(OTf)_2$) exhibited 159 mAh/g (50 mA/g) at first discharge and dense dendrite-free Zn anode upon long term cycling. In terms of rate capability, the DMSO system exhibited greater capacity retention during cycling at high current (118 and 108 mAh/g at 150 and 200 mA/g) than that of the ChCl/urea DES system (63 and 51 mAh/g at 150 and 200 mA/g). Results indicate that the DMSO electrolyte provided higher ion transport and lower desolvation penalty than that of the ChCl/urea DES electrolyte. In addition, incredible cycling stability (60 % capacity retention upon 1,000 cycles) was achieved using the DMSO electrolyte. It is noted that both the DMSO system and ChCl/urea DES system revealed lower capacity than the average value of aqueous Zn/MnO_2 (~ 200 mAh/g), indicating an absence of H^+ contribution. In comparison with other NZIB systems, Zn/MnO_2 having the DMSO electrolyte proves to be one of the most promising systems as regards performance and stability. Lastly, the author hopes that this contribution can benefit those who seek to develop ZIBs on a more practical scale in the future.

5.2 Suggestions

- According to the review section, water is one of the possible choices that may enhance the performance of Zn/MnO_2 having DMSO electrolyte.
- The effect of depth-of-discharge (DOD) of Zn anode should be included in further investigations.
- The desolvation penalty is possibly one of the most precious topics for further investigations.
- "Preconditioning" is another aspect that requires further investigation.

REFERENCES

[1]   L. E. Blanc, D. Kundu, and L. F. Nazar, "Scientific Challenges for the Implementation of Zn-Ion Batteries," *Joule,* vol. 4, no. 4, pp. 771-799, 2020, doi: https://doi.org/10.1016/j.joule.2020.03.002.

[2]   J. Ming, J. Guo, C. Xia, W. Wang, and H. N. Alshareef, "Zinc-ion batteries: Materials, mechanisms, and applications," *Materials Science and Engineering: R: Reports,* vol. 135, pp. 58-84, 2019/01/01/ 2019, doi: https://doi.org/10.1016/j.mser.2018.10.002.

[3]   M. Iturrondobeitia, O. Akizu-Gardoki, O. Amondarain, R. Minguez, and E. Lizundia, "Environmental Impacts of Aqueous Zinc Ion Batteries Based on Life Cycle Assessment," *Advanced Sustainable Systems,* https://doi.org/10.1002/adsu.202100308 vol. n/a, no. n/a, p. 2100308, 2021/10/17 2021, doi: https://doi.org/10.1002/adsu.202100308.

[4]   B. Scrosati, "History of lithium batteries," *Journal of Solid State Electrochemistry,* vol. 15, no. 7, pp. 1623-1630, 2011/07/01 2011, doi: 10.1007/s10008-011-1386-8.

[5]   H. Pan *et al.*, "Reversible aqueous zinc/manganese oxide energy storage from conversion reactions," *Nature Energy,* vol. 1, no. 5, p. 16039, 2016/04/18 2016, doi: 10.1038/nenergy.2016.39.

[6]   L. Wang and J. Zheng, "Recent advances in cathode materials of rechargeable aqueous zinc-ion batteries," *Materials Today Advances,* vol. 7, p. 100078, 2020/09/01/ 2020, doi: https://doi.org/10.1016/j.mtadv.2020.100078.

[7]   L. Ma *et al.*, "Realizing high zinc reversibility in rechargeable batteries," *Nature Energy,* vol. 5, no. 10, pp. 743-749, 2020/10/01 2020, doi: 10.1038/s41560-020-0674-x.

[8]   W. Kao-ian, R. Pornprasertsuk, P. Thamyongkit, T. Maiyalagan, and S. Kheawhom, "Rechargeable Zinc-Ion Battery Based on Choline Chloride-Urea Deep Eutectic Solvent," *Journal of The Electrochemical Society,* vol. 166, no. 6, pp. A1063-A1069, January 1, 2019 2019, doi: https://doi.org/10.1149/2.0641906jes.

[9]   D. Selvakumaran, A. Pan, S. Liang, and G. Cao, "A review on recent developments and challenges of cathode materials for rechargeable aqueous Zn-ion batteries," *Journal of Materials Chemistry A,* 10.1039/C9TA05053A vol. 7, no. 31, pp. 18209-18236, 2019, doi: 10.1039/C9TA05053A.

[10]   P. Chen *et al.*, "Recent Progress in Electrolytes for Zn–Air Batteries," *Frontiers in Chemistry,* 10.3389/fchem.2020.00372 vol. 8, p. 372, 2020. [Online]. Available: https://www.frontiersin.org/article/10.3389/fchem.2020.00372.

[11]   H. Jia *et al.*, "Recent advances in zinc anodes for high-performance aqueous Zn-ion batteries," *Nano Energy,* vol. 70, p. 104523, 2020/04/01/ 2020, doi: https://doi.org/10.1016/j.nanoen.2020.104523.

[12]   A. R. Mainar *et al.*, "An overview of progress in electrolytes for secondary zinc-air batteries and other storage systems based on zinc," *Journal of Energy Storage,* vol. 15, pp. 304-328, 2018/02/01/ 2018, doi: https://doi.org/10.1016/j.est.2017.12.004.

[13]   H. Moon *et al.*, "Direct Proof of the Reversible Dissolution/Deposition of Mn2+/Mn4+ for Mild-Acid Zn-MnO2 Batteries with Porous Carbon Interlayers,"

Advanced Science, https://doi.org/10.1002/advs.202003714 vol. 8, no. 6, p. 2003714, 2021/03/01 2021, doi: https://doi.org/10.1002/advs.202003714.

[14] L. Lei, Y. Sun, X. Wang, Y. Jiang, and J. Li, "Strategies to Enhance Corrosion Resistance of Zn Electrodes for Next Generation Batteries," (in English), *Frontiers in Materials,* Mini Review vol. 7, no. 96, 2020-April-24 2020, doi: https://doi.org/10.3389/fmats.2020.00096.

[15] J. Yi *et al.*, "Challenges, mitigation strategies and perspectives in development of zinc-electrode materials and fabrication for rechargeable zinc–air batteries," *Energy & Environmental Science,* 10.1039/C8EE01991F vol. 11, no. 11, pp. 3075-3095, 2018, doi: 10.1039/C8EE01991F.

[16] M. Song, H. Tan, D. Chao, and H. J. Fan, "Recent Advances in Zn-Ion Batteries," *Advanced Functional Materials,* https://doi.org/10.1002/adfm.201802564 vol. 28, no. 41, p. 1802564, 2018/10/01 2018, doi: https://doi.org/10.1002/adfm.201802564.

[17] K. W. Leong, Y. Wang, M. Ni, W. Pan, S. Luo, and D. Y. C. Leung, "Rechargeable Zn-air batteries: Recent trends and future perspectives," *Renewable and Sustainable Energy Reviews,* vol. 154, p. 111771, 2022/02/01/ 2022, doi: https://doi.org/10.1016/j.rser.2021.111771.

[18] D. Yang, H. Tan, X. Rui, and Y. Yu, "Electrode Materials for Rechargeable Zinc-Ion and Zinc-Air Batteries: Current Status and Future Perspectives," *Electrochemical Energy Reviews,* vol. 2, no. 3, pp. 395-427, 2019/09/01 2019, doi: 10.1007/s41918-019-00035-5.

[19] A. K. Worku, D. W. Ayele, and N. G. Habtu, "Recent advances and future perspectives in engineering of bifunctional electrocatalysts for rechargeable zinc–air batteries," *Materials Today Advances,* vol. 9, p. 100116, 2021/03/01/ 2021, doi: https://doi.org/10.1016/j.mtadv.2020.100116.

[20] C. Xu, B. Li, H. Du, and F. Kang, "Energetic Zinc Ion Chemistry: The Rechargeable Zinc Ion Battery," *Angewandte Chemie International Edition,* vol. 51, no. 4, pp. 933-935, 2012, doi: https://doi.org/10.1002/anie.201106307.

[21] W. Zhang *et al.*, "Application of Manganese-Based Materials in Aqueous Rechargeable Zinc-Ion Batteries," *Frontiers in Energy Research,* 10.3389/fenrg.2020.00195 vol. 8, p. 195, 2020. [Online]. Available: https://www.frontiersin.org/article/10.3389/fenrg.2020.00195.

[22] P. Xu, C. Wang, B. Zhao, Y. Zhou, and H. Cheng, "An interfacial coating with high corrosion resistance based on halloysite nanotubes for anode protection of zinc-ion batteries," *Journal of Colloid and Interface Science,* vol. 602, pp. 859-867, 2021/11/15/ 2021, doi: https://doi.org/10.1016/j.jcis.2021.06.057.

[23] Q. Zhang *et al.*, "Issues and rational design of aqueous electrolyte for Zn-ion batteries," *SusMat,* https://doi.org/10.1002/sus2.20 vol. 1, no. 3, pp. 432-447, 2021/09/01 2021, doi: https://doi.org/10.1002/sus2.20.

[24] F. Wang *et al.*, "Highly reversible zinc metal anode for aqueous batteries," *Nature Materials,* vol. 17, no. 6, pp. 543-549, 2018/06/01 2018, doi: 10.1038/s41563-018-0063-z.

[25] P. Liang *et al.*, "Highly Reversible Zn Anode Enabled by Controllable Formation of Nucleation Sites for Zn-Based Batteries," *Advanced Functional Materials,* https://doi.org/10.1002/adfm.201908528 vol. 30, no. 13, p. 1908528, 2020/03/01 2020, doi: https://doi.org/10.1002/adfm.201908528.

[26]   Z. Zhao *et al.*, "Long-life and deeply rechargeable aqueous Zn anodes enabled by a multifunctional brightener-inspired interphase," *Energy & Environmental Science,* 10.1039/C9EE00596J vol. 12, no. 6, pp. 1938-1949, 2019, doi: 10.1039/C9EE00596J.

[27]   H. He, H. Tong, X. Song, X. Song, and J. Liu, "Highly stable Zn metal anodes enabled by atomic layer deposited Al2O3 coating for aqueous zinc-ion batteries," *Journal of Materials Chemistry A,* 10.1039/D0TA00748J vol. 8, no. 16, pp. 7836-7846, 2020, doi: 10.1039/D0TA00748J.

[28]   L. Cao *et al.*, "Solvation Structure Design for Aqueous Zn Metal Batteries," *Journal of the American Chemical Society,* vol. 142, no. 51, pp. 21404-21409, 2020/12/23 2020, doi: 10.1021/jacs.0c09794.

[29]   J. Abdulla, J. Cao, P. Wangyao, and J. Qin, "Review on the suppression of Zn dendrite for high performance of Zn ion battery," *Journal of Metals, Materials and Minerals,* vol. 30, no. 3, 09/29 2020. [Online]. Available: http://jmmm.material.chula.ac.th/index.php/jmmm/article/view/900.

[30]   L. Ma *et al.*, "Hydrogen-Free and Dendrite-Free All-Solid-State Zn-Ion Batteries," *Advanced Materials,* vol. 32, no. 14, p. 1908121, 2020, doi: https://doi.org/10.1002/adma.201908121.

[31]   W. Kao-ian *et al.*, "Highly Stable Rechargeable Zinc-ion Battery using Dimethyl Sulfoxide Electrolyte," *Materials Today Energy,* p. 100738, 2021/04/02/ 2021, doi: 10.1016/j.mtener.2021.100738.

[32]   M. Kar and C. Pozo-Gonzalo, "Emergence of nonaqueous electrolytes for rechargeable zinc batteries," *Current Opinion in Green and Sustainable Chemistry,* vol. 28, p. 100426, 2021/04/01/ 2021, doi: 10.1016/j.cogsc.2020.100426.

[33]   J. Zhao *et al.*, ""Water-in-deep eutectic solvent" electrolytes enable zinc metal anodes for rechargeable aqueous batteries," *Nano Energy,* vol. 57, pp. 625-634, 2019/03/01/ 2019, doi: 10.1016/j.nanoen.2018.12.086.

[34]   H. Qiu *et al.*, "Zinc anode-compatible in-situ solid electrolyte interphase via cation solvation modulation," *Nature Communications,* vol. 10, no. 1, p. 5374, 2019/11/26 2019, doi: 10.1038/s41467-019-13436-3.

[35]   S.-D. Han *et al.*, "Origin of Electrochemical, Structural, and Transport Properties in Nonaqueous Zinc Electrolytes," *ACS Applied Materials & Interfaces,* vol. 8, no. 5, pp. 3021-3031, 2016/02/10 2016, doi: 10.1021/acsami.5b10024.

[36]   E. Knipping, C. Aucher, G. Guirado, and L. Aubouy, "Room temperature ionic liquids versus organic solvents as lithium–oxygen battery electrolytes," *New Journal of Chemistry,* 10.1039/C8NJ00449H vol. 42, no. 6, pp. 4693-4699, 2018, doi: 10.1039/C8NJ00449H.

[37]   Y. Zhang *et al.*, "Pursuit of reversible Zn electrochemistry: a time-honored challenge towards low-cost and green energy storage," *NPG Asia Materials,* vol. 12, no. 1, p. 4, 2020/01/24 2020, doi: https://doi.org/10.1038/s41427-019-0167-1.

[38]   X. Gao, H. Zhang, X. Liu, and X. Lu, "Flexible Zn-ion batteries based on manganese oxides: Progress and prospect," *Carbon Energy,* https://doi.org/10.1002/cey2.63 vol. 2, no. 3, pp. 387-407, 2020/09/01 2020, doi: https://doi.org/10.1002/cey2.63.

[39]   A. J Brad and L. R Faulkner, *Electrochemical Methods: Fundamentals and Applications*. 2000.

[40] M. Orazem and B. Tribollet, *Tribollet, B.: Electrochemical Impedance Spectroscopy. Wiley-Interscience, New York*. 2008.

[41] D. Aurbach, *Nonaqueous Electrochemistry*. 1999.

[42] A. Eftekhari, "Lithium-Ion Batteries with High Rate Capabilities," *ACS Sustainable Chemistry & Engineering,* vol. 5, no. 4, pp. 2799-2816, 2017/04/03 2017, doi: 10.1021/acssuschemeng.7b00046.

[43] G. Yang *et al.*, "Improving the cyclability performance of lithium-ion batteries by introducing lithium difluorophosphate (LiPO2F2) additive," *RSC Advances,* 10.1039/C7RA03926C vol. 7, no. 42, pp. 26052-26059, 2017, doi: 10.1039/C7RA03926C.

[44] T. Zhang *et al.*, "Fundamentals and perspectives in developing zinc-ion battery electrolytes: a comprehensive review," *Energy & Environmental Science,* 10.1039/D0EE02620D vol. 13, no. 12, pp. 4625-4665, 2020, doi: 10.1039/D0EE02620D.

[45] N. H. F. Ismail, S. F. Toha, N. A. M. Azubir, N. H. Md Ishak, M. K. Hassan, and B. S. Ksm Ibrahim, "Simplified Heat Generation Model for Lithium ion battery used in Electric Vehicle," *IOP Conference Series: Materials Science and Engineering,* vol. 53, p. 012014, 2013/12/20 2013, doi: 10.1088/1757-899x/53/1/012014.

[46] D. Kundu, S. Hosseini Vajargah, L. Wan, B. Adams, D. Prendergast, and L. F. Nazar, "Aqueous vs. nonaqueous Zn-ion batteries: consequences of the desolvation penalty at the interface," *Energy & Environmental Science,* 10.1039/C8EE00378E vol. 11, no. 4, pp. 881-892, 2018, doi: 10.1039/C8EE00378E.

[47] G. G. Eshetu *et al.*, "Production of high-energy Li-ion batteries comprising silicon-containing anodes and insertion-type cathodes," *Nature Communications,* vol. 12, no. 1, p. 5459, 2021/09/15 2021, doi: 10.1038/s41467-021-25334-8.

[48] W. Zhang, S. Liang, G. Fang, Y. Yang, and J. Zhou, "Ultra-High Mass-Loading Cathode for Aqueous Zinc-Ion Battery Based on Graphene-Wrapped Aluminum Vanadate Nanobelts," *Nano-Micro Letters,* vol. 11, no. 1, p. 69, 2019/08/26 2019, doi: 10.1007/s40820-019-0300-2.

[49] N. Wang *et al.*, "A review of zinc-based battery from alkaline to acid," *Materials Today Advances,* vol. 11, p. 100149, 2021/09/01/ 2021, doi: 10.1016/j.mtadv.2021.100149.

[50] X. Zhu *et al.*, "Superior-Performance Aqueous Zinc-Ion Batteries Based on the In Situ Growth of MnO2 Nanosheets on V2CTX MXene," *ACS Nano,* vol. 15, no. 2, pp. 2971-2983, 2021/02/23 2021, doi: 10.1021/acsnano.0c09205.

[51] T. Xue and H. J. Fan, "From aqueous Zn-ion battery to Zn-MnO2 flow battery: A brief story," *Journal of Energy Chemistry,* vol. 54, pp. 194-201, 2021/03/01/ 2021, doi: 10.1016/j.jechem.2020.05.056.

[52] X. Jia, C. Liu, Z. G. Neale, J. Yang, and G. Cao, "Active Materials for Aqueous Zinc Ion Batteries: Synthesis, Crystal Structure, Morphology, and Electrochemistry," *Chemical Reviews,* vol. 120, no. 15, pp. 7795-7866, 2020/08/12 2020, doi: 10.1021/acs.chemrev.9b00628.

[53] C. Xie, Y. Li, Q. Wang, D. Sun, Y. Tang, and H. Wang, "Issues and solutions toward zinc anode in aqueous zinc-ion batteries: A mini review," *Carbon Energy,* vol. 2, no. 4, pp. 540-560, 2020, doi: 10.1002/cey2.67.

[54] H. Liu, Y. Zhang, C. Wang, J. N. Glazer, Z. Shan, and N. Liu, "Understanding and Controlling the Nucleation and Growth of Zn Electrodeposits for Aqueous Zinc-Ion Batteries," *ACS Applied Materials & Interfaces,* vol. 13, no. 28, pp. 32930-32936, 2021/07/21 2021, doi: 10.1021/acsami.1c06131.

[55] X. Guo *et al.*, "Alleviation of Dendrite Formation on Zinc Anodes via Electrolyte Additives," *ACS Energy Letters,* vol. 6, no. 2, pp. 395-403, 2021/02/12 2021, doi: 10.1021/acsenergylett.0c02371.

[56] J. Hao *et al.*, "Designing Dendrite-Free Zinc Anodes for Advanced Aqueous Zinc Batteries," *Advanced Functional Materials,* vol. 30, no. 30, p. 2001263, 2020, doi: 10.1002/adfm.202001263.

[57] Q. Li, J. Chen, L. Fan, X. Kong, and Y. Lu, "Progress in electrolytes for rechargeable Li-based batteries and beyond," *Green Energy & Environment,* vol. 1, no. 1, pp. 18-42, 2016/04/01/ 2016, doi: 10.1016/j.gee.2016.04.006.

[58] N. Nitta, F. Wu, J. T. Lee, and G. Yushin, "Li-ion battery materials: present and future," *Materials Today,* vol. 18, no. 5, pp. 252-264, 2015/06/01/ 2015, doi: 10.1016/j.mattod.2014.10.040.

[59] N. Wang *et al.*, "Zinc–Organic Battery with a Wide Operation-Temperature Window from −70 to 150 °C," *Angewandte Chemie International Edition,* vol. 59, no. 34, pp. 14577-14583, 2020, doi: 10.1002/anie.202005603.

[60] Q. Li, K. Ma, G. Yang, and C. Wang, "High-voltage non-aqueous Zn/K1.6Mn1.2Fe(CN)6 batteries with zero capacity loss in extremely long working duration," *Energy Storage Materials,* vol. 29, pp. 246-253, 2020/08/01/ 2020, doi: 10.1016/j.ensm.2020.04.030.

[61] A. Naveed, H. Yang, J. Yang, Y. Nuli, and J. Wang, "Highly Reversible and Rechargeable Safe Zn Batteries Based on a Triethyl Phosphate Electrolyte," *Angewandte Chemie International Edition,* vol. 58, no. 9, pp. 2760-2764, 2019, doi: https://doi.org/10.1002/anie.201813223.

[62] C. Pan, R. G. Nuzzo, and A. A. Gewirth, "ZnAlxCo2–xO4 Spinels as Cathode Materials for Non-Aqueous Zn Batteries with an Open Circuit Voltage of ≤2 V," *Chemistry of Materials,* vol. 29, no. 21, pp. 9351-9359, 2017/11/14 2017, doi: https://doi.org/10.1021/acs.chemmater.7b03340.

[63] C. Pan, R. Zhang, R. G. Nuzzo, and A. A. Gewirth, "ZnNixMnxCo2–2xO4 Spinel as a High-Voltage and High-Capacity Cathode Material for Nonaqueous Zn-Ion Batteries," *Advanced Energy Materials,* vol. 8, no. 22, p. 1800589, 2018, doi: 10.1002/aenm.201800589.

[64] Y. Dong *et al.*, "Nonaqueous electrolyte with dual-cations for high-voltage and long-life zinc batteries," *Journal of Materials Chemistry A,* 10.1039/C9TA13068C vol. 8, no. 6, pp. 3252-3261, 2020, doi: 10.1039/C9TA13068C.

[65] J. Fan, Q. Xiao, Y. Fang, L. Li, and W. Yuan, "A rechargeable Zn/graphite dual-ion battery with an ionic liquid-based electrolyte," *Ionics,* vol. 25, no. 3, pp. 1303-1313, 2019/03/01 2019, doi: 10.1007/s11581-018-2644-x.

[66] N. Zhang *et al.*, "Ultrafast Rechargeable Zinc Battery Based on High-Voltage Graphite Cathode and Stable Nonaqueous Electrolyte," *ACS Applied Materials & Interfaces,* vol. 11, no. 36, pp. 32978-32986, 2019/09/11 2019, doi: https://doi.org/10.1021/acsami.9b10399.

[67] A. S. Etman, M. Carboni, J. Sun, and R. Younesi, "Acetonitrile-Based Electrolytes for Rechargeable Zinc Batteries," *Energy Technology,* vol. 8, no. 9, p. 2000358, 2020, doi: 10.1002/ente.202000358.

[68] V. Verma *et al.*, "Layered VOPO4 as a Cathode Material for Rechargeable Zinc-Ion Battery: Effect of Polypyrrole Intercalation in the Host and Water Concentration in the Electrolyte," *ACS Applied Energy Materials,* vol. 2, no. 12, pp. 8667-8674, 2019/12/23 2019, doi: 10.1021/acsaem.9b01632.

[69] S.-D. Han *et al.*, "Mechanism of Zn Insertion into Nanostructured δ-MnO2: A Nonaqueous Rechargeable Zn Metal Battery," *Chemistry of Materials,* vol. 29, no. 11, pp. 4874-4884, 2017/06/13 2017, doi: https://doi.org/10.1021/acs.chemmater.7b00852.

[70] M. S. Chae, J. W. Heo, H. H. Kwak, H. Lee, and S.-T. Hong, "Organic electrolyte-based rechargeable zinc-ion batteries using potassium nickel hexacyanoferrate as a cathode material," *Journal of Power Sources,* vol. 337, pp. 204-211, 2017/01/01/ 2017, doi: https://doi.org/10.1016/j.jpowsour.2016.10.083.

[71] P. Senguttuvan *et al.*, "A High Power Rechargeable Nonaqueous Multivalent Zn/V2O5 Battery," *Advanced Energy Materials,* vol. 6, no. 24, p. 1600826, 2016, doi: 10.1002/aenm.201600826.

[72] A. Guerfi *et al.*, "High cycling stability of zinc-anode/conducting polymer rechargeable battery with non-aqueous electrolyte," *Journal of Power Sources,* vol. 248, pp. 1099-1104, 2014/02/15/ 2014, doi: 10.1016/j.jpowsour.2013.09.082.

[73] A. Naveed *et al.*, "A Highly Reversible Zn Anode with Intrinsically Safe Organic Electrolyte for Long-Cycle-Life Batteries," *Advanced Materials,* vol. 31, no. 36, p. 1900668, 2019, doi: 10.1002/adma.201900668.

[74] R. D. Corpuz *et al.*, "Binder-Free α-MnO2 Nanowires on Carbon Cloth as Cathode Material for Zinc-Ion Batteries," *International Journal of Molecular Sciences,* vol. 21, no. 9, p. 3113, 2020, doi: 10.3390/ijms21093113.

[75] X. Qiu *et al.*, "A High-Voltage Zn–Organic Battery Using a Nonflammable Organic Electrolyte," *Angewandte Chemie International Edition,* vol. 60, no. 38, pp. 21025-21032, 2021, doi: 10.1002/anie.202108624.

[76] G. M. Asselin, O. Paden, W. Qiu, Z. Yang, and N. Sa, "A Systematic Electrochemical Investigation of a Dimethylamine Cosolvent-Assisted Nonaqueous Zinc(II) Bis(trifluoromethylsulfonyl)imide Electrolyte," *Journal of The Electrochemical Society,* vol. 168, no. 3, p. 030516, 2021/03/01 2021, doi: 10.1149/1945-7111/abe9cb.

[77] A. M. O'Mahony, D. S. Silvester, L. Aldous, C. Hardacre, and R. G. Compton, "Effect of Water on the Electrochemical Window and Potential Limits of Room-Temperature Ionic Liquids," *Journal of Chemical & Engineering Data,* vol. 53, no. 12, pp. 2884-2891, 2008/12/11 2008, doi: 10.1021/je800678e.

[78] G. Damilano, D. Kalebić, K. Binnemans, and W. Dehaen, "One-pot synthesis of symmetric imidazolium ionic liquids N,N-disubstituted with long alkyl chains," *RSC Advances,* 10.1039/D0RA03358H vol. 10, no. 36, pp. 21071-21081, 2020, doi: 10.1039/D0RA03358H.

[79] T. J. Simons, D. R. MacFarlane, M. Forsyth, and P. C. Howlett, "Zn Electrochemistry in 1-Ethyl-3-Methylimidazolium and N-Butyl-N-Methylpyrrolidinium Dicyanamides: Promising New Rechargeable Zn Battery

Electrolytes," *ChemElectroChem,* vol. 1, no. 10, pp. 1688-1697, 2014, doi: 10.1002/celc.201402177.

[80] L. Zhang, G. Wang, J. Feng, Q. Ma, Z. Liu, and X. Yan, "Designing a Zn(BF4)2-Based Ionic Liquid Electrolyte to Realize Superior Energy Density in a Carbon-Based Zinc-Ion Hybrid Capacitor," *ChemElectroChem,* vol. 8, no. 7, pp. 1289-1297, 2021, doi: 10.1002/celc.202100003.

[81] M. S. Ghazvini, G. Pulletikurthi, A. Lahiri, and F. Endres, "Electrochemical and Spectroscopic Studies of Zinc Acetate in 1-Ethyl-3-methylimidazolium Acetate for Zinc Electrodeposition," *ChemElectroChem,* vol. 3, no. 4, pp. 598-604, 2016, doi: 10.1002/celc.201500444.

[82] G. García, S. Aparicio, R. Ullah, and M. Atilhan, "Deep Eutectic Solvents: Physicochemical Properties and Gas Separation Applications," *Energy & Fuels,* vol. 29, no. 4, pp. 2616-2644, 2015/04/16 2015, doi: 10.1021/ef5028873.

[83] A. P. Abbott, G. Capper, D. L. Davies, R. K. Rasheed, and V. Tambyrajah, "Novel solvent properties of choline chloride/urea mixtures," *Chemical Communications,* 10.1039/B210714G no. 1, pp. 70-71, 2003, doi: 10.1039/B210714G.

[84] E. L. Smith, A. P. Abbott, and K. S. Ryder, "Deep Eutectic Solvents (DESs) and Their Applications," *Chemical Reviews,* vol. 114, no. 21, pp. 11060-11082, 2014/11/12 2014, doi: 10.1021/cr300162p.

[85] T. J. Simons, P. C. Howlett, A. A. J. Torriero, D. R. MacFarlane, and M. Forsyth, "Electrochemical, Transport, and Spectroscopic Properties of 1-Ethyl-3-methylimidazolium Ionic Liquid Electrolytes Containing Zinc Dicyanamide," *The Journal of Physical Chemistry C,* vol. 117, no. 6, pp. 2662-2669, 2013/02/14 2013, doi: 10.1021/jp311886h.

[86] T. J. Simons, A. A. J. Torriero, P. C. Howlett, D. R. MacFarlane, and M. Forsyth, "High current density, efficient cycling of Zn2+ in 1-ethyl-3-methylimidazolium dicyanamide ionic liquid: The effect of Zn2+ salt and water concentration," *Electrochemistry Communications,* vol. 18, pp. 119-122, 2012/01/01/ 2012, doi: 10.1016/j.elecom.2012.02.034.

[87] B. Ji, W. Yao, and Y. Tang, "High-performance rechargeable zinc-based dual-ion batteries," *Sustainable Energy & Fuels,* 10.1039/C9SE00744J vol. 4, no. 1, pp. 101-107, 2020, doi: 10.1039/C9SE00744J.

[88] B. Dilasari, Y. Jung, and K. Kwon, "Effect of water on the stability of zinc in 1-butyl-1-methylpyrrolidinium bis(trifluoromethylsulfonyl)imide ionic liquid," *Journal of Industrial and Engineering Chemistry,* vol. 45, pp. 375-379, 2017/01/25/ 2017, doi: 10.1016/j.jiec.2016.10.005.

[89] M. Xu, D. G. Ivey, Z. Xie, W. Qu, and E. Dy, "The state of water in 1-butly-1-methyl-pyrrolidinium bis(trifluoromethanesulfonyl)imide and its effect on Zn/Zn(II) redox behavior," *Electrochimica Acta,* vol. 97, pp. 289-295, 2013/05/01/ 2013, doi: 10.1016/j.electacta.2013.03.027.

[90] K. R. Harris, L. A. Woolf, M. Kanakubo, and T. Rüther, "Transport Properties of N-Butyl-N-methylpyrrolidinium Bis(trifluoromethylsulfonyl)amide," *Journal of Chemical & Engineering Data,* vol. 56, no. 12, pp. 4672-4685, 2011/12/08 2011, doi: 10.1021/je2006049.

[91] T. J. Simons *et al.*, "Influence of Zn2+ and Water on the Transport Properties of a Pyrrolidinium Dicyanamide Ionic Liquid," *The Journal of Physical Chemistry B,* vol. 118, no. 18, pp. 4895-4905, 2014/05/08 2014, doi: 10.1021/jp501665g.

[92] C. Du, B. Zhao, X.-B. Chen, N. Birbilis, and H. Yang, "Effect of water presence on choline chloride-2urea ionic liquid and coating platings from the hydrated ionic liquid," *Scientific Reports,* vol. 6, no. 1, p. 29225, 2016/07/06 2016, doi: 10.1038/srep29225.

[93] N. S. Venkata Narayanan, B. V. Ashokraj, and S. Sampath, "Ambient temperature, zinc ion-conducting, binary molten electrolyte based on acetamide and zinc perchlorate: Application in rechargeable zinc batteries," *Journal of Colloid and Interface Science,* vol. 342, no. 2, pp. 505-512, 2010/02/15/ 2010, doi: https://doi.org/10.1016/j.jcis.2009.10.034.

[94] J. Xie and Y.-C. Lu, "A retrospective on lithium-ion batteries," *Nature Communications,* vol. 11, no. 1, p. 2499, 2020/05/19 2020, doi: 10.1038/s41467-020-16259-9.

[95] L. Ma *et al.*, "Critical Factors Dictating Reversibility of the Zinc Metal Anode," *ENERGY & ENVIRONMENTAL MATERIALS,* vol. 3, no. 4, pp. 516-521, 2020, doi: 10.1002/eem2.12077.

[96] D. Chen *et al.*, "Persistent zinc-ion storage in mass-produced V2O5 architectures," *Nano Energy,* vol. 60, pp. 171-178, 2019/06/01/ 2019, doi: 10.1016/j.nanoen.2019.03.034.

[97] S. Asha, K. P. Vijayalakshmi, and B. K. George, "Pyrrolidinium-based ionic liquids as electrolytes for lithium batteries: A Computational Study," *International Journal of Quantum Chemistry,* vol. 119, no. 22, p. e26014, 2019, doi: 10.1002/qua.26014.

[98] M.-J. Deng, P.-C. Lin, J.-K. Chang, J.-M. Chen, and K.-T. Lu, "Electrochemistry of Zn(II)/Zn on Mg alloy from the N-butyl-N-methylpyrrolidinium dicyanamide ionic liquid," *Electrochimica Acta,* vol. 56, no. 17, pp. 6071-6077, 2011/07/01/ 2011, doi: 10.1016/j.electacta.2011.04.082.

[99] A. P. Abbott, J. C. Barron, G. Frisch, S. Gurman, K. S. Ryder, and A. Fernando Silva, "Double layer effects on metal nucleation in deep eutectic solvents," *Physical Chemistry Chemical Physics,* 10.1039/C0CP02244F vol. 13, no. 21, pp. 10224-10231, 2011, doi: 10.1039/C0CP02244F.

[100] R. Bernasconi, G. Panzeri, G. Firtin, B. Kahyaoglu, L. Nobili, and L. Magagnin, "Electrodeposition of ZnNi Alloys from Choline Chloride/Ethylene Glycol Deep Eutectic Solvent and Pure Ethylene Glycol for Corrosion Protection," *The Journal of Physical Chemistry B,* vol. 124, no. 47, pp. 10739-10751, 2020/11/25 2020, doi: 10.1021/acs.jpcb.0c04784.

[101] L. Vieira, R. Schennach, and B. Gollas, "The effect of the electrode material on the electrodeposition of zinc from deep eutectic solvents," *Electrochimica Acta,* vol. 197, pp. 344-352, 2016/04/10/ 2016, doi: 10.1016/j.electacta.2015.11.030.

[102] N. M. Pereira, C. M. Pereira, J. P. Araújo, and A. Fernando Silva, "Zinc Electrodeposition from deep eutectic solvent containing organic additives," *Journal of Electroanalytical Chemistry,* vol. 801, pp. 545-551, 2017/09/15/ 2017, doi: 10.1016/j.jelechem.2017.08.019.

[103] M. Metzger *et al.*, "Carbon Coating Stability on High-Voltage Cathode Materials in H2O-Free and H2O-Containing Electrolyte," *Journal of The Electrochemical Society,* vol. 162, no. 7, pp. A1227-A1235, 2015, doi: 10.1149/2.0461507jes.

[104] H. Yang and R. G. Reddy, "Electrochemical deposition of zinc from zinc oxide in 2:1 urea/choline chloride ionic liquid," *Electrochimica Acta,* vol. 147, pp. 513-519, 2014/11/20/ 2014, doi: 10.1016/j.electacta.2014.09.137.

[105] X. Guo *et al.*, "The energy storage mechanisms of MnO2 in batteries," *Current Opinion in Electrochemistry,* vol. 30, p. 100769, 2021/12/01/ 2021, doi: 10.1016/j.coelec.2021.100769.

[106] R. D. Corpuz *et al.*, "Annealing induced a well-ordered single crystal δ-MnO2 and its electrochemical performance in zinc-ion battery," *Scientific Reports,* vol. 9, no. 1, p. 15107, 2019/10/22 2019, doi: 10.1038/s41598-019-51692-x.

[107] J. Shin, J. K. Seo, R. Yaylian, A. Huang, and Y. S. Meng, "A review on mechanistic understanding of MnO2 in aqueous electrolyte for electrical energy storage systems," *International Materials Reviews,* vol. 65, no. 6, pp. 356-387, 2020/08/17 2020, doi: 10.1080/09506608.2019.1653520.

[108] S. Khamsanga, R. Pornprasertsuk, T. Yonezawa, A. A. Mohamad, and S. Kheawhom, "δ-MnO2 nanoflower/graphite cathode for rechargeable aqueous zinc ion batteries," *Scientific Reports,* vol. 9, no. 1, p. 8441, 2019/06/11 2019, doi: 10.1038/s41598-019-44915-8.

[109] S. Khamsanga *et al.*, "MnO2 Heterostructure on Carbon Nanotubes as Cathode Material for Aqueous Zinc-Ion Batteries," *International Journal of Molecular Sciences,* vol. 21, no. 13, p. 4689, 2020, doi: 10.3390/ijms21134689.

[110] D. A. Kitchaev, H. Peng, Y. Liu, J. Sun, J. P. Perdew, and G. Ceder, "Energetics of MnO2 polymorphs in density functional theory," *Physical Review B,* vol. 93, no. 4, p. 045132, 01/26/ 2016, doi: 10.1103/PhysRevB.93.045132.

[111] Y. Xie, Y. Jin, and L. Xiang, "Understanding Mn-Based Intercalation Cathodes from Thermodynamics and Kinetics," *Crystals,* vol. 7, no. 7, p. 221, 2017, doi: 10.3390/cryst7070221.

[112] N. Nakayama, T. Nozawa, Y. Iriyama, T. Abe, Z. Ogumi, and K. Kikuchi, "Interfacial lithium-ion transfer at the LiMn2O4 thin film electrode/aqueous solution interface," *Journal of Power Sources,* vol. 174, no. 2, pp. 695-700, 2007/12/06/ 2007, doi: 10.1016/j.jpowsour.2007.06.113.

[113] T. Zhang, D. Li, Z. Tao, and J. Chen, "Understanding electrode materials of rechargeable lithium batteries via DFT calculations," *Progress in Natural Science: Materials International,* vol. 23, no. 3, pp. 256-272, 2013/06/01/ 2013, doi: https://doi.org/10.1016/j.pnsc.2013.04.005.

[114] L. M. De Juan-Corpuz *et al.*, "Binder-Free Centimeter-Long V2O5 Nanofibers on Carbon Cloth as Cathode Material for Zinc-Ion Batteries," *Energies,* vol. 13, no. 1, p. 31, 2020, doi: 10.3390/en13010031.

[115] N. Zhang *et al.*, "Rechargeable Aqueous Zn–V2O5 Battery with High Energy Density and Long Cycle Life," *ACS Energy Letters,* vol. 3, no. 6, pp. 1366-1372, 2018/06/08 2018, doi: 10.1021/acsenergylett.8b00565.

[116] J. Zhou, L. Shan, Z. Wu, X. Guo, G. Fang, and S. Liang, "Investigation of V2O5 as a low-cost rechargeable aqueous zinc ion battery cathode," *Chemical Communications,* 10.1039/C8CC02250J vol. 54, no. 35, pp. 4457-4460, 2018, doi: https://doi.org/10.1039/C8CC02250J.

[117] P. He *et al.*, "Layered VS2 Nanosheet-Based Aqueous Zn Ion Battery Cathode," *Advanced Energy Materials,* vol. 7, no. 11, p. 1601920, 2017, doi: 10.1002/aenm.201601920.

[118] G. Li *et al.*, "Towards polyvalent ion batteries: A zinc-ion battery based on NASICON structured Na3V2(PO4)3," *Nano Energy,* vol. 25, pp. 211-217, 2016/07/01/ 2016, doi: 10.1016/j.nanoen.2016.04.051.

[119] J.-Z. Guo *et al.*, "High-Energy/Power and Low-Temperature Cathode for Sodium-Ion Batteries: In Situ XRD Study and Superior Full-Cell Performance," *Advanced Materials,* vol. 29, no. 33, p. 1701968, 2017, doi: 10.1002/adma.201701968.

[120] Y. Lyu *et al.*, "An Overview on the Advances of LiCoO2 Cathodes for Lithium-Ion Batteries," *Advanced Energy Materials,* vol. 11, no. 2, p. 2000982, 2021, doi: 10.1002/aenm.202000982.

[121] F. Cheng *et al.*, "Conducting Poly(aniline) Nanotubes and Nanofibers: Controlled Synthesis and Application in Lithium/Poly(aniline) Rechargeable Batteries," *Chemistry – A European Journal,* vol. 12, no. 11, pp. 3082-3088, 2006, doi: 10.1002/chem.200500883.

[122] J. Liao *et al.*, "Controlling the morphology, size and phase of Nb2O5 crystals for high electrochemical performance," *Chinese Chemical Letters,* vol. 29, no. 12, pp. 1785-1790, 2018/12/01/ 2018, doi: https://doi.org/10.1016/j.cclet.2018.11.018.

[123] J. Huang, Z. Wei, J. Liao, W. Ni, C. Wang, and J. Ma, "Molybdenum and tungsten chalcogenides for lithium/sodium-ion batteries: Beyond MoS2," *Journal of Energy Chemistry,* vol. 33, pp. 100-124, 2019/06/01/ 2019, doi: https://doi.org/10.1016/j.jechem.2018.09.001.

[124] K. Wongrujipairoj, L. Poolnapol, A. Arpornwichanop, S. Suren, and S. Kheawhom, "Suppression of zinc anode corrosion for printed flexible zinc-air battery," *physica status solidi (b),* https://doi.org/10.1002/pssb.201600442 vol. 254, no. 2, p. 1600442, 2017/02/01 2017, doi: https://doi.org/10.1002/pssb.201600442.

[125] S. Suren and S. Kheawhom, "Development of a High Energy Density Flexible Zinc-Air Battery," *Journal of The Electrochemical Society,* vol. 163, no. 6, pp. A846-A850, 2016, doi: 10.1149/2.0361606jes.

[126] D. Larcher and J. M. Tarascon, "Towards greener and more sustainable batteries for electrical energy storage," *Nature Chemistry,* vol. 7, no. 1, pp. 19-29, 2015/01/01 2015, doi: 10.1038/nchem.2085.

[127] D. Kundu, B. D. Adams, V. Duffort, S. H. Vajargah, and L. F. Nazar, "A high-capacity and long-life aqueous rechargeable zinc battery using a metal oxide intercalation cathode," *Nature Energy,* vol. 1, no. 10, p. 16119, 2016/08/26 2016, doi: 10.1038/nenergy.2016.119.

[128] G. Fang, J. Zhou, A. Pan, and S. Liang, "Recent Advances in Aqueous Zinc-Ion Batteries," *ACS Energy Letters,* vol. 3, no. 10, pp. 2480-2501, 2018/10/12 2018, doi: 10.1021/acsenergylett.8b01426.

[129] W. Lao-atiman, T. Julaphatachote, P. Boonmongkolras, and S. Kheawhom, "Printed Transparent Thin Film Zn-MnO2Battery," *Journal of The Electrochemical Society,* vol. 164, no. 4, pp. A859-A863, 2017, doi: 10.1149/2.1511704jes.

[130] R. Trócoli and F. La Mantia, "An Aqueous Zinc-Ion Battery Based on Copper Hexacyanoferrate," *ChemSusChem,* https://doi.org/10.1002/cssc.201403143 vol. 8, no. 3, pp. 481-485, 2015/02/01 2015, doi: https://doi.org/10.1002/cssc.201403143.

[131] K. Xu and C. Wang, "Batteries: Widening voltage windows," *Nature Energy,* vol. 1, no. 10, p. 16161, 2016/10/06 2016, doi: 10.1038/nenergy.2016.161.

[132] N. Alias and A. A. Mohamad, "Morphology study of electrodeposited zinc from zinc sulfate solutions as anode for zinc-air and zinc-carbon batteries," *Journal of King Saud University - Engineering Sciences,* vol. 27, no. 1, pp. 43-48, 2015/01/01/ 2015, doi: https://doi.org/10.1016/j.jksues.2013.03.003.

[133] Z. Liu, G. Pulletikurthi, A. Lahiri, T. Cui, and F. Endres, "Suppressing the dendritic growth of zinc in an ionic liquid containing cationic and anionic zinc complexes for battery applications," *Dalton Transactions,* 10.1039/C6DT00969G vol. 45, no. 19, pp. 8089-8098, 2016, doi: 10.1039/C6DT00969G.

[134] M. Armand, F. Endres, D. R. MacFarlane, H. Ohno, and B. Scrosati, "Ionic-liquid materials for the electrochemical challenges of the future," *Nature Materials,* vol. 8, no. 8, pp. 621-629, 2009/08/01 2009, doi: 10.1038/nmat2448.

[135] S. Kazemiabnavi, Z. Zhang, K. Thornton, and S. Banerjee, "Electrochemical Stability Window of Imidazolium-Based Ionic Liquids as Electrolytes for Lithium Batteries," *The Journal of Physical Chemistry B,* vol. 120, no. 25, pp. 5691-5702, 2016/06/30 2016, doi: 10.1021/acs.jpcb.6b03433.

[136] A. P. Abbott, J. C. Barron, and K. S. Ryder, "Electrolytic deposition of Zn coatings from ionic liquids based on choline chloride," *Transactions of the IMF,* vol. 87, no. 4, pp. 201-207, 2009/07/01 2009, doi: 10.1179/174591909X438857.

[137] J. P. Tafur, J. Abad, E. Román, and A. J. Fernández Romero, "Charge storage mechanism of MnO2 cathodes in Zn/MnO2 batteries using ionic liquid-based gel polymer electrolytes," *Electrochemistry Communications,* vol. 60, pp. 190-194, 2015/11/01/ 2015, doi: https://doi.org/10.1016/j.elecom.2015.09.011.

[138] T. J. Simons, M. Salsamendi, P. C. Howlett, M. Forsyth, D. R. MacFarlane, and C. Pozo-Gonzalo, "Rechargeable Zn/PEDOT Battery with an Imidazolium-Based Ionic Liquid as the Electrolyte," *ChemElectroChem,* https://doi.org/10.1002/celc.201500278 vol. 2, no. 12, pp. 2071-2078, 2015/12/01 2015, doi: https://doi.org/10.1002/celc.201500278.

[139] A. Fdz De Anastro *et al.*, "Poly(ionic liquid) iongels for all-solid rechargeable zinc/PEDOT batteries," *Electrochimica Acta,* vol. 278, pp. 271-278, 2018/07/10/ 2018, doi: https://doi.org/10.1016/j.electacta.2018.05.044.

[140] L. Millia *et al.*, "Bio-inspired choline chloride-based deep eutectic solvents as electrolytes for lithium-ion batteries," *Solid State Ionics,* vol. 323, pp. 44-48, 2018/10/01/ 2018, doi: https://doi.org/10.1016/j.ssi.2018.05.016.

[141] Y. Liu, J. Wei, Y. Tian, and S. Yan, "The structure–property relationship of manganese oxides: highly efficient removal of methyl orange from aqueous solution," *Journal of Materials Chemistry A,* 10.1039/C5TA05507E vol. 3, no. 37, pp. 19000-19010, 2015, doi: 10.1039/C5TA05507E.

[142] A. P. Abbott, J. C. Barron, G. Frisch, K. S. Ryder, and A. F. Silva, "The effect of additives on zinc electrodeposition from deep eutectic solvents," *Electrochimica Acta,* vol. 56, no. 14, pp. 5272-5279, 2011/05/30/ 2011, doi: https://doi.org/10.1016/j.electacta.2011.02.095.

[143] A. P. Abbott, G. Capper, D. L. Davies, R. K. Rasheed, and P. Shikotra, "Selective Extraction of Metals from Mixed Oxide Matrixes Using Choline-Based Ionic Liquids," *Inorganic Chemistry,* vol. 44, no. 19, pp. 6497-6499, 2005/09/01 2005, doi: 10.1021/ic0505450.

[144] M.-S. Wu, P.-C. J. Chiang, and J.-C. Lin, "Electrochemical Investigations on Capacity Fading of Advanced Lithium-Ion Batteries after Storing at Elevated Temperature," *Journal of The Electrochemical Society,* vol. 152, no. 6, p. A1041, 2005, doi: 10.1149/1.1896325.

[145] M. H. Alfaruqi *et al.*, "A layered δ-MnO2 nanoflake cathode with high zinc-storage capacities for eco-friendly battery applications," *Electrochemistry Communications,* vol. 60, pp. 121-125, 2015/11/01/ 2015, doi: https://doi.org/10.1016/j.elecom.2015.08.019.

[146] J. Wang, J. Polleux, J. Lim, and B. Dunn, "Pseudocapacitive Contributions to Electrochemical Energy Storage in TiO2 (Anatase) Nanoparticles," *The Journal of Physical Chemistry C,* vol. 111, no. 40, pp. 14925-14931, 2007/10/01 2007, doi: 10.1021/jp074464w.

[147] N. Ogihara, Y. Itou, T. Sasaki, and Y. Takeuchi, "Impedance Spectroscopy Characterization of Porous Electrodes under Different Electrode Thickness Using a Symmetric Cell for High-Performance Lithium-Ion Batteries," *The Journal of Physical Chemistry C,* vol. 119, no. 9, pp. 4612-4619, 2015/03/05 2015, doi: 10.1021/jp512564f.

[148] T. T. Yu *et al.*, "Zn2GeO4 nanorods grown on carbon cloth as high performance flexible lithium-ion battery anodes," *RSC Advances,* 10.1039/C7RA09273C vol. 7, no. 82, pp. 51807-51813, 2017, doi: 10.1039/C7RA09273C.

[149] W. Lao-atiman, K. Bumroongsil, A. Arpornwichanop, P. Bumroongsakulsawat, S. Olaru, and S. Kheawhom, "Model-Based Analysis of an Integrated Zinc-Air Flow Battery/Zinc Electrolyzer System," (in English), *Frontiers in Energy Research,* Original Research vol. 7, no. 15, 2019-February-22 2019, doi: https://doi.org/10.3389/fenrg.2019.00015.

[150] Y. Huang *et al.*, "Novel Insights into Energy Storage Mechanism of Aqueous Rechargeable Zn/MnO2 Batteries with Participation of Mn2+," *Nano-Micro Letters,* journal article vol. 11, no. 1, p. 49, June 06 2019, doi: https://doi.org/10.1007/s40820-019-0278-9.

[151] W. Lao-atiman *et al.*, "Linear parameter-varying model for a refuellable zinc–air battery," *Royal Society Open Science,* vol. 7, no. 12, p. 201107, 2020, doi: doi:10.1098/rsos.201107.

[152] W. Lao-atiman, S. Olaru, A. Arpornwichanop, and S. Kheawhom, "Discharge performance and dynamic behavior of refuellable zinc-air battery," *Scientific Data,* vol. 6, no. 1, p. 168, 2019/09/09 2019, doi: 10.1038/s41597-019-0178-3.

[153] R. Khezri, K. Jirasattayaporn, A. Abbasi, T. Maiyalagan, A. A. Mohamad, and S. Kheawhom, "Three-Dimensional Fibrous Iron as Anode Current Collector for Rechargeable Zinc–Air Batteries," *Energies,* vol. 13, no. 6, p. 1429, 2020, doi: 10.3390/en13061429.

[154] H. Chen, S. Cai, Y. Wu, W. Wang, M. Xu, and S. J. Bao, "Successive electrochemical conversion reaction to understand the performance of aqueous Zn/MnO2 batteries with Mn2+ additive," *Materials Today Energy,* vol. 20, p. 100646, 2021/06/01/ 2021, doi: 10.1016/j.mtener.2021.100646.

[155] A. Abbasi, S. Hosseini, A. Somwangthanaroj, R. Cheacharoen, S. Olaru, and S. Kheawhom, "Discharge profile of a zinc-air flow battery at various electrolyte flow rates and discharge currents," *Scientific Data,* vol. 7, no. 1, p. 196, 2020/06/22 2020, doi: 10.1038/s41597-020-0539-y.

[156] L. Gao *et al.*, "A High-Performance Aqueous Zinc-Bromine Static Battery," *iScience,* vol. 23, no. 8, p. 101348, 2020/08/21/ 2020, doi: https://doi.org/10.1016/j.isci.2020.101348.

[157] P. Tangthuam, J. Pimoei, A. A. Mohamad, F. Mahlendorf, A. Somwangthanaroj, and S. Kheawhom, "Carboxymethyl cellulose-based polyelectrolyte as cationic exchange membrane for zinc-iodine batteries," *Heliyon,* vol. 6, no. 10, p. e05391, 2020/10/01/ 2020, doi: 10.1016/j.heliyon.2020.e05391.

[158] A. Abbasi, S. Hosseini, A. Somwangthanaroj, A. A. Mohamad, and S. Kheawhom, "Poly(2,6-Dimethyl-1,4-Phenylene Oxide)-Based Hydroxide Exchange Separator Membranes for Zinc–Air Battery," *International Journal of Molecular Sciences,* vol. 20, no. 15, p. 3678, 2019, doi: 10.3390/ijms20153678.

[159] S. Zhang *et al.*, "An adaptive and stable bio-electrolyte for rechargeable Zn-ion batteries," *Journal of Materials Chemistry A,* 10.1039/C8TA04298E vol. 6, no. 26, pp. 12237-12243, 2018, doi: 10.1039/C8TA04298E.

[160] W. Sun *et al.*, "Zn/MnO2 Battery Chemistry With H+ and Zn2+ Coinsertion," *Journal of the American Chemical Society,* vol. 139, no. 29, pp. 9775-9778, 2017/07/26 2017, doi: https://doi.org/10.1021/jacs.7b04471.

[161] X. Gao *et al.*, "H+-Insertion Boosted α-MnO2 for an Aqueous Zn-Ion Battery," *Small,* vol. 16, no. 5, p. 1905842, 2020, doi: 10.1002/smll.201905842.

[162] M. Han *et al.*, "Reaction mechanisms and optimization strategies of manganese-based materials for aqueous zinc batteries," *Materials Today Energy,* vol. 20, p. 100626, 2021/06/01/ 2021, doi: 10.1016/j.mtener.2020.100626.

[163] M. H. Alfaruqi *et al.*, "Electrochemically Induced Structural Transformation in a γ-MnO2 Cathode of a High Capacity Zinc-Ion Battery System," *Chemistry of Materials,* vol. 27, no. 10, pp. 3609-3620, 2015/05/26 2015, doi: https://doi.org/10.1021/cm504717p.

[164] N. Qiu, H. Chen, Z. Yang, S. Sun, and Y. Wang, "Low-cost birnessite as a promising cathode for high-performance aqueous rechargeable batteries," *Electrochimica Acta,* vol. 272, pp. 154-160, 2018/05/10/ 2018, doi: https://doi.org/10.1016/j.electacta.2018.04.012.

[165] J. Lai, H. Zhu, X. Zhu, H. Koritala, and Y. Wang, "Interlayer-Expanded V6O13·nH2O Architecture Constructed for an Advanced Rechargeable Aqueous Zinc-Ion Battery," *ACS Applied Energy Materials,* vol. 2, no. 3, pp. 1988-1996, 2019/03/25 2019, doi: https://doi.org/10.1021/acsaem.8b02054.

[166] K. E. K. Sun *et al.*, "Suppression of Dendrite Formation and Corrosion on Zinc Anode of Secondary Aqueous Batteries," *ACS Applied Materials & Interfaces,* vol. 9, no. 11, pp. 9681-9687, 2017/03/22 2017, doi: https://doi.org/10.1021/acsami.6b16560.

[167] W. Guo *et al.*, "Multifunctional tin layer enabled long-life and stable anode for aqueous zinc-ion batteries," *Materials Today Energy,* vol. 20, p. 100675, 2021/06/01/ 2021, doi: 10.1016/j.mtener.2021.100675.

[168] Y. Zuo *et al.*, "Zinc dendrite growth and inhibition strategies," *Materials Today Energy,* vol. 20, p. 100692, 2021/06/01/ 2021, doi: 10.1016/j.mtener.2021.100692.

[169] B. Tang, L. Shan, S. Liang, and J. Zhou, "Issues and opportunities facing aqueous zinc-ion batteries," *Energy & Environmental Science,* 10.1039/C9EE02526J 2019, doi: https://doi.org/10.1039/C9EE02526J.

[170] W. Du, E. H. Ang, Y. Yang, Y. Zhang, M. Ye, and C. C. Li, "Challenges in the material and structural design of zinc anode towards high-performance aqueous zinc-ion batteries," *Energy & Environmental Science,* 10.1039/D0EE02079F vol. 13, no. 10, pp. 3330-3360, 2020, doi: 10.1039/D0EE02079F.

[171] B. Chakrabarti *et al.*, "Evaluation of a Non-Aqueous Vanadium Redox Flow Battery Using a Deep Eutectic Solvent and Graphene-Modified Carbon Electrodes via Electrophoretic Deposition," *Batteries,* vol. 6, no. 3, p. 38, 2020, doi: https://doi.org/10.3390/batteries6030038.

[172] K. W. Nam *et al.*, "The High Performance of Crystal Water Containing Manganese Birnessite Cathodes for Magnesium Batteries," *Nano Letters,* vol. 15, no. 6, pp. 4071-4079, 2015/06/10 2015, doi: https://doi.org/10.1021/acs.nanolett.5b01109.

[173] I. Soroko, Y. Bhole, and A. G. Livingston, "Environmentally friendly route for the preparation of solvent resistant polyimide nanofiltration membranes," *Green Chemistry,* 10.1039/C0GC00155D vol. 13, no. 1, pp. 162-168, 2011, doi: https://doi.org/10.1039/C0GC00155D.

[174] S. Hosseini *et al.*, "The Influence of Dimethyl Sulfoxide as Electrolyte Additive on Anodic Dissolution of Alkaline Zinc-Air Flow Battery," *Scientific Reports,* vol. 9, no. 1, p. 14958, 2019/10/18 2019, doi: https://doi.org/10.1038/s41598-019-51412-5.

[175] B. Liu *et al.*, "Stabilization of Li Metal Anode in DMSO-Based Electrolytes via Optimization of Salt–Solvent Coordination for Li–O2 Batteries," *Advanced Energy Materials,* vol. 7, no. 14, p. 1602605, 2017, doi: https://doi.org/10.1002/aenm.201602605.

[176] A. Martínez-de la Cruz, U. Amador, J. Rodríguez-Carvajal, and F. García-Alvarado, "Electrochemical zinc insertion into W18O49: Synthesis and characterization of new bronzes," *Journal of Solid State Chemistry,* vol. 178, no. 10, pp. 2998-3003, 2005/10/01/ 2005, doi: https://doi.org/10.1016/j.jssc.2005.07.008.

[177] R. E. Dueber, S. Patat, and P. G. Dickens, "Thermochemical and electrochemical study of sodium and zinc insertion into α-UO3 − y and α-U3O8," *Solid State Ionics,* vol. 80, no. 3, pp. 231-238, 1995/09/01/ 1995, doi: https://doi.org/10.1016/0167-2738(95)00119-Q.

[178] W. Kaveevivitchai and A. Manthiram, "High-capacity zinc-ion storage in an open-tunnel oxide for aqueous and nonaqueous Zn-ion batteries," *Journal of Materials Chemistry A,* 10.1039/C6TA07747A vol. 4, no. 48, pp. 18737-18741, 2016, doi: 10.1039/C6TA07747A.

[179] J. Shin, J. Lee, Y. Park, and J. W. Choi, "Aqueous zinc ion batteries: focus on zinc metal anodes," *Chemical Science,* 10.1039/D0SC00022A vol. 11, no. 8, pp. 2028-2044, 2020, doi: https://doi.org/10.1039/D0SC00022A.

[180] W. Dong, J.-L. Shi, T.-S. Wang, Y.-X. Yin, C.-R. Wang, and Y.-G. Guo, "3D zinc@carbon fiber composite framework anode for aqueous Zn–MnO2 batteries," *RSC Advances,* 10.1039/C8RA03226B vol. 8, no. 34, pp. 19157-19163, 2018, doi: https://doi.org/10.1039/C8RA03226B.

[181] L. Chen *et al.*, "Ultrathin MnO2 nanoflakes grown on N-doped hollow carbon spheres for high-performance aqueous zinc ion batteries," *Materials Chemistry*

Frontiers, 10.1039/C9QM00675C vol. 4, no. 1, pp. 213-221, 2020, doi: 10.1039/C9QM00675C.

[182] D. Y. Putro *et al.*, "Quasi-solid-state zinc-ion battery based on α-MnO2 cathode with husk-like morphology," *Electrochimica Acta,* vol. 345, p. 136189, 2020/06/10/ 2020, doi: https://doi.org/10.1016/j.electacta.2020.136189.

[183] G. Zhao, L. Zhang, and K. Sun, "Capacitive contribution to lithium storage capacity in porous MoO3 films," *Journal of Electroanalytical Chemistry,* vol. 694, pp. 61-67, 2013/04/01/ 2013, doi: 10.1016/j.jelechem.2013.02.005.

[184] D. Wang *et al.*, "A Superior δ-MnO2 Cathode and a Self-Healing Zn-δ-MnO2 Battery," *ACS Nano,* vol. 13, no. 9, pp. 10643-10652, 2019/09/24 2019, doi: 10.1021/acsnano.9b04916.

[185] G. Li *et al.*, "Rechargeable Zn-ion batteries with high power and energy densities: a two-electron reaction pathway in birnessite MnO2 cathode materials," *Journal of Materials Chemistry A,* 10.1039/C9TA11985J vol. 8, no. 4, pp. 1975-1985, 2020, doi: 10.1039/C9TA11985J.

[186] Y.-Z. Wang *et al.*, "A Desolvated Solid–Solid Interface for a High-Capacitance Electric Double Layer," *Advanced Energy Materials,* vol. 9, no. 12, p. 1803715, 2019, doi: https://doi.org/10.1002/aenm.201803715.

[187] Y.-Z. Wang, X.-Y. Shan, D.-W. Wang, H.-M. Cheng, and F. Li, "Mitigating self-discharge of carbon-based electrochemical capacitors by modifying their electric-double layer to maximize energy efficiency," *Journal of Energy Chemistry,* vol. 38, pp. 214-218, 2019/11/01/ 2019, doi: https://doi.org/10.1016/j.jechem.2019.04.004.

[188] K. Nadendla, B. Sarode, and S. H. Friedman, "Chapter Six - Chemical modification of proteins with photocleavable groups," in *Methods in Enzymology*, vol. 624, A. Deiters Ed.: Academic Press, 2019, pp. 113-128.

[189] A. Zahoor, J. S. Jeon, H. S. Jang, M. Christy, Y. Hwang, and K. S. Nahm, "Mechanistic Study on Phase and Morphology Conversion of MnO2 Nanostructures Grown by Controlled Hydrothermal Synthesis," *Science of Advanced Materials,* vol. 6, no. 12, pp. 2712-2723, // 2014, doi: 10.1166/sam.2014.1990.

[190] W. Choi, H.-C. Shin, J. M. Kim, J.-Y. Choi, and W.-S. Yoon, "Modeling and Applications of Electrochemical Impedance Spectroscopy (EIS) for Lithium-ion Batteries," *J. Electrochem. Sci. Technol,* vol. 11, no. 1, pp. 1-13, 2 2020, doi: 10.33961/jecst.2019.00528.

[191] F. Single, B. Horstmann, and A. Latz, "Theory of Impedance Spectroscopy for Lithium Batteries," *The Journal of Physical Chemistry C,* vol. 123, no. 45, pp. 27327-27343, 2019/11/14 2019, doi: 10.1021/acs.jpcc.9b07389.

[192] M.-J. Uddin and S.-J. Cho, "Reassessing the bulk ionic conductivity of solid-state electrolytes," *Sustainable Energy & Fuels,* 10.1039/C8SE00139A vol. 2, no. 7, pp. 1458-1462, 2018, doi: 10.1039/C8SE00139A.

[193] K. Vuorilehto, "Materials and function," in *Lithium-Ion Batteries: Basics and Applications*, R. Korthauer Ed. Berlin, Heidelberg: Springer Berlin Heidelberg, 2018, pp. 21-28.

[194] J. P. Pender *et al.*, "Electrode Degradation in Lithium-Ion Batteries," *ACS Nano,* vol. 14, no. 2, pp. 1243-1295, 2020/02/25 2020, doi: 10.1021/acsnano.9b04365.

[195] E. Tavčar, E. Turk, and S. Kreft, "Simple Modification of Karl-Fischer Titration Method for Determination of Water Content in Colored Samples," *Journal of Analytical Methods in Chemistry,* vol. 2012, p. 379724, 2012/03/19 2012, doi: 10.1155/2012/379724.

APPENDIX A
SUPPLEMENTARY INFORMATION

Supplementary Information: Highly Stable Rechargeable Zinc-ion Battery using Dimethyl Sulfoxide Electrolyte

Wathanyu Kao-ian[1], Mai Thanh Nguyen[2], Tetsu Yonezawa[2,3], Rojana Pornprasertsuk[4,5,6], Jiaqian Qin[6,7], Siwaruk Siwamogsatham[8] and Soorathep Kheawhom[1,6,*]

[1] Department of Chemical Engineering, Faculty of Engineering, Chulalongkorn University, Bangkok 10330, Thailand; wathanyu.k@student.chula.ac.th (W.K.-i.)

[2] Division of Materials Science and Engineering, Faculty of Engineering, Hokkaido University, Hokkaido 060-8628, Japan; mai_nt@eng.hokudai.ac.jp (M.T.N.); tetsu@eng.hokudai.ac.jp (T.Y.)

[3] Institute for the Promotion of Business-Regional Collaboration, Hokkaido University, Sapporo, Japan

[4] Department of Materials Science, Faculty of Science, Chulalongkorn University, Bangkok 10330, Thailand; rojana.p@chula.ac.th (R.P.)

[5] Center of Excellence in Petrochemical and Materials Technology, Chulalongkorn University, Bangkok 10330, Thailand

[6] Research Unit of Advanced Materials for Energy Storage, Chulalongkorn University, Bangkok 10330, Thailand

[7] Metallurgy and Materials Science Research Institute, Chulalongkorn University, Bangkok 10330, Thailand; Jiaqian.Q@chula.ac.th (J.Q.)

[8] National Science and Technology Development Agency, Pathumthani 12120, Thailand; siwaruk.siw@nstda.or.th (S.S.)

* Correspondence: soorathep.k@chula.ac.th (S.K.)

A.1 Experimental Procedures

A.1.1 Materials

Zn foil (99.99%, thickness: 0.1 mm) was procured from Shandong AME Energy Co. Ltd., China. Ni/Cu fabric (thickness: 0.08 mm) was purchased from Qijing Trading Co., Ltd (Wenzhou, China). Carbon paper (SIGRACET® GDL 24 BA, thickness: 190 μm) was acquired from Ion Power, Inc. Conductive carbon black (Super P) was purchased from TIMCAL Ltd. Polyvinylidene fluoride (PVDF, MW~180,000), anhydrous DMSO (99.9%) and $Zn(OTf)_2$ (98%) were procured from Sigma Aldrich. Manganese Sulfate Monohydrate ($MnSO_4 \cdot H_2O$, 99.0%) and N-Methyl-2-pyrrolidone (NMP, 99.5%) were acquired from QReC. $ZnSO_4$ ($ZnSO_4 \cdot 7H_2O$, 99.0%) was purchased from LOBA CHEMIE. Potassium Permanganate ($KMnO_4$, 99.0%) was obtained from Ajax Finechem. Glass microfiber (Whatman 1822-047 GF/C, 1.2 μm) was acquired from Whatman Plc.
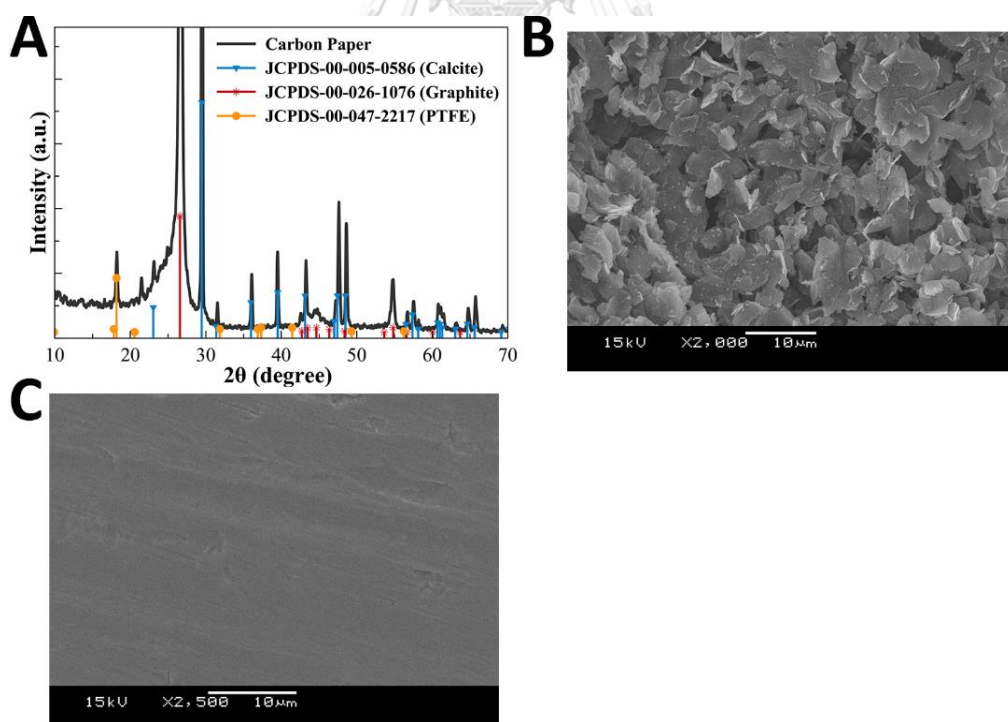

Figure A1 Characterization of raw materials: (a) XRD spectra of carbon paper (SIGRACET) (b) SEM image of carbon paper (SIGRACET), and (c) SEM image of zinc foil.

A.1.2 δ-MnO₂ synthesis

δ-MnO$_2$ nanoflowers were synthesized via the method as used by Liu et al., [141]. Firstly, 0.948 g KMnO4 was dissolved in 35 ml of deionized (DI) water and stirred at medium rotational speed. Then, 0.169 g MnSO4•H2O was slowly added dropwise to the solution and left for 30 min. After that, the mixture was put in a PTFE lined autoclave and heated at 160 °C for 12 h. Next, the autoclave was left to cool down naturally, under ambient environment. Eventually, the synthesized product was filtered, washed several times with DI water and ethanol, and dried overnight at 60°C under vacuum, respectively. As illustrated in Fig. A2, the crystallography and nanostructure of δ-MnO2 was confirmed via X-ray diffraction (XRD) technique and scanning electron microscope (SEM).
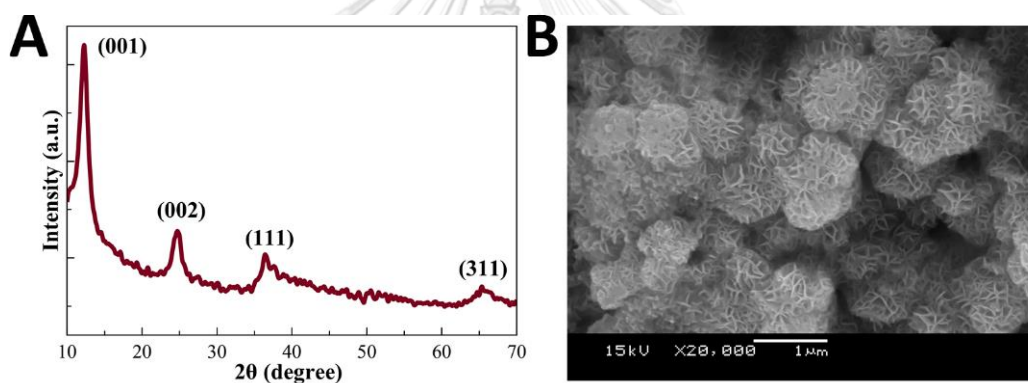

Figure A2 Characterization of synthesized δ-MnO$_2$: (a) XRD spectra and (b) SEM image.

A.1.3 Electrode and electrolyte preparations

In this study, two types of negative electrode were applied: Zn foil and electrodeposited Zn on Ni/Cu fabric. The first electrode, raw Zn foil, was used in a Zn-symmetrical cell study for clearer observation of the Zn morphology. The second electrode was used in a full cell (Zn/δ-MnO$_2$) study in order to minimize the voltage polarization of the negative electrode. The second electrode was prepared by the electrodeposition of Zn from 1 M ZnSO4 solution at 40 mA/cm^2 onto Ni/Cu fabric; the counter side was Zn foil. The resultant Zn loading was 15 mg/cm^2.

The δ-MnO$_2$ (positive) electrode was prepared via slurry mixing of δ-MnO$_2$ (80 %wt.), conductive carbon black (15 %wt.) and PVDF (5 %wt.) in NMP. The mixture was repeatedly stirred and shook, using a magnetic stirrer and ultrasonic cleaner to ensure it was well mixed. Next, it was coated onto the carbon paper using doctor blade coater (AOT-FCM-250, AOT Electronic Technology) and dried at 80°C for 3 h. Subsequently, the coated paper was rolled several times to make a denser coated layer, which would decrease its electronic resistivity. Finally, the coated paper was dried again at 60°C under vacuum. The average δ-MnO$_2$ loading on the electrode was 2.06 mg/ cm^2. The Zn(OTf)$_2$/DMSO solution, as an electrolyte, was prepared by the common mixing method of Zn(OTf)$_2$ and anhydrous DMSO. The Zn(OTf)$_2$ powder and DMSO were poured into a bottle together under nitrogen (N$_2$) atmospheric (water content < 0.1 ppm). Then, the bottle was vigorously shaken by a vortex mixer until all the Zn(OTf)$_2$ totally dissolved in the solvent. Finally, it was stored under N$_2$.

A.1.4 Electrochemical and material characterization

In Fig. A3a, a three-electrode cell used for the Zn half-cell test is presented. The cell consists of a cylindrical glass container having a three-hole PTFE cap. As seen, the container has a working electrode (Pt wire), a counter electrode (1 cm^2 Pt sheet) and a reference electrode (Ag/AgCl, sat. KCl). The cell is filled with the electrolyte solution.

The cell for the two-electrode test was a CR2025 button cell. In order to fabricate this type of cell, electrodes were punched into a 15 mm diameter disk using electrode punching machine (TOB-CP60). Furthermore, a glass microfiber was punched into a 19 mm diameter disk and used as the separator. As illustrated in Fig. A3b, all parts of the cell were arranged in the following order: the negative electrode cap, conical spring, spacer, negative electrode, two separators, positive electrode and positive electrode cap. Then, 0.25 ml of the electrolyte solution was added to the assembled cell. After that, the cell was crimped using coin cell crimping machine (TOB-MR120). Eventually, the cell was preconditioned by galvanostatic discharging/charging at low current density (25 mA/g) within the voltage range of (0.5-1.85) V. The voltage polarization profile is shown, as in Fig. A4. Both CV and EIS were performed via Potentiostat/Galvanostat (AMETEK-Princeton Applied Research,

VersaSTAT 3F). The galvanostatic test was conducted using battery analyzer (NEWARE, BTS4000-5V50mA). The synthesized samples and some other materials were characterized ex-situ via scanning electron microscope (JEOL, JSM-5800LV) and X-ray diffractometer (Bruker, D2 PHASER) employing Cu Kα radiation. To prepare electrodes for characterization, the electrodes were detached from the cell and washed with DI water and ethanol, several times, to remove the electrolyte solution and Zn salt from their surface. Finally, they were dried overnight at 60°C under vacuum.
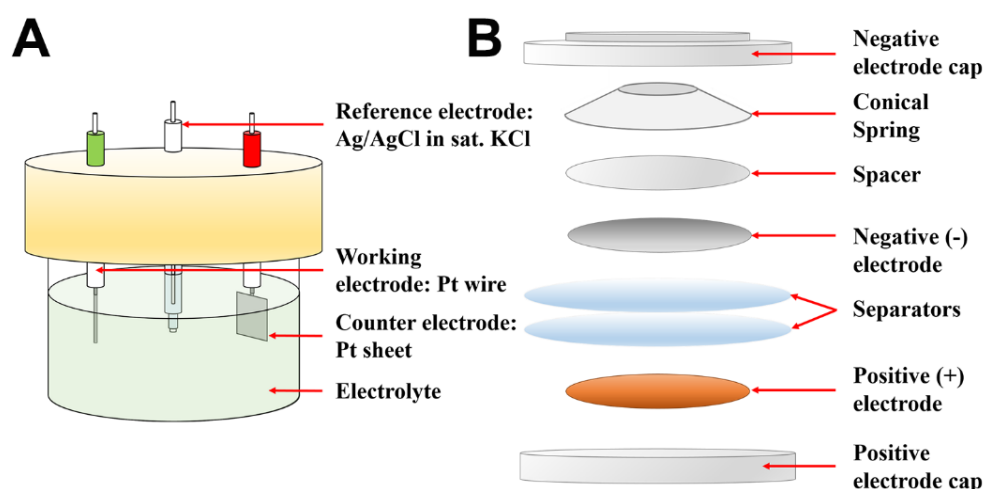

Figure A3 Cell configurations for electrochemical tests: (a) three-electrode (half-cell) setup and (b) two-electrode (full-cell) setup.
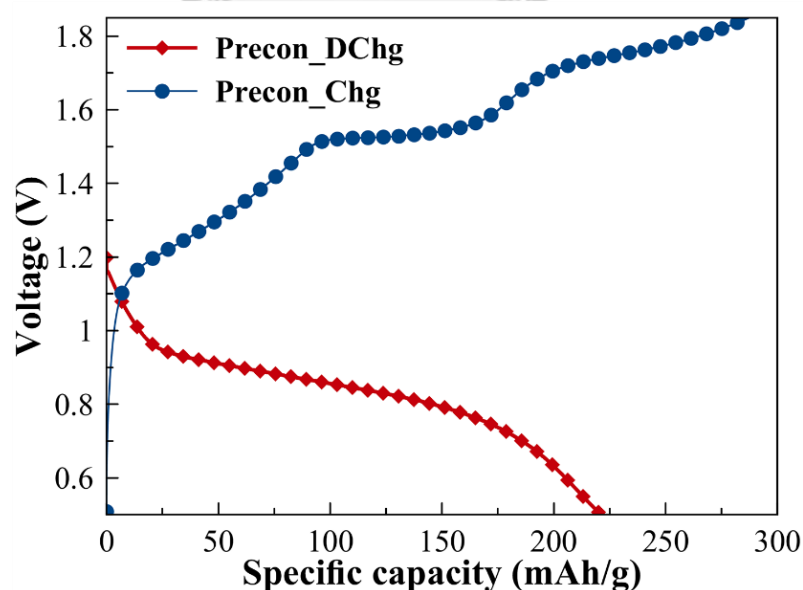

Figure A4 Preconditioning voltage profile

A.1.5 Ionic conductivity

In Fig. A5a, the ionic conductivity of DMSO solution was measured via EIS analysis. The EIS measurement was carried out using a frequency range of 1000 kHz to 1 Hz under N_2 environment (< 0.1 ppm of H_2O) and temperature control. Three temperatures: namely, 30, 50 and 70°C, were used in the test. Then, the ionic conductivity value was calculated using the equation as follows [192]

$$\sigma = \frac{L}{RA} \qquad\qquad\qquad (A1)$$

where σ, A, L and R is ionic conductivity (mS/cm), area of electrode (cm^2), distance between electrode (cm) and the intercept-value of EIS spectral with real impedance axis (kΩ). The calculation results are as shown in Fig. A5b.
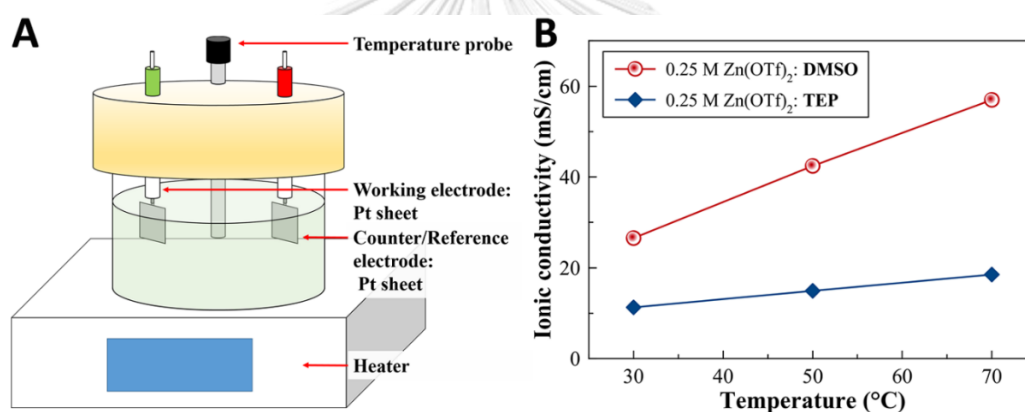

Figure A5 Ionic conductivity measurement: (a) cell configuration for ionic conductivity measurement and (b) ionic conductivity of 0.25M Zn(OTf)$_2$/ DMSO and TEP: at 30, 50 and 70°C.

A.1.6 Zn plating efficiency

The plating efficiency was evaluated through the discharging capacity of Zn after charged. Hence, in order to measure this value, the cell must contain one blank current collector and one Zn electrode. In the setup, the 15 mm stainless steel (SS) spacer disk was used as a negative electrode and the 15 mm Zn disk was used as the positive electrode. The CR2025 configuration was applied to this test along with the 19mm glass microfiber separator. The cell was cycled at 0.5 mA/cm^2 having a charging time of 10

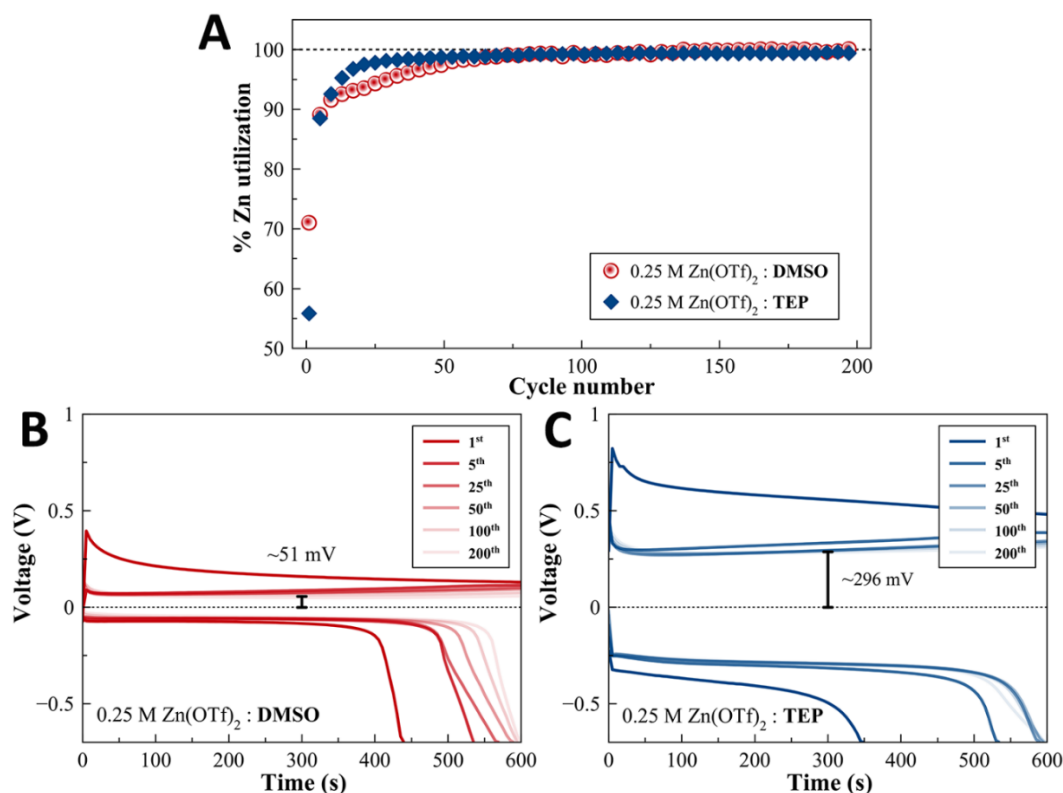min and discharging cut-off voltage of -0.7 V. Results of this experiment are illustrated as shown in Fig. A6 below.

Figure A6 Plating efficiency results: (a) percentage of Zn utilization vs. cycle number (b) voltage profile of SS |0.25 M Zn(OTf)2/DMSO| Zn cell at 1st,5th,25th, 50th, 100th and 200th, and (c) voltage profile of SS |0.25 M Zn(OTf)2/TEP| Zn cell at 1st,5th,25th, 50th, 100th and 200th.

A.1.7 H$_2$ evolution and self-corrosion test

Due to the difficulty in observing the production of hydrogen in the coin cell, an extra experiment was performed using the same glass cell, which was used in the CV experiment of the negative electrode. Regarding hydrogen production, two issues were of concern viz. hydrogen production from HER and hydrogen production owing to self-corrosion of Zn in the electrolyte. The occurrence of such phenomena was investigated by testing the electrodeposited Zn on the Ni/Cu fabric. Two tests were carried out: (1) multiple cycle CV and (2) soaking the electrode in the electrolyte.

As illustrated in Fig. A7, with regard to the multiple cycle CV, the Zn electrode, 1 cm^2 Pt sheet electrode and Ag/AgCl (sat. KCl) electrode were used as working electrode, counter electrode and reference electrode, respectively. Multiple cycle CV, having a scan rate of 15 mV/s and potential range of (+0.2 to -0.2) V versus OCV, was applied to this cell using different electrolytes (water-based and DMSO-based) for the duration of 100 cycles. Then, a picture was taken after the 50th and 100th cycle, as shown in Figs. 2E and 2F.

Subsequently, the second test was performed whereby the electrode was soaked in different electrolytes. Then, a photo was taken at the start and another 24 h. later. In Figs. 2G and 2H, results are shown.
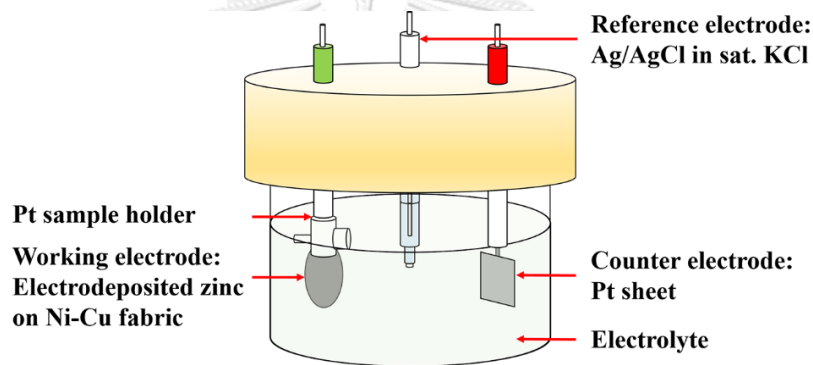

Figure A7. Cell configuration for hydrogen evolution test

A.1.8 Charge-storage mechanism and capacitive contribution of δ-MnO₂ cathode

In order to distinguish the charge-storage mechanism of this system, the form of equation that is commonly used for analysis of voltammetric response is shown, as in Eq. (1):

$$i = av^b \tag{A1}$$

where i and v is measured current density (mA/cm^2) and scan rate (mV/s), respectively, while a and b are empirical constants. The charge-storage mechanism, therefore, is diffusion-controlled in which $b=0.5$ and capacitive when it is 1.0. Calculation results are as shown in Fig. A8b.

To investigate the contribution of the capacitive reaction, in the overall charge-storage process at every potential, an equation in terms of the sum of the capacitive and diffusion-controlled current was applied. This equation can be written, as follows in Eq. (2):

$$i = k_1 v + k_2 v^{1/2} \qquad\qquad (A2)$$

where k_1 is the constant corresponding to the capacitive current and k_2 is the constant corresponding to the diffusion-controlled current. Calculation results are as shown in Figs. S8C and S8D.
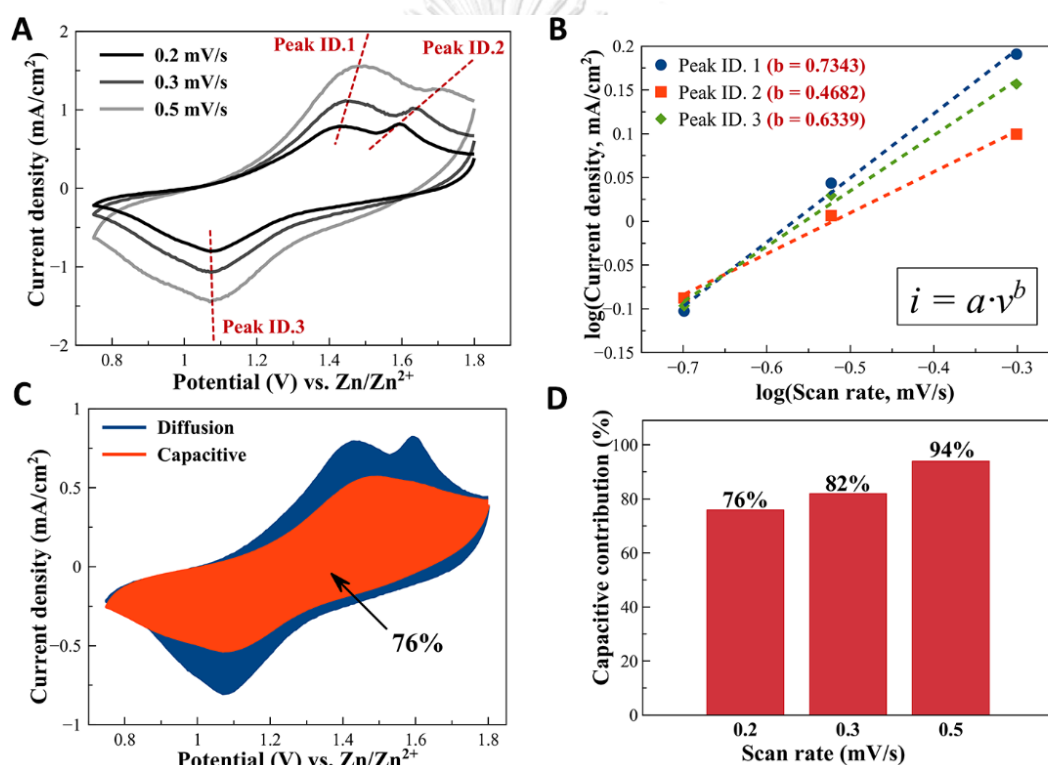

Figure A8. Electrochemical data of the δ-MnO$_2$ electrode within 0.25 M Zn(OTf)$_2$/DMSO: (a) cyclic voltammograms of Zn|0.25 M Zn(OTf)$_2$/DMSO |δ-MnO$_2$ cell, at various scan rates (b) the b-value analysis for all peaks (c) capacitive contribution plot, at a scan rate of 0.2 mV/s, and (d) capacitive contribution percentages, at different scan rates.

A.1.9 Water Content of Electrolyte (Before/After Cycling)

The moisture content of the electrolyte is one of the factors which may disrupt the performance and stability of the battery [193, 194]. Thus, the initial amount of water in an electrolyte and the its effect upon cycling are pivotal to this discussion. To identify the amount of water within the organic solvent, Karl Fischer titration, one of the most powerful techniques, was used for this purpose [195].

Due to the large amount of electrolyte solution required for the Karl Fischer titration (~0.5-1 ml per time), a special setup of the cell (Fig. A9) was used instead of CR2025 button cell; 5 ml of electrolyte was poured into the cell. The cell was cycled at 50 mA/g within the voltage range of 0.75-1.8 V for 25 cycles. Titration was carried out via the automatic titrator (Karl Fischer moisture titrator, MKV-710S, Kyoto Electronics Manufacturing) at its initial and after cycling. Results are as shown in Table A1
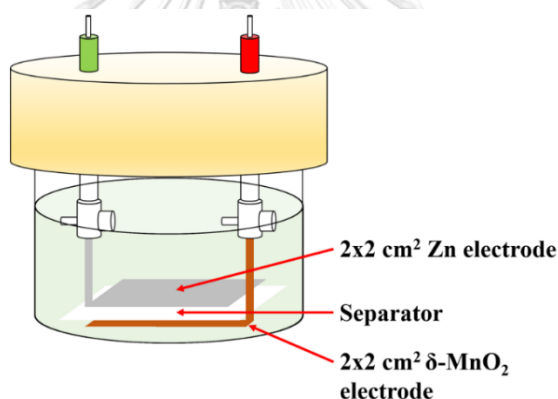

Figure A9 $Zn|0.25$ M $Zn(OTf)_2/DMSO$ $|\delta\text{-}MnO_2$ cell for the electrolyte sampling

Table A1 Water content of the electrolyte

Cycling position	Water content (ppm)			
	1st	2nd	3rd	Average
As-prepare	270.86	259.59	304.92	**278.46**
25th cycle	469.8	468.84	469.36	**469.33**

A.1.10 Water content of δ-MnO₂ electrode (before/after cycling)

In general, δ-MnO$_2$ contains water molecules within its structure [69, 189]. Hence, an increase in the amount of water in an electrolyte may occur due to the water emission from δ-MnO$_2$ structure. The answer to this phenomena can be obtained through the water content measurement of the electrode. The water content of δ-MnO$_2$ was measured using thermogravimetric analysis (TGA). Three samples viz. δ-MnO$_2$ powder, bare electrode and cycled electrode were applied in this experiment in order to observe the change in water content of δ-MnO$_2$ structure upon cycling. The cycled electrode was prepared from the CR2025 Zn|0.25 M Zn(OTf)$_2$/DMSO |δ-MnO$_2$ cell. Thus, galvanostatic charge-discharge cycling at 50 mA/g within a voltage range of 0.75-1.8 V for 25 cycles was carried out. Then, the electrode was detached from the cell and repeatedly washed with water and ethanol. Next it was dried under vacuum at 60°C overnight. Finally, all samples were characterized using simultaneous thermogravimetry - differential scanning calorimetry (STA/TG-DSC) (STA 449 F1 Jupiter, NETZSCH Group). Results are as shown in Fig. A10.
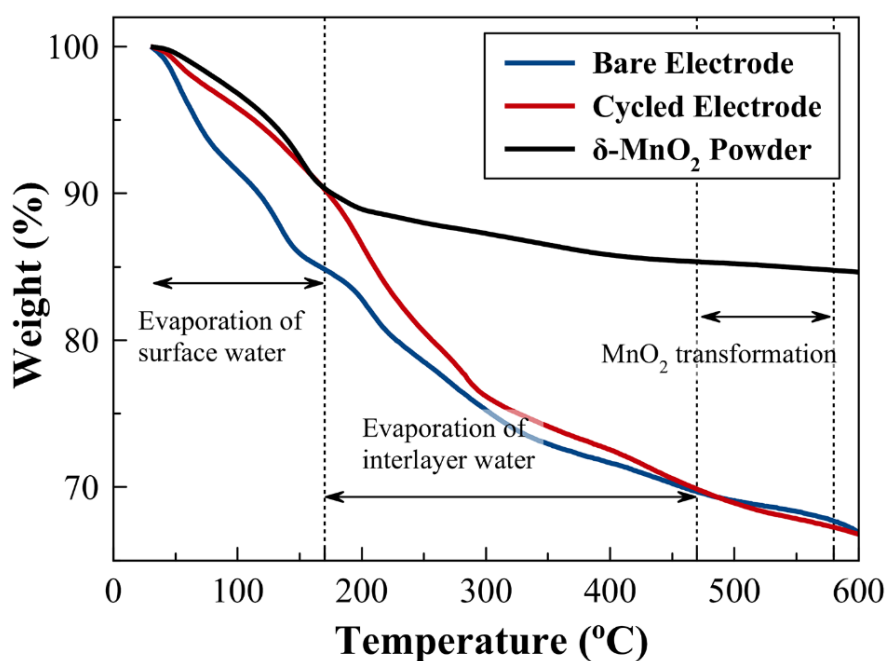

Figure A10. TGA analysis result
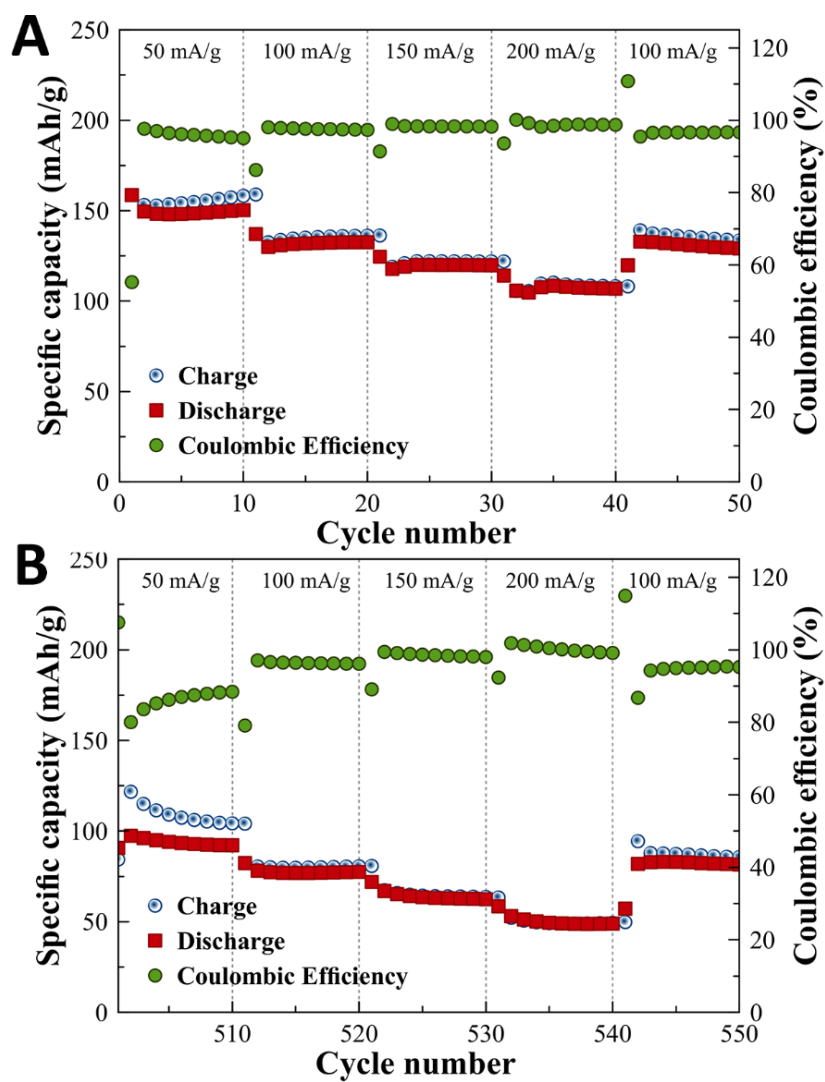
A.2 Aditional Results and Data From the Literature

Figure A11 Rate capability of Zn|0.25 M Zn(OTf)$_2$/DMSO |δ-MnO$_2$ cell: (a) 1st to 50th cycle and (b) 501st to 550th cycle.
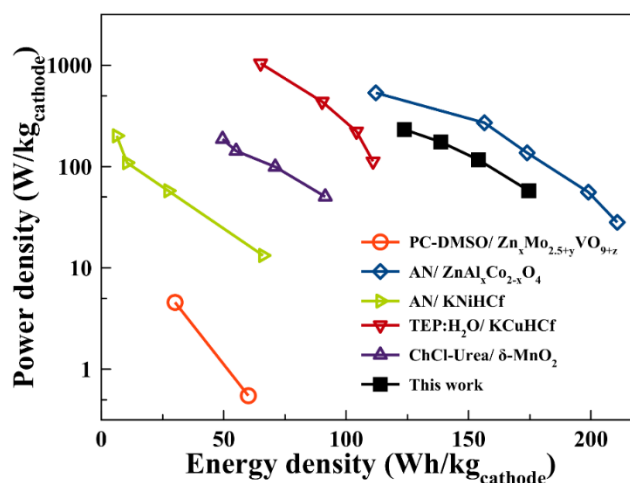
Figure A12 Ragone plot of nonaqueous Zn intercalation batteries

Table A2 Cyclability comparison of nonaqueous Zn intercalation batteries

Electrolyte	Negative Electrode	Positive Electrode	Voltage Window & Current Density	Starting Capacity of Cyclability Test (mAh/g)	Ending Capacity (mAh/g) & Capacity Fading Rate (per cycle)	Refs.
$Zn(TFSI)_2$/AN	Zinc metal	δ-MnO_2	0.05-1.9 V, 12.3 mA/g	100 at 1st cycle	72 at 100th cycle (0.28%)	[69]
$Zn(OTf)_2$/AN	Zinc metal	$ZnAl_xCo_{2-x}O_4$	1.4-2.15 V, 32 mA/g	134 at 1st cycle	100 at 100th cycle (0.25%)	[62]
$Zn(OTf)_2$/AN	Zinc metal	$V_3O_7 \cdot H_2O$	0.5-1.8 V, 5 mA/g	50 at 1st cycle	177 at 50th cycle (capacity increase)	[46]
$Zn(ClO_4)_2$/AN	Zinc metal	Potassium Nickel Hexacyanoferrate (KNiHCf)	0.7-1.8 V, 11.2 mA/g	49 at 1st cycle	N/A	[70]
0.5M $Zn(OTf)_2$/ TEP:H_2O (7:3)	Zinc foil	Potassium Copper Hexacyanoferrate (KCuHCf)	1.3-2.0 V, 1C	73.3 at 1st cycle	54.2 at 1000th cycle (0.026%)	[61]
$Zn(OTf)_2$/PC-DMSO	Zinc metal	$Zn_xMo_{2.5+y}VO_{9+z}$	0.5-1.8 V, 20 mA/g	188 at 1st cycle	114 at 35th cycle (1.12%)	[178]
$ZnCl_2$/ChCl-urea	Zinc on Ni-foam	δ-MnO_2	0.4-1.9 V, 50 mA/g	67 at 51st cycle	36 at 150th cycle (0.46%)	[8]
$Zn(ClO_4)_2$/ Acetamide	Zinc sheet	γ-MnO_2	0.5-1.9 V, 100 μA/cm^2	190 at 1st cycle	72 at 35th cycle (1.77%)	[93]
$Zn(OTf)_2$/DMSO	Zinc on Ni-Cu fabric	δ-MnO_2	0.75-1.8 V, 50 mA/g	129 at 51st cycle	75 at 1000th cycle (0.047%)	This work

VITA

NAME   Wathanyu Kao-ian

DATE OF BIRTH 13 March 1994

PLACE OF BIRTH Suratthani

INSTITUTIONS   B.Eng. King Mongkut's Institute of Technology
ATTENDED   Ladkrabang
HOME ADDRESS 126/29 Pattanakarn-Kukwang Road, Nai Mueang,
Mueang, Nakhon Si Thammarat, Postcode: 80000

PUBLICATION   Kao-ian, W., Nguyen, M. T., Yonezawa, T.,
Pornprasertsuk, R., Qin, J., Siwamogsatham, S., &
Kheawhom, S. (2021). Highly Stable Rechargeable Zinc-
ion Battery using Dimethyl Sulfoxide Electrolyte.
Materials Today Energy, 100738.

Kao-ian, W., Pornprasertsuk, R., Thamyongkit, P.,
Maiyalagan, T., & Kheawhom, S. (2019). Rechargeable
Zinc-Ion Battery Based on Choline Chloride-Urea Deep
Eutectic Solvent. Journal of The Electrochemical Society,
166(6), A1063-A1069.

จุฬาลงกรณ์มหาวิทยาลัย

CHULALONGKORN UNIVERSITY